

# Progress Report on SIMULINK Modelling of RF Cavity Control for SPL Extension to LINAC4

---

*Theory and Analysis behind Simulation Results of SPL Model Using  
I/Q Components in SIMULINK to Date, Including Lorentz Force  
Effects and Multiple Cavities Driven by Single Feedback Loop*

Matias Hernandez

Supervisor: Wolfgang Hofle

Acknowledgements:

CEA team, in particular O.Piquet (SIMULINK model)

W. Hofle G. Kotzian J. Tuckmantel D. Valuch

Geneva, October 2010

## Abstract

In the context of a luminosity upgrade for the LHC within the coming years, works have started on LINAC4 to provide an infrastructure for updating the LHC supplier chain. In order to achieve energy levels and particles per bunch necessary for the expected rate of events at LHC detectors and related experiments, a project proposal is underway for an appended Superconducting Proton LINAC (SPL) that will run from the normal conducting LINAC4 and LP-SPL onto the LHC supplier chain. Thus, the SPL will have two main functions: Firstly, to provide  $H^-$  beam for injection into the PS2 which is compatible with LHC luminosity. For this purpose the SPL will accelerate the output beam of LINAC4 from 1GeV to 4GeV, removing, at the same time, the necessity for PSB operation in the LHC supply chain. Secondly, it will provide an infrastructure upgradeable to meet the needs of all potential high-power proton users at CERN (EURISOL) and possibly neutrino production facilities. For high-power applications of this nature the SPL will need to provide a 5GeV beam whose time-structure can be tailored to meet the specifications of each application. As of now, the design of the SPL is planned to make use of high-Q, 5-cell superconducting elliptical cavities pulsed at a resonant frequency of 704.4 MHz by MultiMegawatt Klystrons with a max repetition rate of 50 Hz, accelerating a 20/40 mA  $H^-$  beam with a field of approximately 25 MV/m, depending on the output requirements of different applications. In the context of the development of a proposal for this conceptual design by mid-2011, this report consists on the progress to date of a SIMULINK model that follows the design specifications and will provide a useful means to foresee any issues that might arise with construction of the SPL, as well as a relatively precise feel for the costs involved in terms of power consumption and technology.

# Contents

<b>1</b>	<b>Introduction</b>	<b>5</b>
<b>2</b>	<b>RF Cavity Theory</b>	<b>6</b>
2.1	Cavity Equivalent Circuit . . . . .	6
2.2	Coupling Between RF Generator, Cavity and Beam . . . . .	9
2.2.1	Steady-State Analysis . . . . .	9
2.2.2	Transient Analysis . . . . .	12
2.3	Beam loading Theorem . . . . .	16
<b>3</b>	<b>RF Control of a 5-Cell 704.4 MHz Resonant Cavity</b>	<b>21</b>
3.1	SPL Parameters and Power Considerations . . . . .	21
3.2	Sources of Perturbation . . . . .	24
3.3	Feedback and Feed-Forward Control . . . . .	26
3.4	Kalman Filtering . . . . .	28
<b>4</b>	<b>SIMULINK I-Q Model for SPL RF Components</b>	<b>33</b>
4.1	Generator, Generator-Cavity Coupling . . . . .	37
4.2	Resonant Cavity Model . . . . .	40
4.3	RF Feedback Loop . . . . .	44
4.4	Dual Cavity Model . . . . .	47
4.5	Graphical User Interface (GUI) . . . . .	52
<b>5</b>	<b>Results of Model Analysis</b>	<b>56</b>
5.1	Single Cavity in the Absence of Lorentz Detuning . . . . .	56
5.1.1	Open Loop . . . . .	56
5.1.2	Closed Loop . . . . .	60
5.2	Single Cavity with Lorentz Detuning Effects . . . . .	66
5.2.1	Open Loop . . . . .	66
5.2.2	Closed Loop . . . . .	71
5.2.3	Variation of Source Beam Current: Low and High Power SPL Operation . . . . .	77
5.3	Dual-Cavity Case . . . . .	80
5.3.1	The Need for Feed-Forward . . . . .	80
5.3.2	Dual Cavity with Feed-Forward . . . . .	84
5.3.3	Loaded Quality Factor Mismatch . . . . .	85
5.4	Error Analysis and Stability Considerations . . . . .	87



# List of Figures

2.1	Pillbox cavity [Le 00]	6
2.2	Cavity equivalent circuit	8
2.3	Cavity coupled to beam and generator [Sch98]	9
2.4	Steady-state cavity [Tuc04]	10
2.5	Fourier spectrum relation between RF and DC beam current	12
2.6	Cavity-beam interaction [Sch98]	13
2.7	Cavity voltage gradients induced by generator and beam	15
2.8	Effect of single bunch passage on cavity voltage [Wil78]	17
2.9	Voltage decay in detuned cavity [Wil78]	18
2.10	Overall effect of beam loading on detuned cavity [Wil78]	19
2.11	Generator-beam power interaction in tuned cavity	20
3.1	General SPL parameters [Ger07]	22
3.2	Transient power distribution [Hof09]	22
3.3	Negative feedback operation	26
3.4	Effects of PID gain on output control performance [AM]	27
3.5	Feedback and feed-forward complementary control	28
3.6	Kalman filtering operation [WB06]	32
4.1	I/Q Equivalence [Hol07]	34
4.2	SPL 1 cavity control high level diagram	35
4.3	SPL single-cavity control SIMULINK model overview	36
4.4	Coupler SIMULINK model (1/N)	37
4.5	Circulator SIMULINK model	37
4.6	RF generator high level diagram	38
4.7	RF generator SIMULINK model	39
4.8	Beam and generator-induced voltage gradients in cavity	40
4.9	Cavity high level diagram with beam loading and Lorentz detuning	42
4.10	Cavity SIMULINK model with beam loading and Lorentz detuning	43
4.11	PID feedback loop high-level diagram	45
4.12	PID feedback SIMULINK model	46
4.13	Vector average block	47
4.14	PID feedback loop high-level diagram	48
4.15	PID feedback SIMULINK model	49
4.16	Kalman filter high-level diagram	50
4.17	Kalman filter SIMULINK model	51
4.18	Graphical user interface (1-Cavity)	53
4.19	Graphical user interface (2-cavities)	54

4.20	Graphical user interface (4-cavities) . . . . .	55
5.1	Cavity voltage magnitude and phase in the absence of Lorentz detuning (open loop) . . . . .	57
5.2	Forward and reflected power in the absence of Lorentz detuning (open loop) . . . . .	58
5.3	Power phasor diagram for open loop system . . . . .	59
5.4	Cavity voltage magnitude and phase in the absence of Lorentz detuning (closed loop) . . . . .	61
5.5	Cavity voltage magnitude detail . . . . .	62
5.6	Forward and reflected power in closed loop operation . . . . .	63
5.7	Feedback power added . . . . .	64
5.8	Power phasor diagram for closed loop system . . . . .	65
5.9	Resonant frequency shift due to Lorentz force cavity deformation . .	66
5.10	Cavity voltage magnitude and phase with Lorentz detuning (Open Loop) . . . . .	67
5.11	Cavity voltage magnitude and phase detail . . . . .	68
5.12	Forward and reflected power with Lorentz detuning . . . . .	69
5.13	Power phasor diagram for open loop system . . . . .	70
5.14	Cavity voltage magnitude and phase with Lorentz detuning (Open Loop) . . . . .	72
5.15	Cavity voltage magnitude and phase detail . . . . .	73
5.16	Forward and reflected power with Lorentz detuning . . . . .	74
5.17	Feedback power added . . . . .	75
5.18	Power phasor diagram for open loop system . . . . .	76
5.19	Effect of beam current variation on feedback power (matched operation)	77
5.20	Low-power operation of SPL (power considerations) . . . . .	78
5.21	Effect of beam current variation on feedback loop power consumption (mismatched operation) . . . . .	79
5.22	Cavity voltage magnitude and phase of vector sum output, feedback loop is ON . . . . .	81
5.23	Cavity voltage magnitude and phase for cavity 1 . . . . .	82
5.24	Cavity voltage magnitude and phase for cavity 2 . . . . .	83
5.25	Cavity phase for cavities controlled by a single loop, feed-forward correction is applied . . . . .	84
5.26	Effect of 20k (1.5%) difference between loaded quality factors of resonant cavities . . . . .	85
5.27	Effect of 30k (2.2%) difference between loaded quality factors of resonant cavities . . . . .	86
5.28	Curve fit for cavity voltage difference with varying loaded quality factor	89
5.29	Curve fit for cavity voltage magnitude difference with varying Lorentz force detuning . . . . .	89
5.30	Curve fit for cavity voltage phase difference with varying Lorentz force detuning . . . . .	90
5.31	Open plot of open-loop system, gain margin of about 43 dBs . . . . .	92

# Chapter 1

## Introduction

In conjunction with the restart of the Large Hadron Collider at CERN, studies on a luminosity upgrade for the machine started in April of 2008. The project, sLHC-PP, is aimed at gradually increasing the luminosity to reach levels up to ten times the original design specifications of the LHC, providing a smooth transition onto a higher discovery potential of the synchrotron [G<sup>+</sup>10]. In order to achieve these goals, technical improvements need to be deployed on several areas of the CERN complex, including new focusing magnets in LHC at the experiment regions. CMS and ATLAS, as general purpose detectors, will need to be prepared to record higher luminosity collisions, and finally, the LHC supplier chain will be updated. Construction has started on LINAC4 to cater for this need. The whole project has been divided into eight areas of interest referred to as Work Packages. WP1, 2, 3 and 4 are concerned with project management and the coordination of accelerator and detector upgrades. WP5 is investigating protection and safety issues related to the increased radiation due to higher luminosity, WP6 has been charged with developing the new focusing quadrupole magnets for the interaction areas of the LHC ring, WP7 is in charge of developing critical components for the injectors such as accelerating cavities and a hadron source, and finally, WP8 will develop the technology necessary for tracking detectors from the power distribution point of view. Within the scope of work package 7, Low-Level Radio Frequency (LLRF) simulations for a new generation of pulsed electric field superconducting LINAC have been commissioned. The idea is to provide a general idea of the possible setbacks that may arise during construction and their solutions. This report is a detailed description of the field stabilisation solutions when dealing with one or more superconducting cavities driven by a single pulsed klystron from the RF point of view.

# Chapter 2

## RF Cavity Theory

Particle physics arose only a few decades ago following the creation of a device capable of reaching far into the nucleus of an atom, and detectors equipped to observe matter constituting the building blocks of atoms. Particle accelerators have redefined particle physics and as they become increasingly more powerful, we are able to penetrate deeper into the standard model. The idea is to accelerate particles to imbue them with energies capable of separating matter, and then make them crash against each other in an infinitely precise point to observe with gigantic detectors what comes out of their collision. In order to achieve this, we insert particles into a vacuum tube, using magnets to ensure they stay within the vacuum, and accelerate them using electric fields contained within resonant cavities along the tube. From the point of view of RF power, we are interested in observing the effects of a time-varying electric field on a beam of particles travelling through a resonant cavity powered by a valve amplifier generator (Klystron). With this information, we can design the RF control system for a linear accelerator to suit a particular application.

### 2.1 Cavity Equivalent Circuit

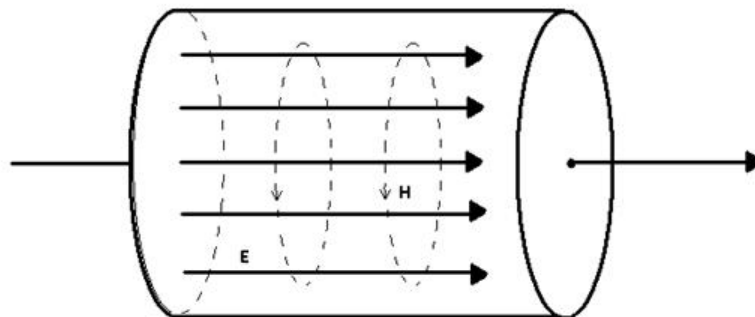


Figure 2.1: Pillbox cavity [Le 00]

Resonant modes of electromagnetic (EM) waves in cavities can be described by



resonant R-C-L circuits. For the simplest case, we limit ourselves to the analysis of a single resonant cavity, which can be closely modelled via a pillbox with perfect electric conducting walls (a circular waveguide with closed ends). In an ideal case, only a finite number of propagating modes, corresponding to a finite number of frequencies will propagate within the pillbox, in the presence of losses, however, cavity modes no longer have a sharp delta function at particular frequencies, but a narrowband peak appears instead. A measure of the sharpness of this peak observed after an external excitation is the quality factor (Q) of that particular mode.

Q is defined as the ratio of time-averaged energy W stored in the cavity to the energy loss per cycle.

$Q_0 = \frac{\omega W}{P_d}$  where  $P_d$  is the dissipated power in the cavity.

Ignoring the effects of losses due to vacuum impurities and surface irregularities (drift tubes) we calculate Q by integrating the power loss of wall currents over the cavity surface and the stored energy over the volume of the cavity

$$P_d = \int_{\delta V} P'_d dA = \frac{1}{2} \int_{\delta V} \sqrt{\frac{\omega \mu}{2\kappa}} |H_{tan}|^2 dA \quad (2.1)$$

$$W = \int_V w dV = \frac{1}{2} \int_V \left( \frac{\epsilon}{2} |\vec{E}|^2 + \frac{\mu}{2} |\vec{H}|^2 \right) dV = \frac{\epsilon}{2} \int_V |\vec{E}|^2 dV \quad (2.2)$$

where  $P'_d$  is the energy loss in the cavity walls per unit area due to surface currents,  $w$  is stored energy within the cavity, and  $\kappa$  is the conductivity of the material [WKS+00]. The Q factor as defined above is one of the main characteristics of an accelerator cavity, and together with the resonant frequency and shunt impedance, it is possible to describe the cavity completely from an electrodynamics point of view. The resonant frequency of a cavity depends mainly on its shape and it is thus too complex to calculate analytically for all but the simplest of shapes, thus it is found by numerical or experimental methods and usually quoted by designer or manufacturer. The shunt impedance of an accelerating cavity relates the voltage between two points in the cavity over (e.g. between drift tubes) to the power dissipated in the cavity walls:

$$R_{sh} = \frac{U^2}{2P_d} (circuit) \quad (2.3)$$

For LINAC purposes, the shunt impedance definition is multiplied by a factor of two; therefore it is important when defining a shunt impedance to specify the convention applied. To calculate the shunt impedance, in any case we find the voltage between two points  $U = |\int_{z_1}^{z_2} \underline{E}_z(z)|$ .

This definition does not take into account the passage of a beam of charged particles and its effect on the cavity voltage and is related to the effective shunt impedance by  $R_{sh,eff} = R_{sh} T^2$ , where the transit-time factor  $T$  is given by

$$T = \frac{|\int_{z_1}^{z_2} \underline{E}_z(z) e^{ik_z z} dz|}{|\int_{z_1}^{z_2} \underline{E}_z(z) dz|} \quad (2.4)$$

$R_{sh}$  is useful to define the characteristic impedance of a resonant cavity, which is defined as

$$\frac{R_{sh}}{Q} = \frac{1}{2\omega W} \left( \int_{z_1}^{z_2} |E_z(z)|^2 dz \right) \quad (2.5)$$

This is a very useful quantity as it depends only on the geometry of the cavity. Going back to our R-C-L circuit, we know that when a cavity resonates on a given mode, the time-averaged energy stored in the electric field equals that in the magnetic field. Within an RF period, the energy oscillates between magnetic and electric field as is the case with an L-C pair. R was defined before and it models the effective shunt impedance due to energy dissipation of the cavity walls [Le 00].

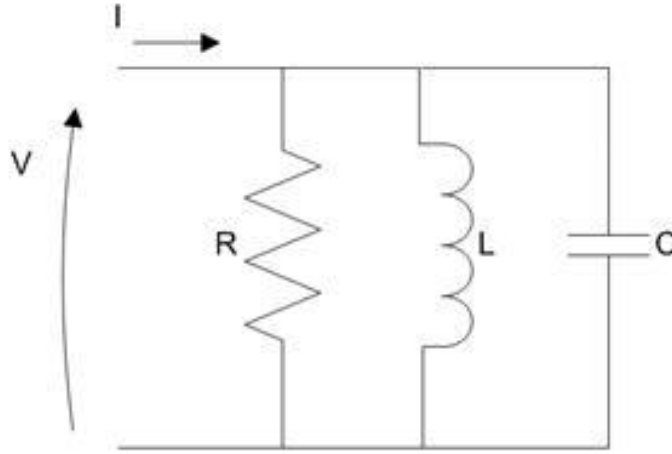


Figure 2.2: Cavity equivalent circuit

If we therefore think of the capacitance as the effect of the electric field on the cavity and the inductance as related to the magnetic field, we find that the average stored energy in the electric and magnetic fields respectively is given by

$$W_{sE} = \frac{1}{4}CV^2 \quad W_{sM} = \frac{1}{4}LI^2 \quad (2.6)$$

where

$$\frac{\varepsilon}{4} \int_V |E|^2 dV = \frac{\mu}{4} \int_V |H|^2 dV$$

At resonance, the total average energy stored is then the addition of both the magnetic and electric:

$$W_s = W_{sE} + W_{sM} = 2W_{sE} = \frac{1}{2}CV^2 \quad (2.7)$$

If we take the power dissipated by the equivalent shunt resistance, bearing in mind  $\omega_0 = \frac{1}{\sqrt{LC}}$  we find  $P_d = \frac{1}{2} \frac{V^2}{R}$  and therefore (CIRCUIT)  $Q_0 = \omega_0 RC$ .

Thus, with the knowledge of the quality factor, resonant frequency and the shunt impedance, it is possible to construct an equivalent circuit for the resonant cavity.

## 2.2 Coupling Between RF Generator, Cavity and Beam

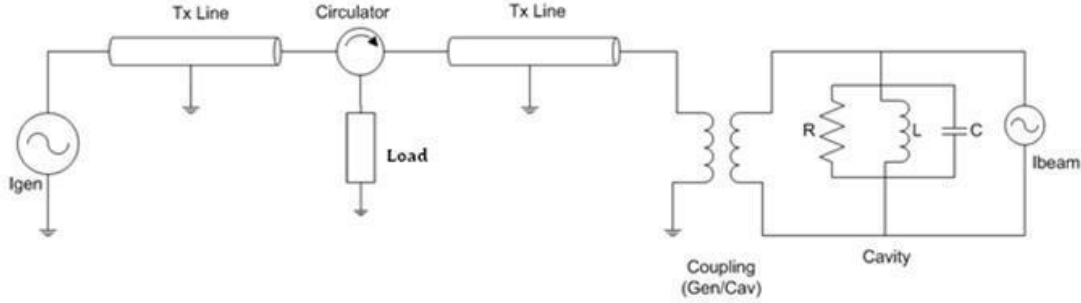


Figure 2.3: Cavity coupled to beam and generator [Sch98]

Until now, we have concentrated on the behaviour of a resonant cavity obtained from a closed pillbox with perfectly conducting walls. We are now interested in the effects on the cavity of coupling to a generator and the passage of beam. We will now observe how the generator transmission line affects the quality factor of the cavity and how beam passage will induce a drop in the cavity voltage. Thus we introduce the concept of the cavity to generator coupling factor

$$\beta_0 = \frac{Q_0}{Q_{ext}} \quad (2.8)$$

which gives rise to the loaded quality factor  $Q_L$

$$\frac{1}{Q_L} = \frac{1}{Q_0} + \frac{1}{Q_{ext}} \quad (2.9)$$

In superconducting cavities in particular, the loaded  $Q$  is virtually equal to the external  $Q$  as the unloaded  $Q$  is much greater than the external. This means the generator to cavity coupling will be of particular importance for the efficient performance of the system.

### 2.2.1 Steady-State Analysis

To start off, we assume steady-state voltages and currents. In figure 2.4, the beam is represented as a current source and the cavity, as previously shown, is equivalent to an L-C-R block, in this case coupled to a transmission line with complex impedance  $Z$ , with an incident current wave (towards the cavity)  $I_g$  and a reflected wave  $I_r$  [Tuc04].

The generator emits a wave with frequency  $\omega$ , which is not necessarily equal to the cavity resonant frequency  $\omega_0$ . We assume all variables are proportional to  $e^{i\omega t}$ . In the case of imperfect tuning, the frequency difference between the resonant frequency and the generator frequency can be described as a mismatch between the generator

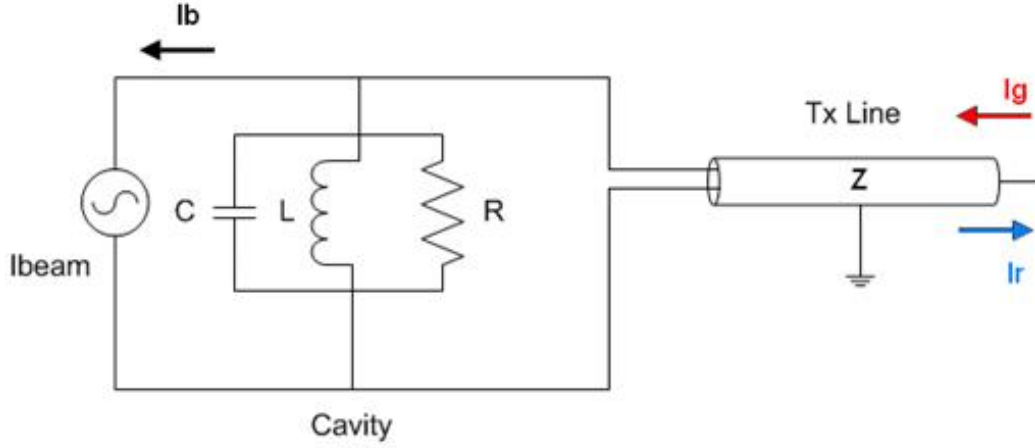


Figure 2.4: Steady-state cavity [Tuc04]

and the cavity angle in phasor terms. We can define the tuning angle between the generator current and cavity voltage as

$$\tan \Psi = 2Q_L \frac{\Delta\omega}{\omega}$$

for small  $\Delta\omega$ .

From transmission line theory, we know  $V = Z(I_g + I_r)$  and therefore  $I_r = \frac{V}{Z} - I_g$ .

From the circuit and the above equation, we get

$$I_{LCR} = I_g - I_r - I_{b,RF} = 2I_g - I_{b,RF} - \frac{V}{Z} \quad (2.10)$$

The current across the L-C-R block is also equal to the individual currents flowing through the passive components. So we can also say (j and i both refer to  $\sqrt{-1}$ )

$$I_{LCR} = I_C + I_L + I_R = V \left( \frac{1}{j\omega L} + j\omega C + \frac{1}{R} \right) \quad (2.11)$$

and equating both sides, we get

$$V \left( j\omega C \left( 1 - \frac{1}{\omega^2 LC} \right) + \frac{1}{R} + \frac{1}{Z} \right) = 2I_g - I_{b,RF} \quad (2.12)$$

If  $\Delta\omega = \omega_0 - \omega$  and  $\Delta\omega \ll \omega$  and , we can say that , and the equation becomes

$$V \left( -i2\Delta\omega C + \frac{1}{R} + \frac{1}{Z} \right) = 2I_g - I_{b,RF} \quad (2.13)$$

where  $\omega_0 = \frac{1}{\sqrt{LC}}$ .

Now we want to express this in cavity parameters. To find expressions for C, R and Z, we use the capacitor voltage-capacitance relation, and the effect of a charge travelling through a resonant cavity (note that all parameters are specified in their LINAC definition):

$$\Delta V = \frac{q}{C} = \frac{q\omega}{2} \left( \frac{R}{Q} \right) \text{ (LINAC)} \quad (2.14)$$

$$C = \frac{2}{\omega(R/Q)} \text{ (LINAC)} \quad (2.15)$$

Using this and the equivalent cavity values for the shunt impedance  $R$  and the external impedance  $Z$ :

$$R = \frac{Q_0}{2} \left( \frac{R}{Q} \right) \text{ (LINAC)} \quad (2.16)$$

$$Z = \frac{Q_{ext}}{2} \left( \frac{R}{Q} \right) \text{ (LINAC)} \quad (2.17)$$

we find the circuit equation using cavity values to be given by the following equation:

$$V \left( -i \frac{2\Delta\omega}{\omega(R/Q)} + \frac{1}{(R/Q)} \left( \frac{1}{Q_0} + \frac{1}{Q_{ext}} \right) \right) = I_g - \frac{1}{2} I_{b,RF} \quad (2.18)$$

The RF beam current is a complex quantity, and as such can be expressed in terms of real and imaginary parts. For simplicity we can define the complex phase of all waves such that the cavity voltage  $V$  is always purely real (this is not the case for the model as shown later). Thus the cavity voltage is at the zero degree point in the complex plane. The synchronous angle  $\phi_s$  is the angle of the RF voltage when the beam arrives. With LINAC machines, as is the case with electron synchrotrons, we generally operate close to maximum power transmission. This means that the synchronous angle is defined from the peak value of the RF voltage, i.e  $\phi_{s, \text{LINAC}} = 0^\circ$ . when the cavity voltage and the beam pulse are in-phase, as opposed to the proton synchrotron case, in which the synchronous angle is taken with 90 degrees of difference. Using the LINAC convention:

$$I_{b,RF} = |I_{b,RF}| (\cos \phi_s - i \sin \phi_s) \quad (2.19)$$

The complex Fourier spectrum of a bunch train passing through the cavity is given by a frequency train which, in case of infinitely short bunches, has equal value for all frequencies  $f = (-\infty, \infty)$ . The corresponding real spectrum has no negative lines and corresponding frequencies add up, except for the DC term. Hence, the RF terms are twice the DC term, in the case of infinitely short bunches.

Thus  $I_{b,RF} = 2I_{b,DC}$ , except for finite bunches, in which case the factor 2 will become lower for higher frequency components. To take this effect into account we add a relative bunch factor  $f_b$  that is normalised to 1 for infinitely short bunches, so

$$I_{b,RF} = 2I_{b,DC} f_b (\cos \phi_s - i \sin \phi_s) \quad (2.20)$$

Substituting back into the previous equation, we find complex expressions for the generator and the reflected powers:

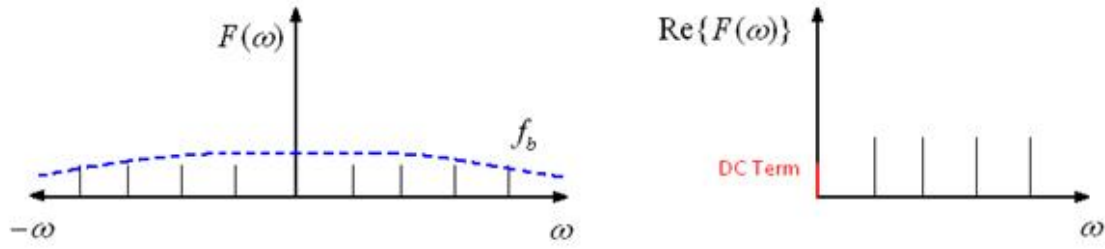


Figure 2.5: Fourier spectrum relation between RF and DC beam current

$$I_g = \left[ \frac{V}{(R/Q)Q_L} + I_{b,DC} f_b \cos \phi_{s, \text{LINAC}} \right] - i \left[ I_{b,DC} f_b \sin \phi_{s, \text{LINAC}} + V \frac{2\Delta\omega}{\omega(R/Q)} \right] \quad (2.21)$$

$$I_r = \left[ \frac{V}{(R/Q)} \left( \frac{1}{Q_{ext}} - \frac{1}{Q_0} \right) - I_{b,DC} f_b \cos \phi_{s, \text{LINAC}} \right] + i \left[ I_{b,DC} f_b \sin \phi_{s, \text{LINAC}} + V \frac{2\Delta\omega}{\omega(R/Q)} \right] \quad (2.22)$$

All equations above are defined using the LINAC convention for synchronous angle and R/Q. The LINAC definition for power, using peak values for current is

$$P_x = \frac{1}{4} R_{\text{LINAC}} |I_x|^2$$

and therefore

$$P_{g,r} = \frac{1}{4} (R/Q) Q_{ext} |I_{g,r}|^2 \quad (2.23)$$

We can also find optimum detuning and loaded quality factor for the superconducting LINAC case using

$$\frac{\Delta\omega_{opt}}{\omega} = \frac{-I_{b,DC} f_b \sin \phi_s (R/Q)}{2V} \quad (2.24)$$

$$Q_{L,opt} = Q_{ext,opt} = \frac{V}{(R/Q) I_{b,DC} f_b \cos \phi_s} \quad (2.25)$$

## 2.2.2 Transient Analysis

The superconducting proton LINAC will make use of pulsed generators, and so does the model developed for it. Hence, the scope of the project is not limited to steady-state analysis, and so it is that we now let go of our initial assumptions and plunge

into the realm of transient analysis. We begin again from the externally driven L-C-R circuit. This time we include the external load in the loaded impedance [Sch98].

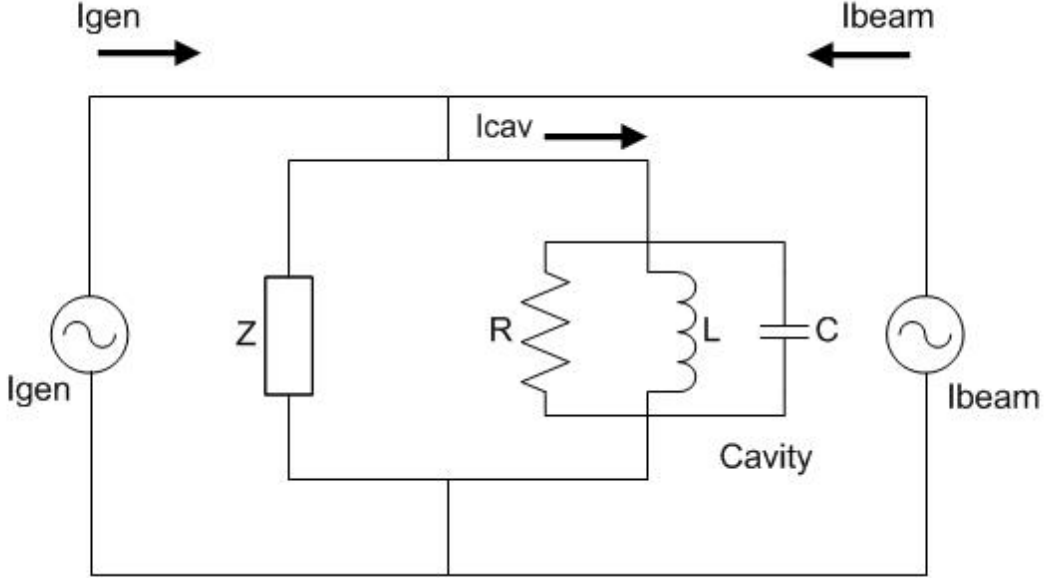


Figure 2.6: Cavity-beam interaction [Sch98]

$$R_L = R || Z_{ext} \quad (2.26)$$

Applying Kirchhoffs current rule

$$I_{cav} = I_{R_L} + I_C + I_L$$

and the formulas

$$\dot{I}_L = V/L \quad \dot{I}_R = 2\dot{V}/R_L \quad \dot{I}_C = C\ddot{V}$$

and translating into cavity values

$$\frac{1}{R_L C} = \frac{\omega_0}{Q_L} \quad \frac{1}{L C} = \omega_0^2$$

we find

$$\ddot{V}(t) + \frac{1}{R_L C} \dot{V}(t) + \frac{1}{L C} V(t) = \frac{1}{C} \dot{I}(t) \quad (2.27)$$

$$\ddot{V}(t) + \frac{\omega_0}{Q_L} \dot{V}(t) + \omega_0^2 V(t) = \frac{\omega_0 R_L}{Q_L} \dot{I}(t) \quad (2.28)$$

The driving current  $I_g$  and the Fourier component of the pulsed beam  $I_{b,RF}$  are harmonic with  $e^{i\omega t}$ . We now separate fast RF oscillation from the slowly changing amplitudes and phases of real and imaginary (I/Q) components of the field vector:

$$\begin{aligned}
V(t) &= (V_r(t) + iV_i(t))e^{i\omega t} \\
I(t) &= (I_r(t) + iI_i(t))e^{i\omega t}
\end{aligned}
\tag{2.29}$$

We insert this into the differential equation 2.28 and we end with the result

$$\begin{aligned}
\dot{V}_{RE} + \omega_{1/2}V_{RE} + \Delta\omega V_{IM} &= R_L\omega_{1/2}I_{RE} \\
\dot{V}_{IM} + \omega_{1/2}V_{IM} - \Delta\omega V_{RE} &= R_L\omega_{1/2}I_{IM}
\end{aligned}
\tag{2.30}$$

Where  $\omega_{1/2} = \frac{\omega_0}{2Q_L}$  is the half bandwidth of the cavity. The driving current in steady-state is given by  $I = 2I_g + I_{b,RF}$ . In the case of on-crest acceleration (zero synchronous angle) for a train of infinitely short bunches passing through a cavity on resonance, we can approximate the resonant frequency component of the beam current to twice its DC value  $I = 2(I_g - I_{b,DC})$ , bearing in mind the 180 phase shift of the beam. Filling a cavity with constant power results in an exponential increase of the cavity voltage

$$V_g = R_L I_g \left(1 - e^{-\frac{t}{\tau}}\right)$$

, where  $V_g$  represents the generator-induced cavity voltage and the LINAC convention is taken for the loaded impedance. Similarly, a beam current injected at time  $t_{inj}$  results in an opposite voltage gradient within the cavity

$$V_b = -R_L I_{b,DC} \left(1 - e^{-\frac{1}{\tau}(t-t_{inj})}\right)$$

where  $V_b$  represents the beam-induced cavity voltage and  $\tau = \frac{1}{\omega_{1/2}} = \frac{2Q_L}{\omega_0}$  is the filling constant of the cavity.

The total cavity voltage is a superposition of the beam-induced and generator-induced voltages.

$$V_{cav}(t) = R_L I_g \left(1 - e^{-\frac{t}{\tau}}\right) \quad \text{for } t < t_{inj} \tag{2.31}$$

$$V_{cav}(t) = R_L I_g \left(1 - e^{-\frac{t}{\tau}}\right) - R_L I_g \left(1 - e^{-\frac{-(t-t_{inj})}{\tau}}\right) \quad \text{for } t_{inj} < t < t_{OFF} \tag{2.32}$$

In the case of superconducting cavities, the generator power is almost entirely transferred to the beam. The injection time can then be chosen to arrive at an immediate steady-state condition. In other words, if we time the beam in such a way that the positive voltage gradient induced by the generator is equal to the negative voltage gradient induced by the beam on the cavity, the cavity voltage will remain constant during beam loading. This can be achieved, for optimal matching and  $I_g = \alpha I_{b,DC}$ , when the cavity field has reached  $1 - \frac{1}{\alpha}$  of its maximum:

$$t_{inj} = \ln \alpha \times \tau \tag{2.33}$$



$$\begin{aligned}
V_{cav}(t) &= R_L I_g \left(1 - e^{-\frac{t}{\tau}}\right) - R_L I_{b,DC} \left(1 - \alpha e^{-\frac{t}{\tau}}\right) \\
V_{cav}(t) &= R_L I_g \left(1 - e^{-\frac{t}{\tau}}\right) - \frac{R_L I_g}{\alpha} \left(1 - \alpha e^{-\frac{t}{\tau}}\right)
\end{aligned} \tag{2.34}$$

$V_{cav} = V_{max} \left(1 - \frac{1}{\alpha}\right)$ , where  $V_{max} = R_L I_g$  (LINAC)

Figure 2.7 shows the effect on the cavity voltage of an infinitely short bunch train, with an average current  $I_{b,DC}$  passing through a cavity at the right injection time  $t_{inj}$  such that the generator-induced gradient is cancelled by that induced by the beam.

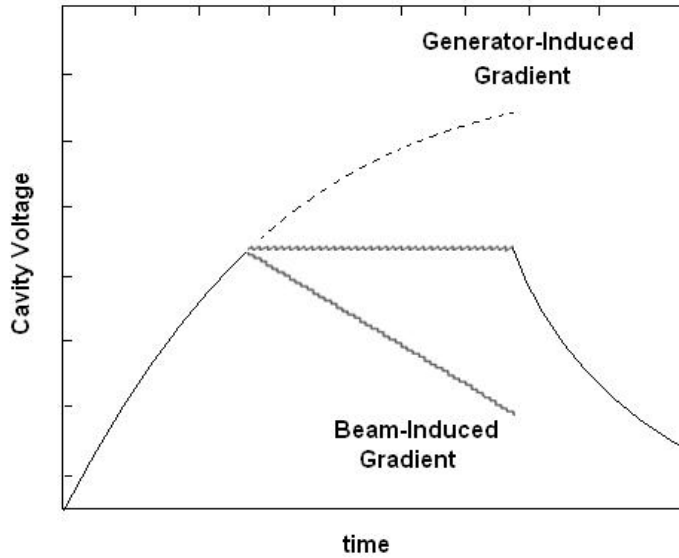


Figure 2.7: Cavity voltage gradients induced by generator and beam

Each infinitely short bunch is seen as an instant drop in the cavity voltage, while the generator-induced voltage has a continuous effect on the cavity. When both the beam and generator are OFF, the cavity voltage decays exponentially.

It is important to note that the above description is somewhat different in the case of out of phase beam loading. It is important to bear in mind that when the beam arrives with a certain synchronous angle, the beam current is expressed by

$$I_{b,RF} = |I_{b,RF}|(\cos \phi_s - i \sin \phi_s) \tag{2.35}$$

and similarly, the generator current is given by

$$\begin{aligned}
I_g &= \left[ \frac{V}{(R/Q)Q_L} + I_{b,DC} f_b \cos \phi_{s, \text{LINAC}} \right] \\
&- i \left[ I_{b,DC} f_b \sin \phi_{s, \text{LINAC}} + V \frac{2\Delta\omega}{\omega(R/Q)} \right]
\end{aligned} \tag{2.36}$$

This means that the relationship between  $I_g$  and  $I_b$  becomes

$$\underline{I}_g = \underline{\alpha} \underline{I}_{b,DC}$$

where the underlining represents complex quantities. This means that the injection time would have to be complex in order to obtain flat-top operation, which is, of course, physically impossible. In practice this means that the cavity voltage flat-top operation can be optimised with respect to the real part by means of optimal coupling and with respect to the imaginary part by detuning the cavity. For the purpose of our analysis, the focus is on the real part and thus the effects of flat-top drift during beam loading due to reactive effects are in practice curbed by a fast feedback loop in both magnitude and phase, though other methods like pre-detuning or half-detuning have proven successful in the past.

## 2.3 Beam loading Theorem

Until now, the passage of the beam through a resonant cavity has been represented by a DC current source pulled from the cavity. This is a good approximation and works well to observe the beam effect on the magnitude of the cavity voltage. In reality, however, beam loading consists on the effects of several single bunches (modelled with infinitely small width) accelerated by a resonant cavity. These bunches not only have an effect in the cavity voltage magnitude, but also its phase. When a beam is perfectly in-phase with the RF voltage in a tuned cavity, the cavity voltage will stay in tune during beam passage, while its amplitude decays, however, the transient effects of a detuned cavity and the beam synchronous angle remain to be discussed. As we will see during the course of this paper in both theory and practice, a beam that arrives at the cavity with a synchronous angle  $\phi_s$  will asymptotically pull the cavity voltage towards this angle (note that we use the LINAC definition for  $\phi_s$ ). Consider a point charge crossing an initially empty cavity. After it has passed, a beam voltage  $V_{bn}$  remains in each resonant mode (for simplicity we will consider the main mode only). What fraction of  $V_{bn}$  does the charge “see”? We will prove this to be  $\frac{1}{2}V_{bn}$ . This result is called the fundamental theorem of beam loading [Wil78]. The fundamental theorem of beam loading relates the energy loss by a charge crossing the cavity to the electromagnetic properties of resonant modes in the cavity computed in the absence of field. By superposition, the beam-induced voltage in a resonant cavity is the same whether or not there is a generator-induced voltage already present. We observe the effect of a charge passing through a cavity, being accelerated by generator-induced field present within said cavity. A single bunch passing through a cavity excites a field within it. Taking into account the fundamental resonant mode only, the excited field can be expressed as an exponentially decaying sine wave oscillating at the resonant frequency of the cavity  $\omega_0$ . In vector terms, the power delivered to the beam by the RF, taking into account the beam-induced cavity voltage is given by

$$P_{b,eff} = -(\vec{V}_g + \vec{V}_b) \bullet \vec{I}_{b,RF}$$

where the generator-induced voltage is not necessarily in-phase with the beam current component at the resonant frequency of the cavity.  $V_b$  represents the effec-

tive beam-induced voltage seen by the beam. To find this voltage, the cavity gap impedance (in transient mode) can be represented by a single capacitor

$$\frac{1}{C} = \frac{R_{sh}}{Q_0} \omega_0$$

and so the bunch-induced voltage in the cavity is given by

$$V_{bunch} = \frac{q_b}{C} = \frac{q_b}{2} \times \left( \frac{R}{Q} \right) (\text{LINAC}) \times \omega_0 \quad (2.37)$$

The energy lost by the bunch and stored in the cavity (Capacitor) is then

$$W = \frac{1}{2} C V_{bunch}^2 = \frac{1}{2} q_b V_{bunch} \quad (2.38)$$

The power received by the beam is then the vector sum of the generator-induced power and the beam self-induced power.

$$P_{b,eff} = -\vec{V}_g \bullet \vec{I}_{b,RF} - \frac{1}{2} \vec{I}_{b,RF} \bullet \vec{V}_{bunch} = -(\vec{V}_g + \frac{1}{2} \vec{V}_{bunch}) \bullet \vec{I}_{b,RF} \quad (2.39)$$

and so, returning to our original result for the power delivered to the beam, it is clear that

$$\vec{V}_b = \frac{1}{2} \vec{V}_{bunch} \quad (2.40)$$

The beam only “sees” half of its own induced voltage in the cavity [Bou86].

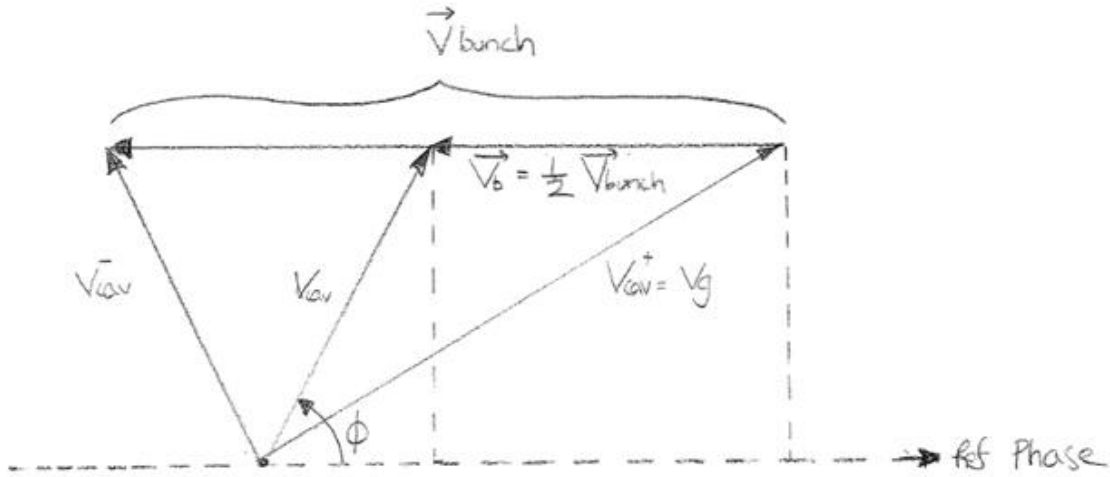


Figure 2.8: Effect of single bunch passage on cavity voltage [Wil78]

Now we are interested in computing the transient variation of the cavity voltage due to the passing of a periodic bunch train (with infinitely small bunches). Consider first an undriven cavity with resonant frequency  $\omega_0$  and a filling time constant  $\tau$ . Suppose the cavity is initially charged to  $V_{cav}(0)$ , and this voltage then decays exponentially with the filling constant, while rotating at the RF frequency  $\omega$ , which

is not necessarily the resonant frequency, i.e. the reference frame for the phasor diagram is chosen as the RF driving frequency.

The time variation in magnitude and phase of the cavity voltage is given by

$$V_{cav}(t) = V_{cav}(0)e^{-\frac{t}{\tau}}e^{jt\Delta\omega}$$

where  $\Delta\omega = \omega_0 - \omega$ , and the tuning angle is the angle between the generator current and the cavity voltage and related to the frequency detuning by

$$\tan \Psi = \tau\Delta\omega$$

These equations, in essence, explain that the RF field within an undriven cavity with a resonant frequency that differs from the RF frequency will rotate in phase as it decays exponentially. Furthermore, the rotation in time will be proportional to the frequency detuning (between RF and resonant frequencies). This effect is shown in figure 2.9.

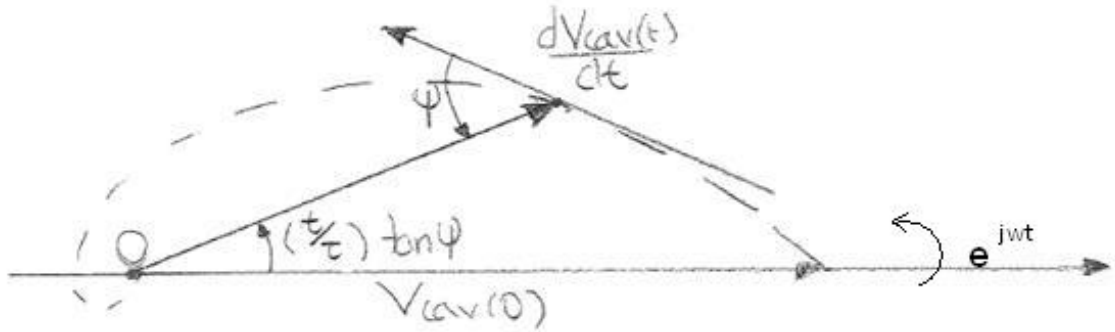


Figure 2.9: Voltage decay in detuned cavity [Wil78]

If we now include the effect of several bunches and the generator voltage, note that the zero degree phase is set as the positive direction of the bunch-induced voltage, we observe the effect of both the frequency detuning and the synchronous angle. If the cavity voltage starts in-phase with the generator voltage, we can see how each bunch passage pulls the cavity voltage towards the synchronous angle (shown in figure 2.11 with the zero phase angle set for the generator current). The spiral path in the figure 2.10 shows the cavity voltage driven by the generator. The cavity voltage tends asymptotically towards the generator voltage, but the beam passage opposes this effect, creating flat-top operation if timed right. The path is not straight, as shown in figure 2.9 due to the mismatch between cavity resonant frequency and RF generator frequency. Interestingly enough, the synchronous angle and the tuning angle can be such that their combined effects are somewhat cancelled, depending on the magnitude of the bunch-induced voltage in the cavity and the frequency of bunch passage in regards to the generator-induced voltage and the filling time constant of the cavity. In the case above, the time between bunch passages is such that  $V_c(t)$  returns to  $V_c^-$  after each bunch passage. If the tuning angle is zero, and

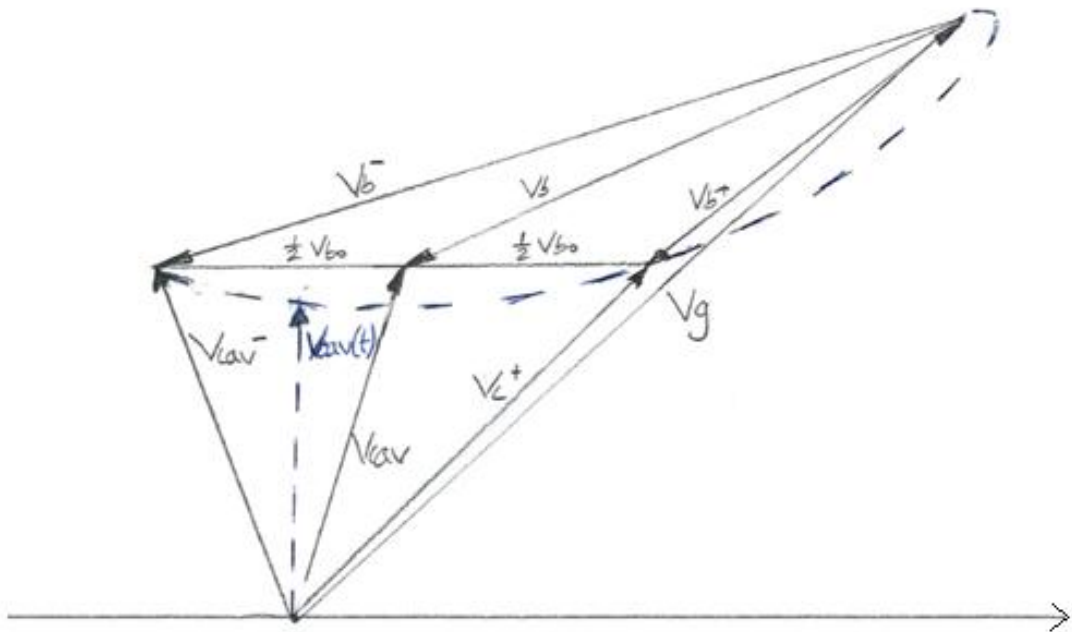


Figure 2.10: Overall effect of beam loading on detuned cavity [Wil78]

the injection time is such that the magnitude of the beam-induced cavity voltage is equal to that of the generator-induced voltage, the phase change of the total cavity voltage will be driven by the beam current, as we will observe in the results section.

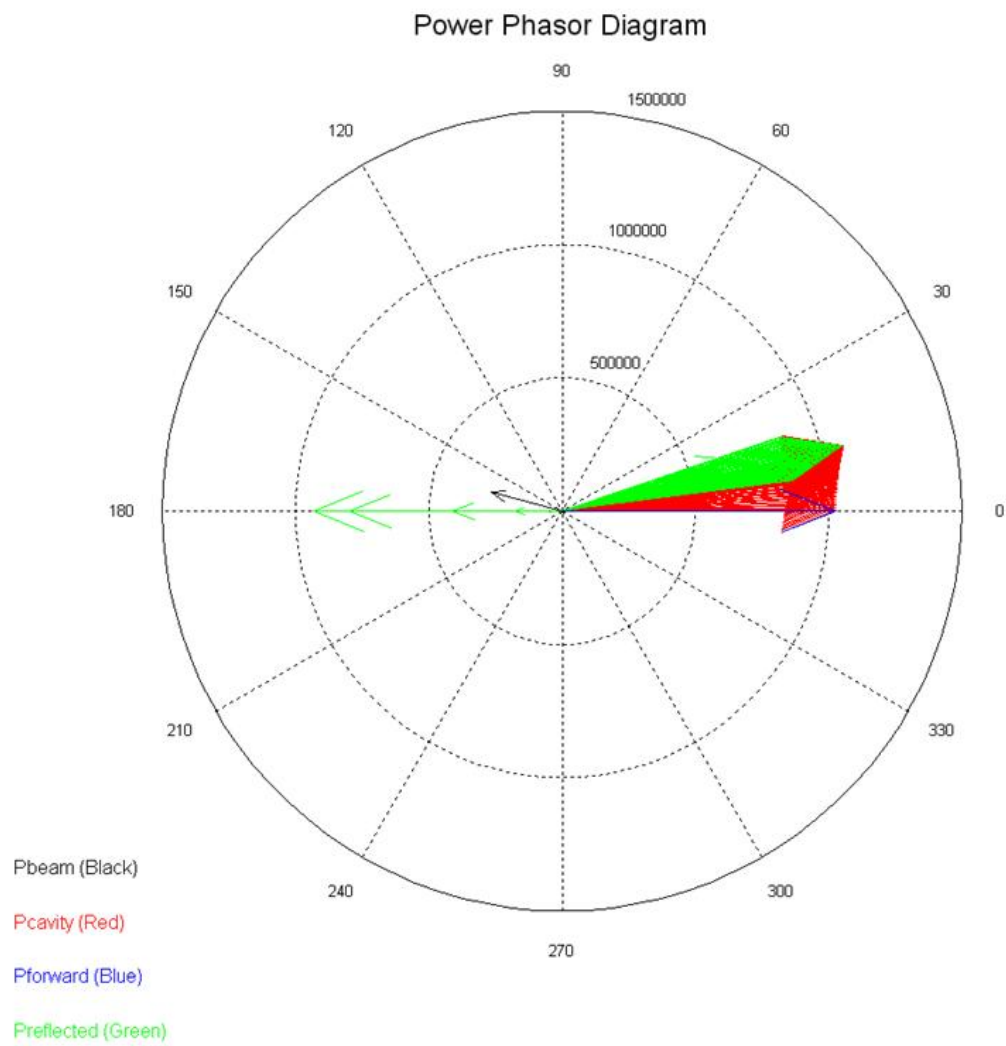


Figure 2.11: Generator-beam power interaction in tuned cavity

# Chapter 3

## RF Control of a 5-Cell 704.4 MHz Resonant Cavity

### 3.1 SPL Parameters and Power Considerations

LINAC4 and the SPL are being developed as a possible generic solution to many of CERNs needs in terms of high-power beam experiments. Perhaps one of the most important features of the SPL, in order to meet these needs, is its flexibility. The SPL is planned to accelerate  $H^-$  ions firstly for the purpose of injecting to the LHC supplier chain, that will include an upgrade to the proton synchrotron and the proton-synchrotron booster referred to as PS2. The second goal of the SPL is to create a beam that is upgradeable to feed all of CERNs high power proton users or neutrino-production facilities. The SPL, as of now, is planned to accelerate a 40mA beam pulse lasting 0.4 ms with a repetition rate of 50 Hz at high current operation, and a 20 mA beam lasting 0.8 ms at low current. The beam bunches arrive with a frequency of 352.2 MHz from LINAC4. The couplers from the RF generator to the resonant cavity will be optimised for 40 mA, where a movable-coupler scheme has been dismissed after budget considerations to favour a slight increase in 20 mA operation power to compensate for the power reflection due to the transmission line mismatch.

The power per cavity value on figure 3.1 is an approximate number. In addition to these specifications, the beam is expected to travel with a 15 degree synchronous angle with respect to the cavity voltage (LINAC convention). This implies that not all of the power delivered to the cavities will be absorbed by the beam, even in the case of a matched coupler. This means the power will need to be raised above 1 MW. The 20 mA case has a similar result due to both coupling mismatch and synchronous angle. As of now, the proposed solution is of maintaining a 25 MV/m accelerating electric field, corresponding to a voltage of 26.6 MV within the cavity. In order to do this the injection time for 20/40 mA operation needs to be calculated as shown below. The total power needed for each scenario can then be specified to match the voltage required at the calculated injection time [Hof09].

### General linac parameters

Parameter	Unit	HP-SPL	LP-SPL	Timestamp
Energy	[GeV]	5	4	15 August 2007
Beam power	[MW]	>4.0	0.192	31 March 2008
Repetition rate	[Hz]	50	2	15 August 2007
Average pulse current	[mA]	20/40	0-20	28 November 2008
Peak pulse current	[mA]	32/64	32	15 August 2007
Source current	[mA]	40/80	40	21 April 2008
Chopping ratio	[%]	62	62	21 November 2008
Beam pulse length	[ms]	0.4 <sup>(1)</sup> - 0.8 <sup>(2)</sup>	0.9	2010-04-13
Number of klystrons (704 MHz, 5 MW)	tbd	tbd	tbd	15 August 2007
Geometric cavity beta		0.65/1.0	0.65/1.0	24 April 2009
Number of cavities		60/184	60/144	2009-10-06
Additional cavities for debunching		0/16	0/16	2009-10-06
Cavities/klystron	tbd	tbd	tbd	22 April 2008
Cavities/cryostat		3/8	3/8	2010-05-04
Max. power/cavity	[MW]	1	0.5	21 April 2008
Length <sup>(3)</sup>	[m]	525	450	2009-11-09

(1) high-current operation

(2) low-current operation

(3) excluding Linac4, including 16 debuncher cavities at linac end, including extraction to ISOLDE and EURISOL

Figure 3.1: General SPL parameters [Ger07]

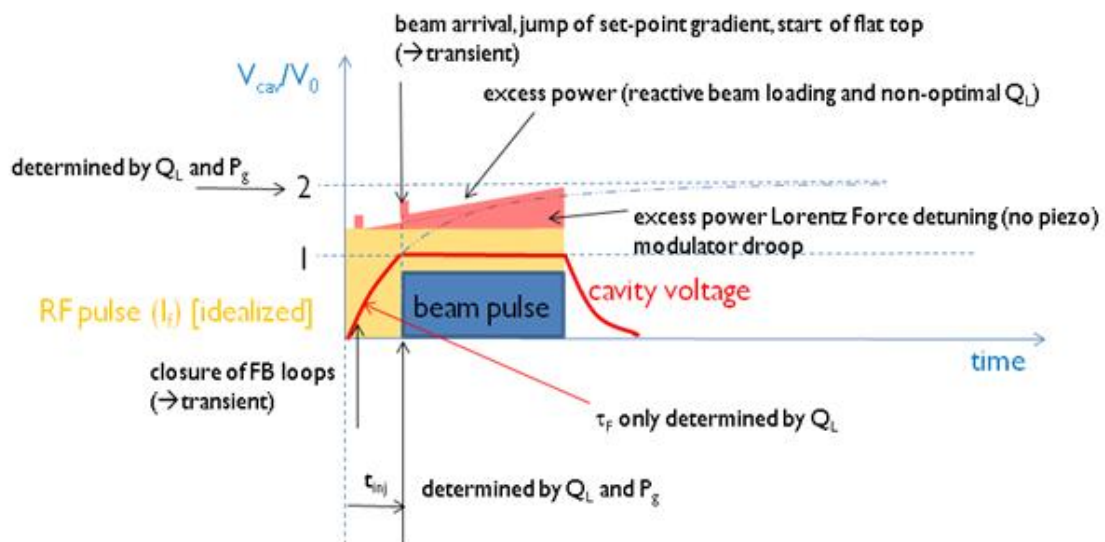


Figure 3.2: Transient power distribution [Hof09]



For 40 mA operation, the following parameters apply:

$$f_{RF} = 704.4 \text{ MHz}$$

$$I_{b,DC} \simeq 40 \text{ mA}$$

$$\phi_s = 15^\circ \text{ (LINAC)}$$

$$E_{acc} = 25 \text{ MV/m}$$

$$\text{length}_{cav} = \beta \times \frac{\lambda_{RF}}{2} \times 5 \text{ (5 cell, } \pi \text{ mode)} = 1.064 \text{ m}$$

$$V_{acc} = E_{acc} \times \text{length}_{cav} = 26.6 \text{ MV}$$

$$P_b = V_{acc} \times I_{b,DC} \times \cos \phi_s = 1.0285 \text{ MW}$$

$$\frac{R}{Q} = 525 \Omega \text{ (LINAC)}$$

$$Q_L = \frac{V_{acc}}{\frac{R}{Q} \times I_{b,DC} \times \cos \phi_s} = 1.3113 \times 10^6$$

$$R_L = Q_L \frac{R}{Q} = 688 \text{ M}\Omega \text{ (LINAC)}$$

$$I_g = \frac{V_{acc}}{R_L} + I_{b,DC} \cos \phi_s = 77.3 \text{ mA}$$

$$\alpha = \frac{I_g}{I_{b,DC} \cos \phi_s} = 2$$

$$\tau_{fill} = \frac{2Q_L}{\omega_{RF}} = 0.5926 \text{ ms}$$

$$t_{inj} = \tau_{fill} \ln \alpha = 0.4108 \text{ ms}$$

$$t_{pulse} = 0.4 \text{ ms}$$

With a power consumption given by  $P_{fwd} = \frac{1}{4} R_L |I_g|^2 = 1.0286 \text{ MW}$ .

Now, if we recall the general equation for the generator current from the steady-state analysis of the theory, we find

$$I_g = \left[ \frac{V}{(R/Q)Q_L} + I_{b,DC} f_b \cos \phi_{s, \text{LINAC}} \right] - i \left[ I_{b,DC} f_b \sin \phi_{s, \text{LINAC}} + V \frac{2\Delta\omega}{\omega(R/Q)} \right] \quad (3.1)$$

It is thus possible to compensate for reactive beam loading

$$P_{reactive\_BL} = \frac{1}{4} |I_b \sin \phi_s|^2 \quad (3.2)$$

This value can be added on the power budget or corrected by detuning the cavity as we can see from the equation above, otherwise the feedback loop will have to compensate for its effects. In these cases, it is also possible to use a half-detuning method, which means the cavity is detuned in between the optimum tuning for filling and beam loading. This will result in compensation being necessary during both filling and beam loading, but at a lower power level.

For the 20 mA case, the same reasoning applies. For the matched case, power consumption is halved while the optimum loaded quality factor and injection and filling times double. This would imply, however, that the loaded quality factor needs to vary between 40 mA and 20 mA operation, which involves using variable coupling between generator and resonant cavity. In practice, this is bulky and very expensive. It is more viable to slightly increase the generator power requirements during mismatched operation. So, if the loaded quality factor is matched for 40 mA operation, the operating values are as follows:

$$I_{b,DC} \simeq 20 \text{ mA}$$

$$P_b = V_{acc} \times I_{b,DC} \times \cos \phi_s = 514 \text{ kW}$$

$$Q_L = 1.3113 \times 10^6$$

$$I_g = \frac{V_{acc}}{R_L} + I_{b,DC} \cos \phi_s = 58 \text{ mA}$$

$$\alpha = \frac{I_g}{I_{b,DC} \cos \phi_s} = 3$$

$$\tau_{fill} = \frac{2Q_L}{\omega_{RF}} = 0.5926 \text{ ms}$$

$$t_{inj} = \tau_{fill} \ln \alpha = 0.6510 \text{ ms}$$

$$I_{ref} = \frac{V_{acc}}{\frac{R}{Q} Q_{ext}} - I_{b,DC} \cos \phi_s = 19.3 \text{ kW}$$

$$P_{ref} = \frac{1}{4} R_L |I_{ref}|^2 = 64 \text{ kW}$$

If we now compare the power requirements with matched operation, for one cavity with 40 mA beam and for two cavities with 20 mA beam respectively, the powers are

$$P_{40 \text{ mA}} = 1.029 \text{ MW}$$

$$P_{2 \times 20 \text{ mA}} = 1.156 \text{ MW}$$

This entails a 12.3% power increase for the mismatched case.

## 3.2 Sources of Perturbation

Due to injection tolerances and stability requirements for the SPL injection onto the LHC supplier chain and other high-energy proton users at CERN, the cavity voltage magnitude and phase have been specified to very accurate values. According

to SPL specifications, the voltage magnitude deviation must be below 0.5% of the total value and its phase deviation must not exceed 0.5 degrees. This is clearly a challenge as the constraints are quite restrictive. It is therefore important to anticipate and analyze the main possible sources of perturbation and their effects on the overall performance of the system. In this way, two main error causes have been identified; namely Microphonics and Lorentz Force Detuning. Superconducting cavities are made of a thin niobium wall and are therefore subject to mechanical deformations due to various external factors. One such factor is the pressure of the liquid helium bath. Other factors can include structural resonances or even external factors such as outside temperature or ground movement. The overall effect is not easily modelled due to the many possible environmental factors that cause cavity deformations. The effects of this deformation due to liquid helium bath pressure are usually referred to as microphonics [LP07]. The detuning may be mathematically described as a sum of slowly modulated harmonic oscillations:

$$\Delta\omega_\mu(t) = \sum_i^N \Delta\bar{\omega}_i(t) \sin(\omega_i t + \phi_i) \quad (3.3)$$

Perhaps a more important source of frequency detuning arises when resonant cavities are filled with very high fields. When a resonant cavity, made of thin niobium is filled with a high-power electric field and its magnetic counterpart, the fields exert a pressure on the cavity walls that can result in mechanic deformation. This is known as Lorentz Force Detuning. In mathematical terms, the wall pressure due to electric and magnetic fields within the cavity is given by

$$P_{\vec{E},\vec{H}} = \frac{1}{4} \left( \mu_0 |\vec{H}|^2 + \varepsilon_0 |\vec{E}|^2 \right) \quad (3.4)$$

This gives rise to a change in volume, and thus a change in resonant frequency of the cavity given by

$$\frac{\omega_0 - \omega}{\omega_0} = \frac{\int_{\Delta V} \left( \varepsilon_0 |\vec{E}|^2 - \mu_0 |\vec{H}|^2 \right)}{\int_V \left( \varepsilon_0 |\vec{E}|^2 + \mu_0 |\vec{H}|^2 \right)} \quad (3.5)$$

the integral of the change in volume over the total volume [Sch98].

In the case of a pillbox-like cavity, the pressure is concentrated in regions with high field. In this way, the electric field close to the irises (drift tubes) contracts the cavity, while the magnetic fields along the equator expand it. This results in a more disk-like cavity which results in a negative frequency change. Thus the frequency deviation is found to be proportional to the negative square of the accelerating field:  $\Delta f_0 = -K \times E_{acc}^2$ , where K is referred to as the Lorentz detuning factor in Hz/(MV/m)<sup>2</sup>. Since the electric field varies and the cavity walls have an inertial mass, Lorentz detuning has a transient variation that can be seen as low frequency damped oscillations with the cavity's mechanical resonant modes. If we now take into account the main mechanical mode, we arrive at a 1st order differential equation:

$$\tau_m \Delta \dot{\omega}(t) = -(\Delta \omega(t) - \Delta \omega_T) + 2\pi K \cdot E_{acc}^2(t) \quad (3.6)$$

This equation describes the time-variation of the frequency deviation with time.  $\tau_m$  is the mechanical damping time constant and  $\Delta \omega_T$  is a frequency shift due to an external mechanical excitation (such as a piezo-electric tuner).

### 3.3 Feedback and Feed-Forward Control

Until now, the sources of error have been identified and the need for a stable cavity voltage in terms of both magnitude and phase has been stressed. In order to effectively control a resonant cavity to meet the necessary specifications, it is necessary to predict errors using mathematical descriptions for the sources identified, and also develop an automated system that can deal with unforeseen variations. The most widely used control technique and one that applies to our necessities is that of negative feedback. The idea is to control a system's output by comparing it to a desired setpoint and feeding the error back to the input dynamically.

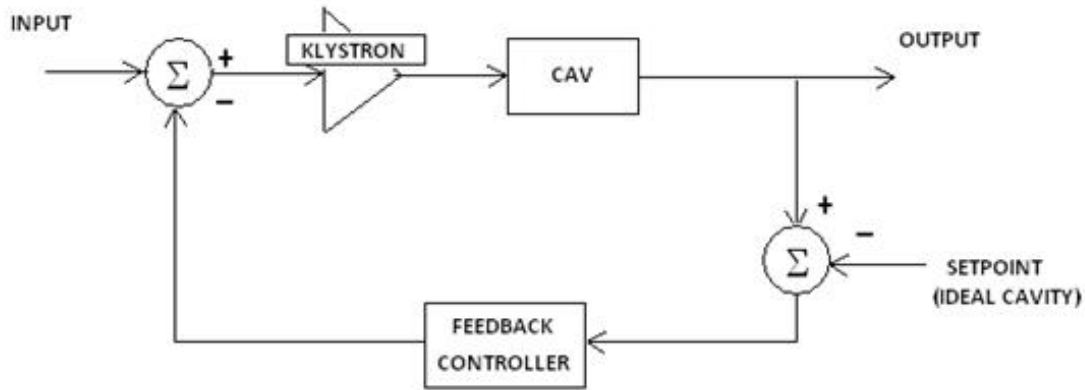


Figure 3.3: Negative feedback operation

The solution used in this particular implementation of the cavity control is done using I/Q components of the signal (refer to chapter 4). The advantage of this is that phase and magnitude can be controlled simultaneously using a setpoint in I/Q description. Common feedback controllers use mathematical information of the error signal  $e(t)$  to determine a signal to be fed to the system input. In the context of this report, PID feedback is of interest. PID feedback stands for Proportional-Integral-Derivative Feedback. This means that not only a fraction of the error signal is fed back to the input, but also of its derivative and integral. The proportional value determines a reaction to the current error, the integral value determines a reaction to the cumulative error, and the derivative term determines a reaction based on the rate at which the error is changing. Together, they form a very powerful means for controlling the output of a system [wik] [AM]:

$$\text{Out}_{FB} = K_p e(t) + K_i \int_0^t e(\tau) d\tau + K_d \frac{d}{dt} e(t) \quad (3.7)$$

A high proportional gain  $K_p$  results in a large change in the output for a given input change. If the proportional gain is too high, the system can become unstable. In contrast, too small a gain can result in poor control effort with respect to the output changes. Pure proportional control, furthermore, will not settle to the setpoint value, but it will retain a steady-state error that depends on the proportional gain and the system (cavity) gain. It is the proportional term that usually contributes the bulk of the control effort. The control contribution from the integral term is proportional to both the magnitude and the duration of the error. Summing the instantaneous error corrects the accumulated offset that results from pure proportional gain. The integral gain  $K_i$  accelerates the process towards the setpoint and eliminates the steady-state error. However, a high integral gain can cause the present value to overshoot responding to accumulated errors from the past. The rate of change of the system output error is calculated by determining its slope over time. The derivative terms effect is most noticeable close to the controller setpoint, as the rate of change varies the most. Derivative control is used to reduce the magnitude of integral overshoot and improve closed-loop stability. Too much differential gain  $K_d$ , however, can result in amplification of noise and instability. The overall effect on a step-change in the output can be observed in figure 3.4 [AM].

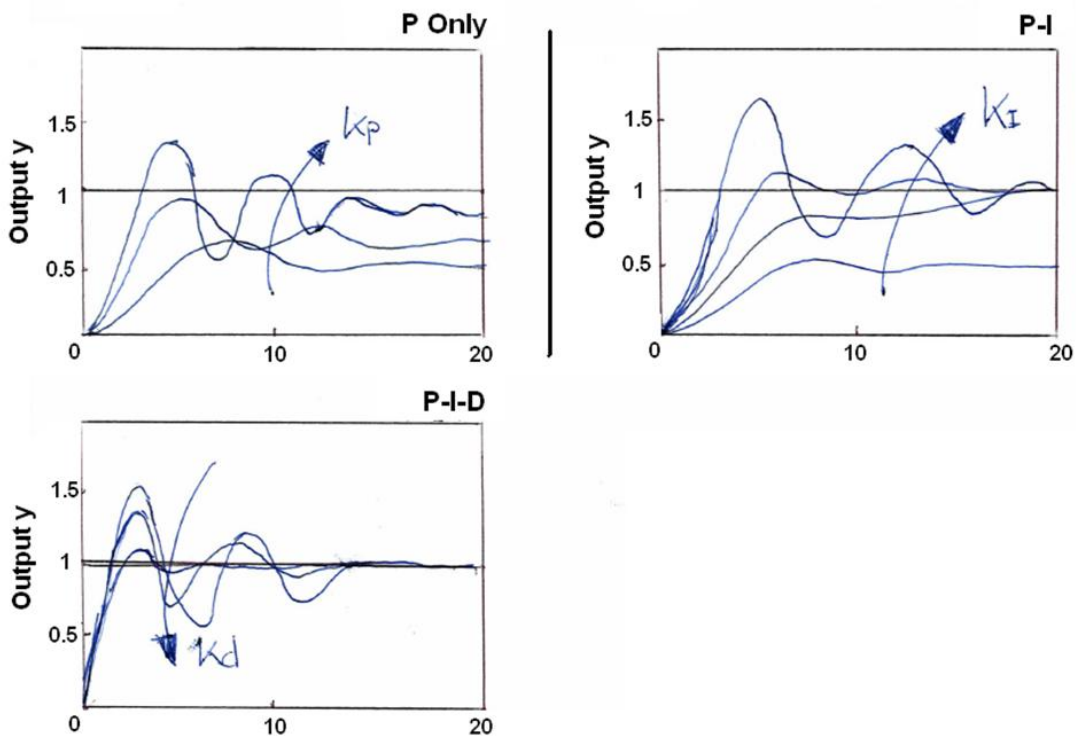


Figure 3.4: Effects of PID gain on output control performance [AM]

Feed-forward is the opposite of feedback, as you might suspect from its name. The idea is to prevent a foreseen error. To do this, the opposite effect is purposely fed to the system to counteract the known error at the time it arises. Combined feedback and feed-forward control can significantly improve performance over simple feedback

architectures when there is a major disturbance to the system that can be measured beforehand [Ore07].

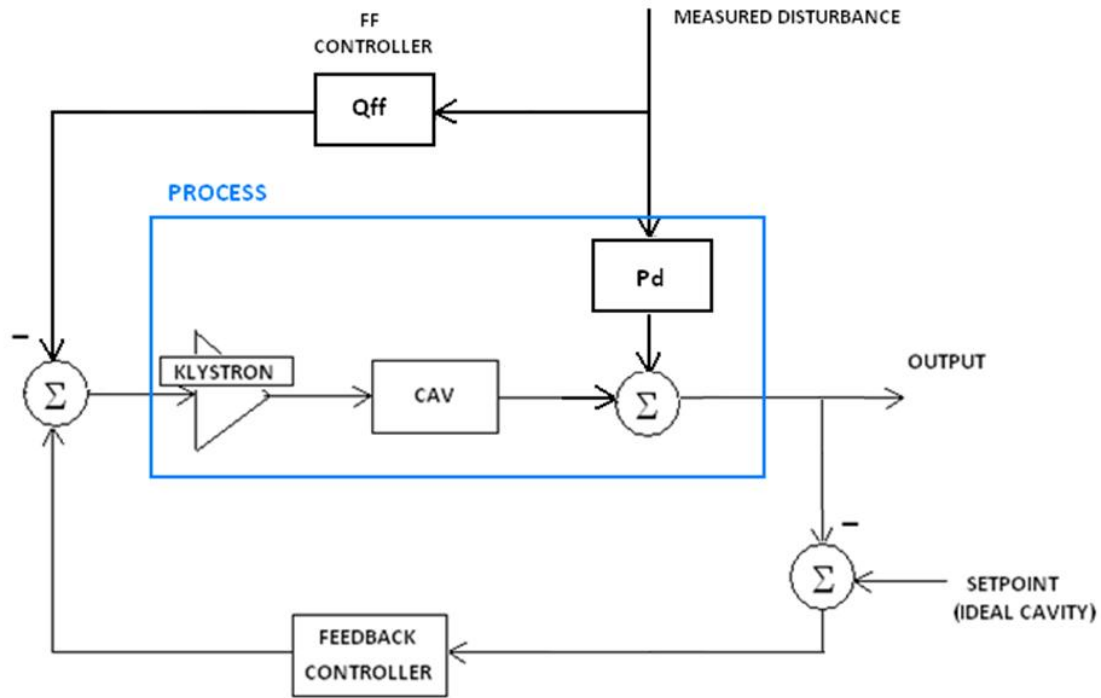


Figure 3.5: Feedback and feed-forward complementary control

To eliminate the effect of the measured disturbance, we need to choose  $Q_{ff}$  so that  $P_d - PQ_{ff} = 0$ , where  $P$  is the effect of the klystron and the cavity on the system. We can do this directly or by using an adaptive scheme. The idea in the context of SPL cavity control is to develop a model for a digital filter that uses ideal statistics to control the output. For this solution, the principles of Kalman filters are appealing.

### 3.4 Kalman Filtering

When the need arises for adaptive feed-forward, we need to develop a practically viable scheme to achieve the best possible efficiency and accuracy. The Kalman filter, in the presence of noisy measurements of a known system, is an ideal optimiser with respect to most criteria in advanced signal processing, and introduces almost no delay in the system as it implements a recursive algorithm. The Kalman filter finds the best possible fit out of a noisy measurement of a known system. This means we can estimate with the minimum possible error the real output of a system from which we have a noisy measurement. The idea is to characterise the system using previous knowledge of its dynamics and compare an estimate given from that model to a real (noisy) measurement taken from the real process. Provided we have an appropriate model for the estimating part of the filter and the statistical description of the system and measurement noises, we can fit the best estimate of the real output using our model, the noise corrupted measurement, and, of course, some very clever

mathematics. Now, it is possible to write whole books on the underlying processes of Kalman filtering and its applications, but we will concentrate on the applications that are relevant to our needs, namely adaptive feed-forward. The secret to Kalman filtering stems from the power of iteration; it is possible to asymptotically reach a best fit by perpetuating trials towards a given value, propagating the probability density function of the estimate, which narrows with each trial [Hof07]. The Kalman filter works with systems that fulfil the following assumptions:

1. Noise is white Gaussian.
2. System is linear.

It might seem like an overly restrictive set of assumptions, but in signal processing, the fact is this is usually the case. Linear systems are common for many real applications, and when a nonlinear system is more appropriate, the standard approach is to linearize about a certain point of interest. White noise has equal power across its whole frequency spectrum, which makes it of infinite power. However, bandpass characteristic of all real systems will limit the noise power, and even when the noise is not equal for all spectra, we can use a shaping filter to whiten the noise, adding the shaping filters characteristics to our system model within the Kalman filter. The Gaussian noise assumption can be defended using the central limit theorem. In many applications, measurement and process noise comes from a variety of sources, making their overall effect close to that of Gaussian noise. This means the mode, median and mean of the noise probability density function are all the same value and thus the Kalman algorithm optimises with respect to all three [May79a]. Consider a system governed by the linear stochastic differential equation

$$\dot{x}(t) = F(t)x(t) + B(t)u(t) + G(t)w(t) \quad (3.8)$$

from which we take a measurement at time  $t$

$$z(t) = H(t)x(t) + v(t) \quad (3.9)$$

With:

$x(t)$  = system state vector (output).

$u(t)$  = control functions vector.

$w(t)$  = white Gaussian model noise vector with zero mean and variance  $Q$ .

$F(t)$  = continuous system dynamics matrix.

$B(t)$  = control input matrix (system dynamics).

$G(t)$  = noise input matrix, equal to 1 for our purposes.

$z(t)$  = measured output vector.

$H(t)$  = measured output matrix, equal to 1 for our purposes.

$v(t)$  = measurement noise vector with zero mean and variance  $R$ .

The Kalman filter, for our particular application, is defined a discrete-time optimal estimator. In order to characterise the hardware necessary to build the filter, it is necessary to investigate the discrete-time **difference equation** of the system.

The solution for this differential equation at time  $t$  is given by:

$$x(t) = \Phi(t, t_0)x_0 + \int_{t_0}^t \Phi(t, \tau)B(\tau)u(t_0)d\tau + \int_{t_0}^t \Phi(t, \tau)G(\tau)d\beta(\tau) \quad (3.10)$$

With:

$$x(t_0) = x_0.$$

$$\beta(\tau) = \text{Brownian motion process [May79b].}$$

$$d\beta(\tau) = w(\tau)d\tau.$$

$$\Phi(t, t_0) = \text{state forward transition matrix.}$$

$\Phi(t, t_0)$  satisfies the differential equation,

$$\begin{aligned} \frac{d(\Phi(t, t_0))}{dt} &= F(t)\Phi(t, t_0) \\ \Phi(t_0, t_0) &= I \end{aligned} \quad (3.11)$$

For a certain sampling time  $\Delta t$ , we can rewrite the process and measurement equations as:

$$\begin{aligned} x(t_{k+1}) &= \Phi(\Delta t)x(t_k) + B_d(t_k)u(t_k) + w_d(t_k) \\ z(t_{k+1}) &= H(t_{k+1})x(t_{k+1}) + v_d(t_{k+1}) \end{aligned} \quad (3.12)$$

With:

$$B_d(t_i) = \int_{t_i}^{t_{i+1}} \Phi(t_{i+1}, \tau)B(\tau)d\tau \text{ is the discrete control input matrix.}$$

$$w_d(t_i) = \text{discrete process noise vector, with mean and variance given by:}$$

$$E\{w_d(t_i)\} = 0$$

$$E\{w_d(t_i)w_d(t_i)^T\} = Q_d(t_i) = \int_{t_i}^{t_{i+1}} \Phi(t_{i+1}, \tau)G(\tau)QG^T(\tau)\Phi^T(t_{i+1}, \tau)d\tau$$

$$v_d(t_i) = \text{discrete measurement noise vector, with mean and variance given by:}$$

$$E\{v_d(t_i)\} = 0$$

$$E\{v_d(t_i)v_d(t_i)^T\} = R_d(t_i)$$

In practice,  $Q$  and  $R$  are the tuning parameters of the Kalman filter and are often set experimentally by trial and error.

The expressions for the forward transition, control input, and noise matrices can be further simplified using the following expressions:

$$\Phi(t_{i+1}, t_i) \simeq I + F(t_i)(t_{i+1} - t_i)$$

$$B_d(t_i) \simeq B(t_i)dt$$



This analysis tells us that all that is necessary to model a system for Kalman filtering applications is:

- A linear system corrupted with white Gaussian noise or the best approximation.
- A differential equation relating the measurable variable or state of interest to its derivative.
- Knowledge of the initial conditions of the system.

Now we can concentrate on the Kalman filtering part of Kalman filtering. For the scope of this project, it is unnecessary, as mentioned previously, to look into the exhaustive proof of the Kalman algorithm. For a more complete explanation of the Kalman filter, refer to [May79a] [May79b].

The process of estimation of a particular state can be separated into two steps; the time update and the measurement update [WB06]. During the time update stage, a prediction of the next value is calculated using our knowledge of the system and the previous outputs. The information of the last outputs propagates through an error covariance matrix that contains information about the innovation or amount of new (unpredicted) data of each new value. In other words, error equals innovation.

$$\begin{aligned} E\{x_k\} &= \hat{x}_k \\ E\{x_k - \hat{x}_k\} &= P_k \end{aligned} \tag{3.13}$$

$P_k$  is the expected value of the innovation; it contains information about how far from the real value the prediction  $\hat{x}_k$  is at time/sample  $k$ .

The measurement update stage incorporates the information given by the noisy measurement of the system of interest, weighting it more or less heavily depending on its accuracy. In order to do this, a matrix known as the “Kalman Gain” becomes a part of the algorithm. The Kalman gain ( $K$ ) is the main feature of the filter; it decides what factor of information to take from the real measurements as opposed to the model prediction. Once the Kalman gain is calculated, the new (measured) value is incorporated to the prediction to create an estimate of the actual output. Finally, a new (a posteriori) error covariance matrix is calculated from the old (a priori) matrix. Just to be clear, a priori and a posterior refer to before and after receiving information from the actual (noisy) measurement.

For the SPL case, we want to measure the frequency detuning of the resonant cavity due to Lorentz force effects, using a noisy measurement of the time-varying cavity voltage. To do this, we measure and model the cavity voltage using a vector state-space with the in-phase and quadrature components of the voltage and their respective differential equations. If we recall the cavity voltage I/Q relationship to the generator current pulse:

$$\begin{bmatrix} V_{re}(t) \\ V_{im}(t) \end{bmatrix} = \begin{bmatrix} \frac{-\omega_0}{2Q_L} & -\omega(t) \\ \omega(t) & \frac{-\omega_0}{2Q_L} \end{bmatrix} \begin{bmatrix} V_{re}(t) \\ V_{im}(t) \end{bmatrix} \begin{bmatrix} \frac{-\omega_0}{2} \frac{R}{Q} & 0 \\ 0 & \frac{-\omega_0}{2} \frac{R}{Q} \end{bmatrix} \begin{bmatrix} I_{re}(t) \\ I_{im}(t) \end{bmatrix} \tag{3.14}$$

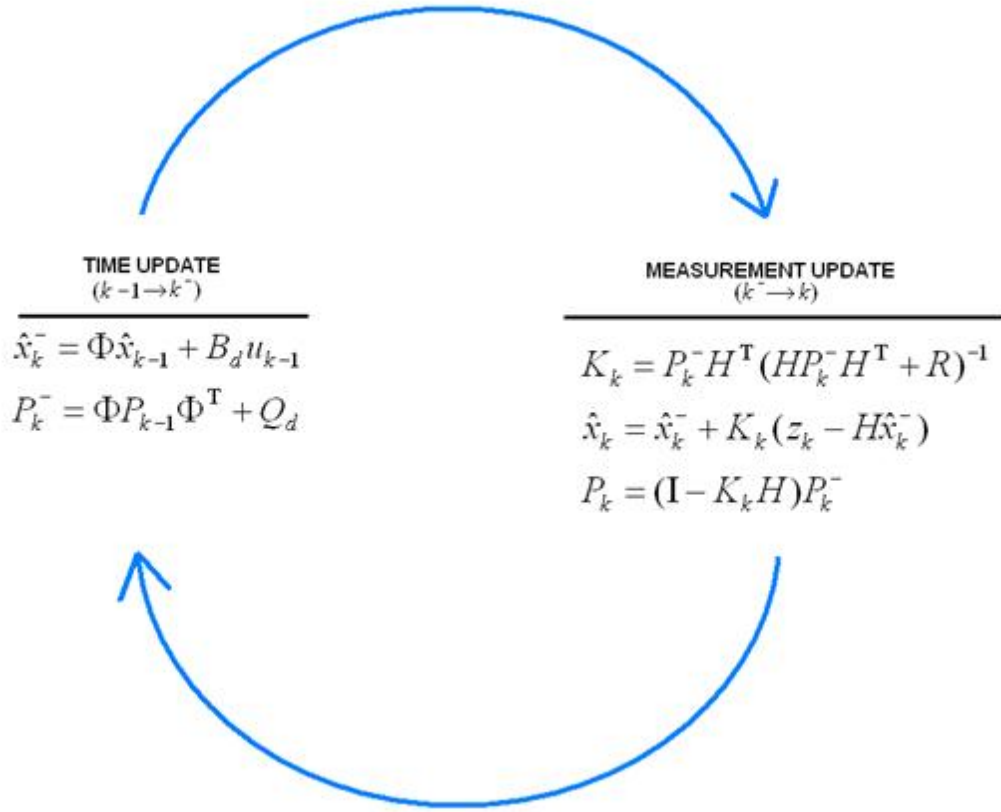


Figure 3.6: Kalman filtering operation [WB06]

If we recall the state transition equation, we can distinguish clearly the Kalman filter parameters:

$$\begin{aligned}
 x(t) &= \begin{bmatrix} V_{re}(t) \\ V_{im}(t) \end{bmatrix} \\
 u(t) &= \begin{bmatrix} I_{re}(t) \\ I_{im}(t) \end{bmatrix} \\
 F(t) &= \begin{bmatrix} \frac{-\omega_0}{2Q_L} & -\omega(t) \\ \omega(t) & \frac{-\omega_0}{2Q_L} \end{bmatrix} \\
 B &= \begin{bmatrix} \frac{-\omega_0}{2} \frac{R}{Q} & 0 \\ 0 & \frac{-\omega_0}{2} \frac{R}{Q} \end{bmatrix}
 \end{aligned} \tag{3.15}$$

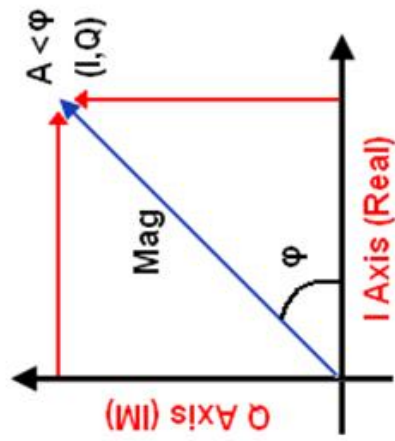
The tuning parameters of the filter will be the process and measurement noise variances; this means that if the process noise adequately follows our models shortcomings, and the filter measurement noise is close to the actual noise, the output of the filter will closely follow the real signal even in very poor SNR conditions. Refer to section 4.4 for detailed schematics of the filter implementation.

## Chapter 4

# SIMULINK I-Q Model for SPL RF Components

Developing a project of great magnitude such as a high-power linear accelerator is a staggering task and demands careful consideration of all elements involved, such as power budget, technology requirements and space and time necessary. In order to foresee difficulties and answer some of the many questions that arise from these considerations, it is useful to develop a virtual model of what we hope to achieve. This section describes the progress to date of a model that hopes to achieve flexibility of design as well as accuracy of results and strives to follow reality as closely and as reliably as possible. The SPL model described in this section (see overleaf) consists of a Generator (Klystron) coupled via a circulator and transmission line to 1, 2 or more resonant cavities, taking into account the effects of beam loading and Lorentz force detuning. The output is controlled by means of PID feedback. The model also includes a versatile GUI (graphical user interface) which will be described further within this chapter. With this layout, it is possible to observe many characteristics of the RF system. The outputs, in addition to the cavity voltage amplitude and phase, include forward and reflected power (to and from cavity) with and without feedback and the additional power due to the feedback loop, all displayed as a function of time. These results can be observed in open and closed loop operation for varying component values, in the presence or absence of Lorentz detuning and source current fluctuation. A phasor diagram of beam, cavity, forward and reflected powers is also available. In addition, for the multiple-cavity cases, the individual cavity waveforms as well as Kalman filtering outputs are displayed. All calculations are done in baseband using Inphase and Quadrature components of complex signals. A band limited signal centered at a carrier frequency  $\omega_0$  can be represented using slow-varying components in-phase  $I(t)$ , named as such because they are  $0^\circ$  or cosine components and in-quadrature  $Q(t)$ , which are the  $90^\circ$  or sine components of the signal [Hol107].

In this section the modelling of each block is explained.



$$x(t) = A(t) \cos(2\pi\omega_o t + \varphi(t)) = I(t) \cos(2\pi\omega_o t) - Q(t) \sin(2\pi\omega_o t)$$

$$Q(t) = A(t) \cos(\varphi(t))$$

$$I(t) = A(t) \sin(\varphi(t))$$

Figure 4.1: I/Q Equivalence [Hol07]

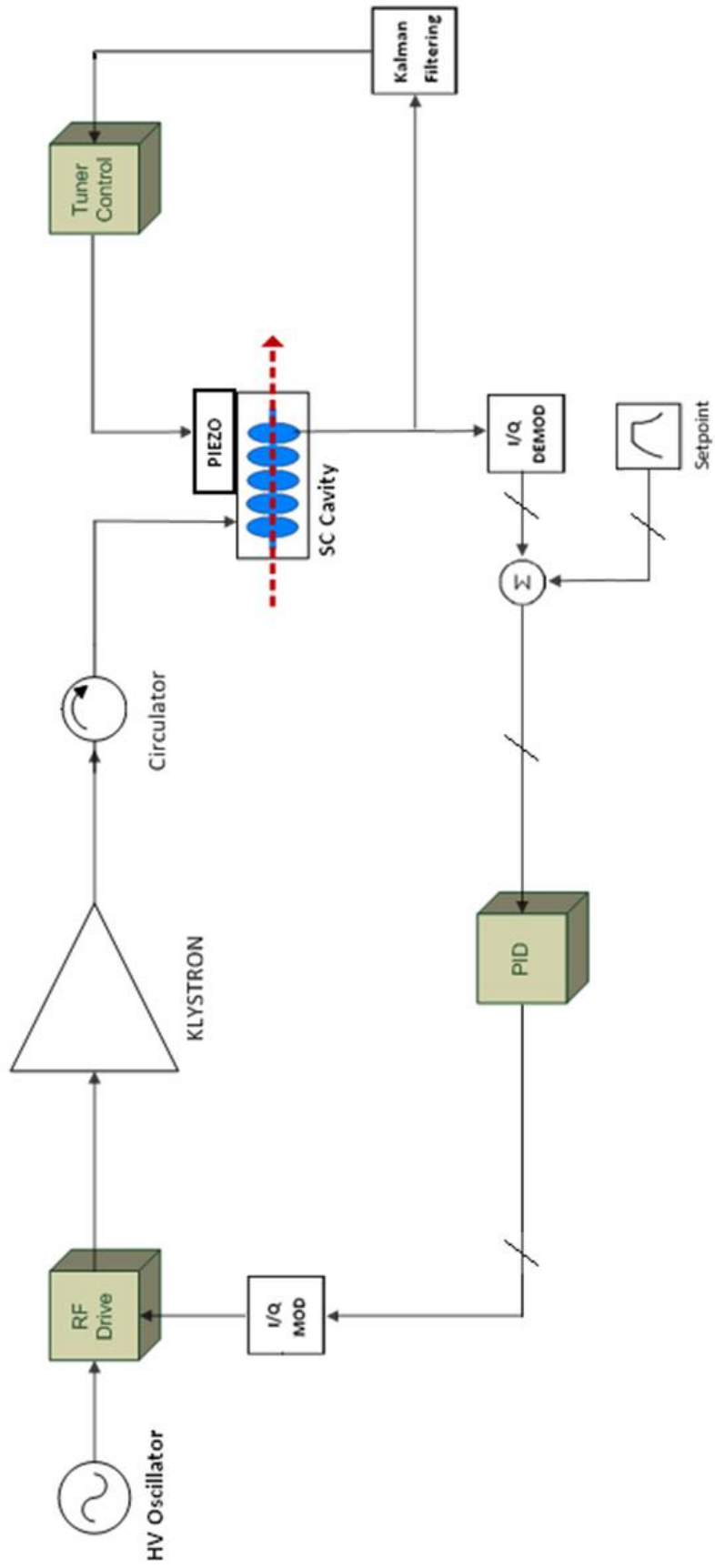


Figure 4.2: SPL 1 cavity control high level diagram

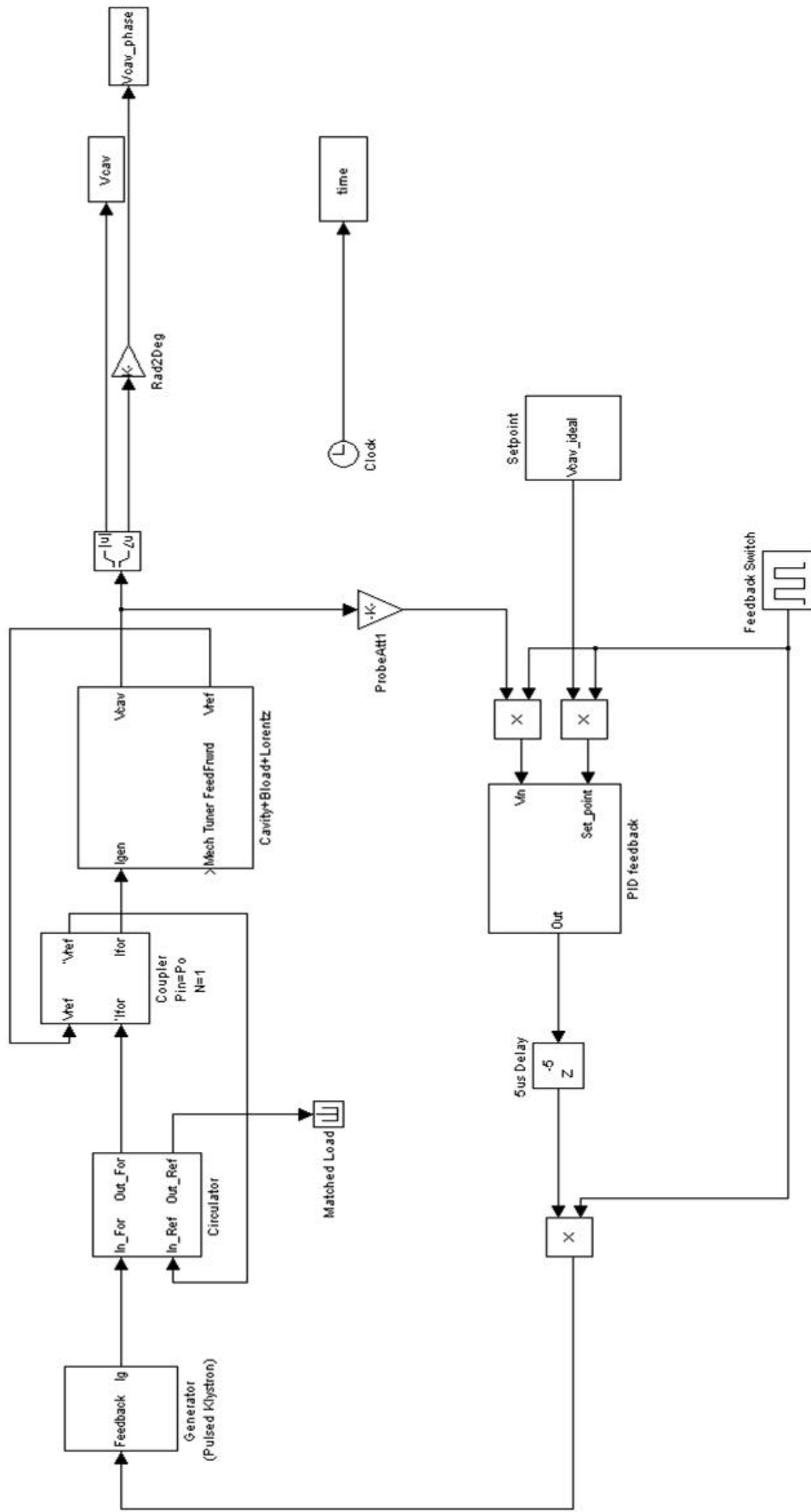


Figure 4.3: SPL single-cavity control SIMULINK model overview

## 4.1 Generator, Generator-Cavity Coupling

The generator is modelled as a square wave current source that emits a current pulse that lasts until cavity filling and beam loading have occurred, the frequency response of the Klystron is modelled as a low pass filter with 1 MHz bandwidth (as we are using I-Q components we work in baseband); this bandwidth is considered high compared to the rest of the system so stability will not be affected by the Klystron bandwidth. The generator angle is set to zero and this is used as the reference angle for the cavity and beam phases. We can also observe the feedback I-Q components adding to the input, all tags(goto) are used to display results. The coupling from the generator to the cavity is set to 1:1 ratio with no circulator loss for present calculations. In future analyses the model will include the effects of an unideal circulator and transmission line length, as well as the coupler efficiency. The diagram for the generator is shown in figures 4.6 and 4.7.

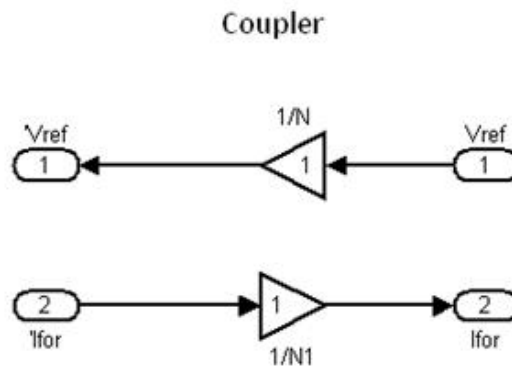


Figure 4.4: Coupler SIMULINK model (1/N)

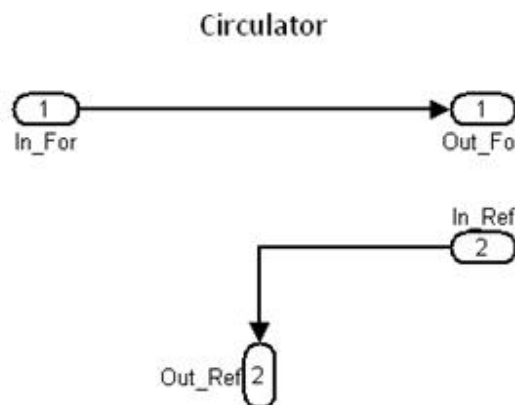


Figure 4.5: Circulator SIMULINK model

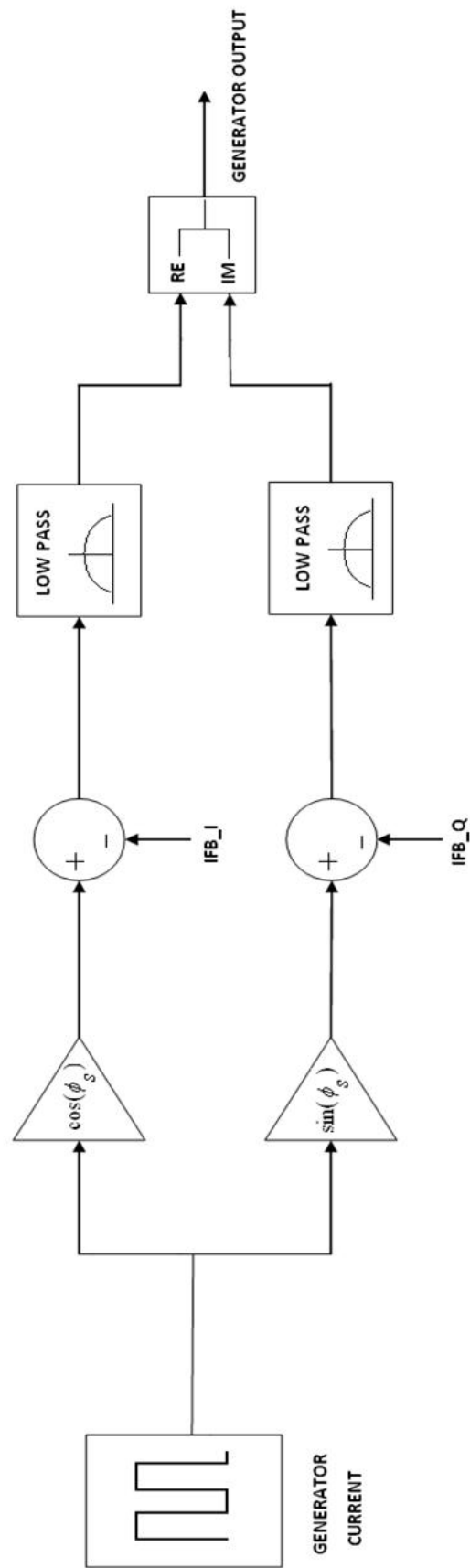


Figure 4.6: RF generator high level diagram



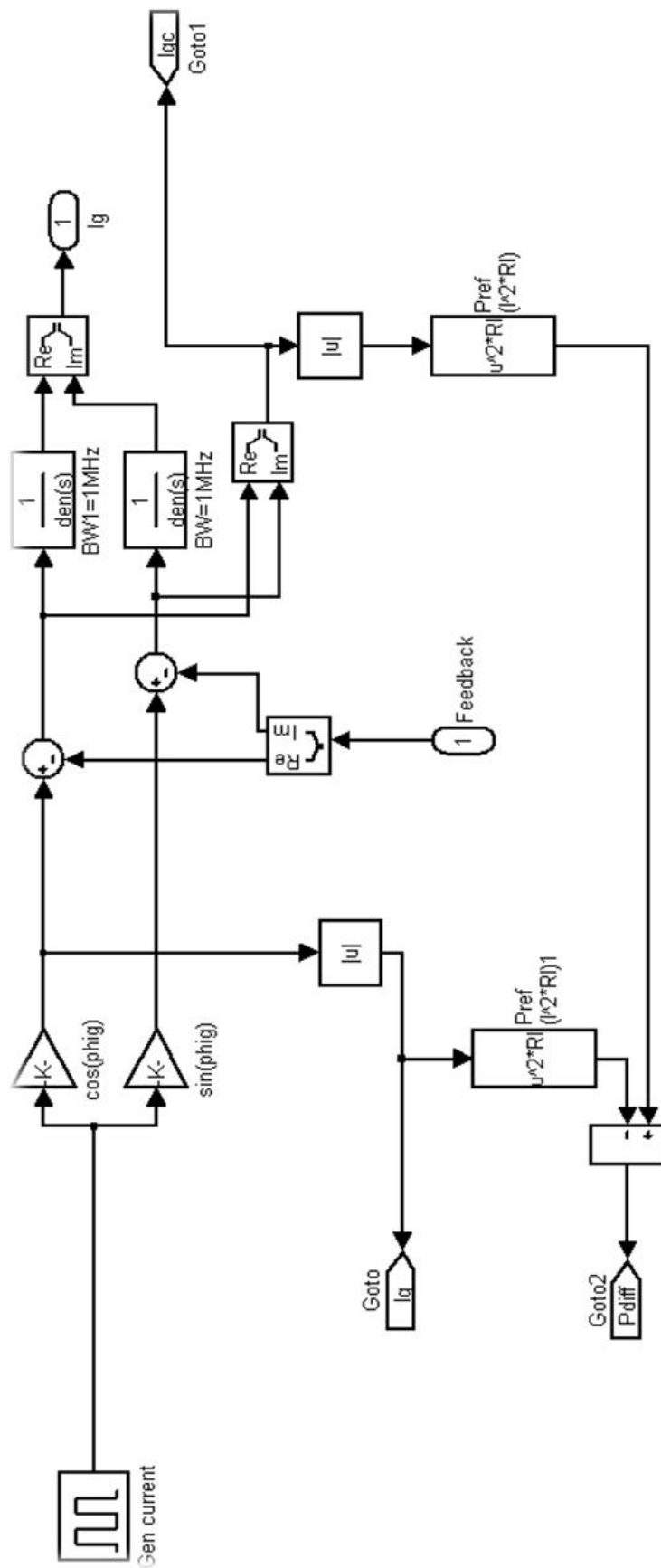


Figure 4.7: RF generator SIMULINK model

## 4.2 Resonant Cavity Model

The resonant cavity is the most important and complex part of the entire model. It contains physical and mathematical descriptions on cavity performance as well as beam loading effects and Lorentz force detuning due to physical deformation at high voltages. In I-Q description, the cavity output behaves like coupled first order differential equations driven by the generator current I-Q components.

$$\begin{aligned} R_L(2I_g + I_b)_{inphase} &= \tau \frac{dV_{inphase}}{dt} + V_{inphase} - yV_{quad} \\ R_L(2I_g + I_b)_{quad} &= \tau \frac{dV_{quad}}{dt} + V_{quad} + yV_{inphase} \end{aligned} \quad (4.1)$$

Where  $y = \tan \Psi = 2Q_L \frac{\Delta\omega}{\omega_0}$  is the detuning caused by a frequency mismatch, and  $\tau = \frac{2Q_L}{\omega_0}$  is the cavity filling time. Beam loading can be viewed as a train of instantaneous voltage drops in the cavity voltage corresponding to infinitely narrow bunches passing every 1.4 nanoseconds. The voltage drop due to each bunch is given by [LP07] [Bou86]:

$$V_{cav.bunch} = \omega_{RF} \times \frac{R}{Q}(\text{circuit}) \times q_b \quad (4.2)$$

Where the synchronous angle  $\phi_s$  is given by its LINAC definition, which means the beam loading occurs with a phase shift of  $\phi_s$  degrees before the positive maximum value of the RF field in the cavity. The injection-time parameter is chosen at a point in the cavity filling time such that the negative gradient induced by the beam on the cavity voltage is equal to the positive gradient induced by the generator, and so we observe flattop operation during the beam pulse. After the beam has been accelerated, the generator is switched off until the next period of operation.

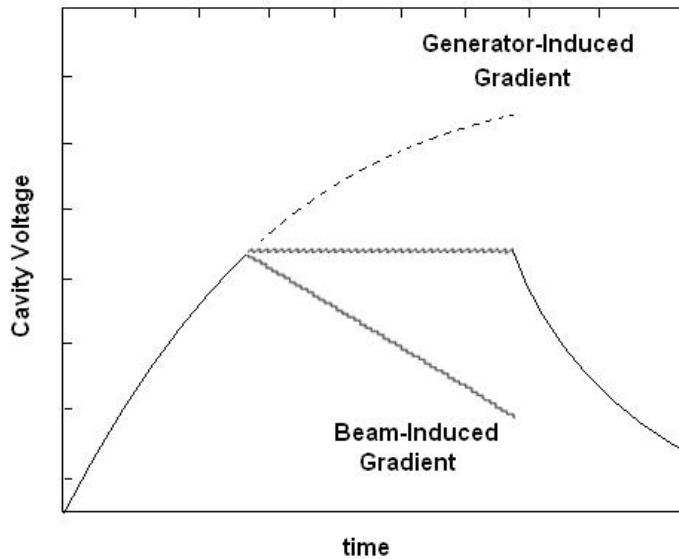


Figure 4.8: Beam and generator-induced voltage gradients in cavity

In I/Q representation, however, the current is modelled simply as a DC driving term to the cavity differential equations. In this way, we are able to observe the envelope of the full effect. For a complete description of the beam effects it is therefore best to investigate the characteristics of the cavity voltage signal and the phasor diagram of the generator-beam-cavity interaction available from the simulation results. The model also includes the effects of variations in the DC current of the beam source during beamloading. Lorentz force effects are added to the tuning angle of the system as an extra shift in the cavity resonant frequency with respect to the generator centre frequency. Lorentz detuning is modelled, as of now, as a 1<sup>st</sup> order differential equation driven by the square of the accelerating field [Sch98].

$$\frac{d\Delta\omega(t)}{dt} = \frac{1}{\tau}(-\Delta\omega(t) + \Delta\omega_T + 2\pi K E_{acc}^2) \quad (4.3)$$

Where  $K$  is known as the Lorentz detuning factor and relates the frequency shift to the square of the electric field inside the cavity, its units being Hz/(MV/m)<sup>2</sup>.

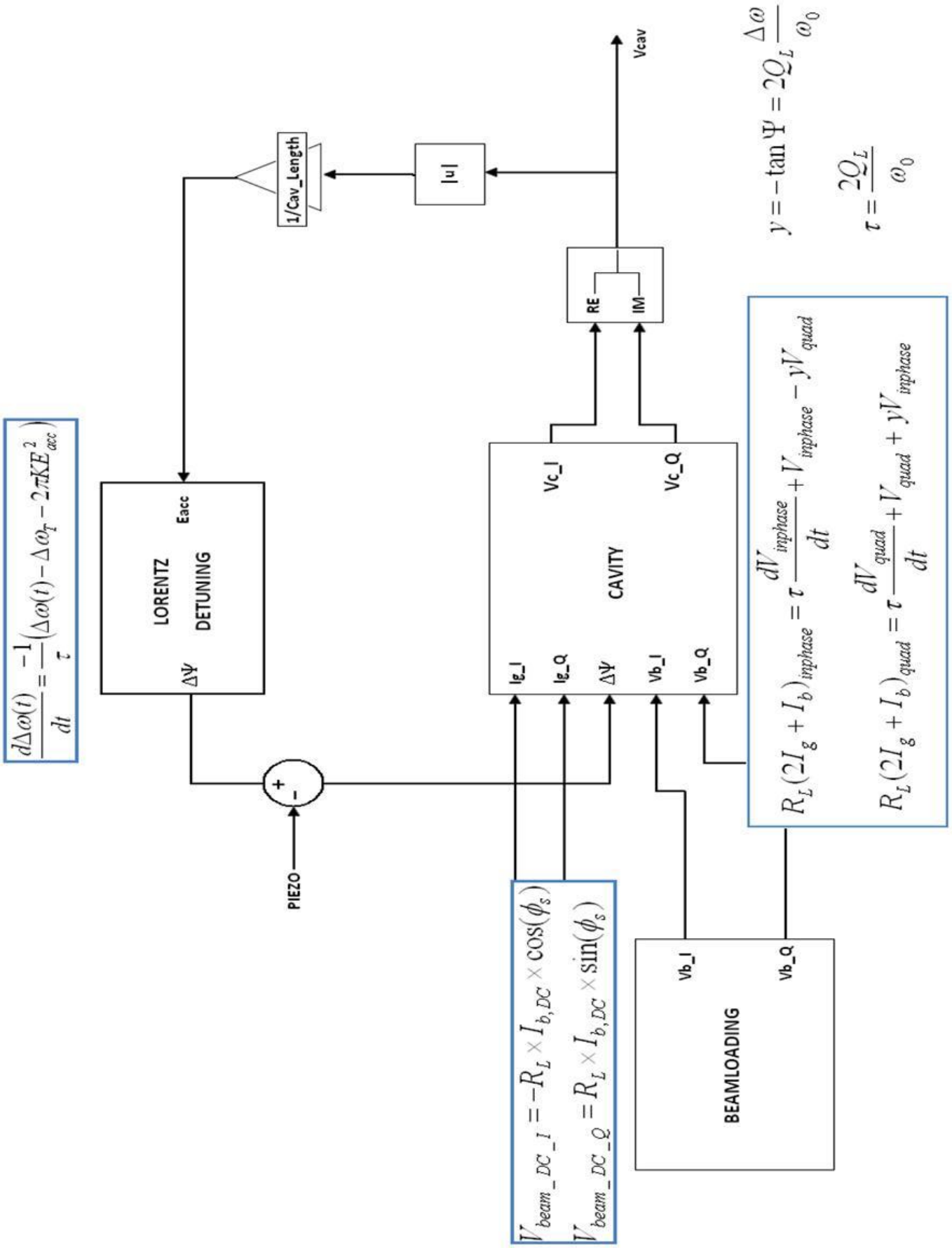


Figure 4.9: Cavity high level diagram with beam loading and Lorentz detuning

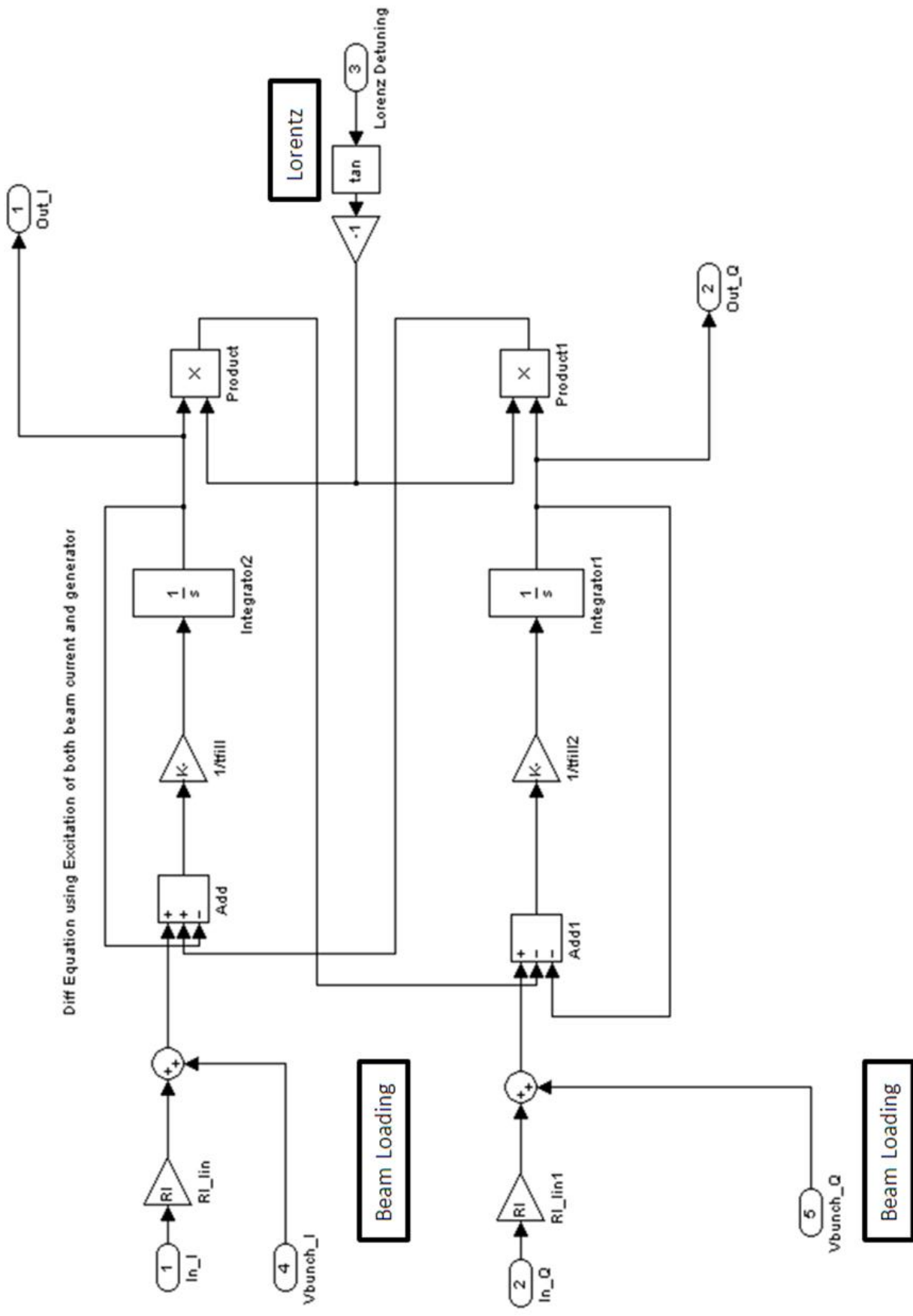


Figure 4.10: Cavity SIMULINK model with beam loading and Lorentz detuning

### 4.3 RF Feedback Loop

The goal of the model for both singular and multiple-cavity cases is to maintain the cavity voltage during beam loading within certain amplitude and phase values. As the output is affected by Lorentz detuning and synchronous angle mismatches as well as microphonics effects and external conditions, a feedback loop is necessary to maintain the output of our system within the specified parameters. In order to achieve this, a PID feedback model was used. The proportional gain was set using stability considerations, taking into account a feedback loop with a 5 microsecond delay and a bandwidth of 100 kHz. The integral and differential gains were found by trial and error to produce stable results shown in section 5. The integral gain was added to suppress any DC offset introduced between the setpoint and the output by the proportional gain and the differential gain results in a smoother operation (less oscillation). The SIMULINK model schematic for this block is shown in figure 4.12.

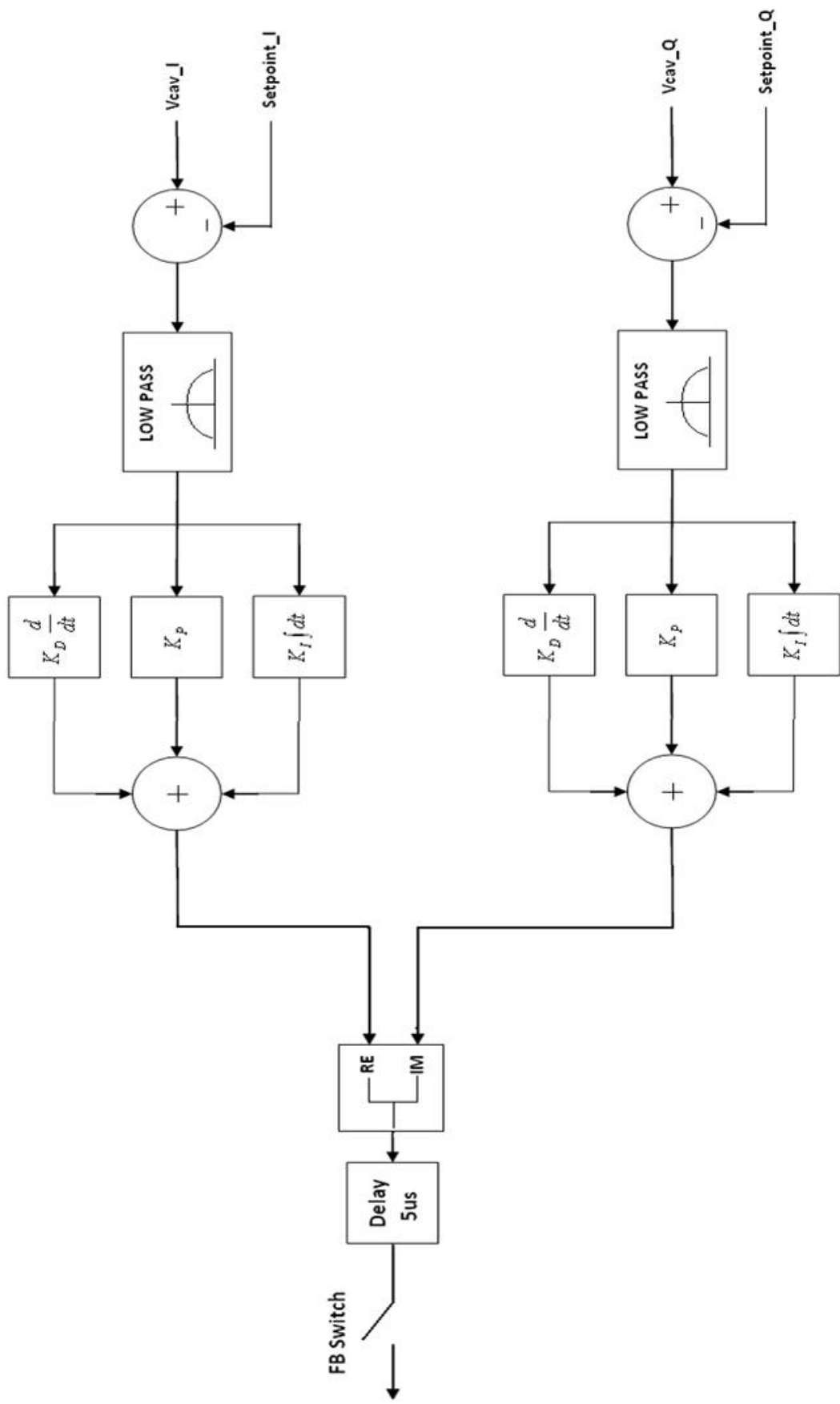


Figure 4.11: PID feedback loop high-level diagram

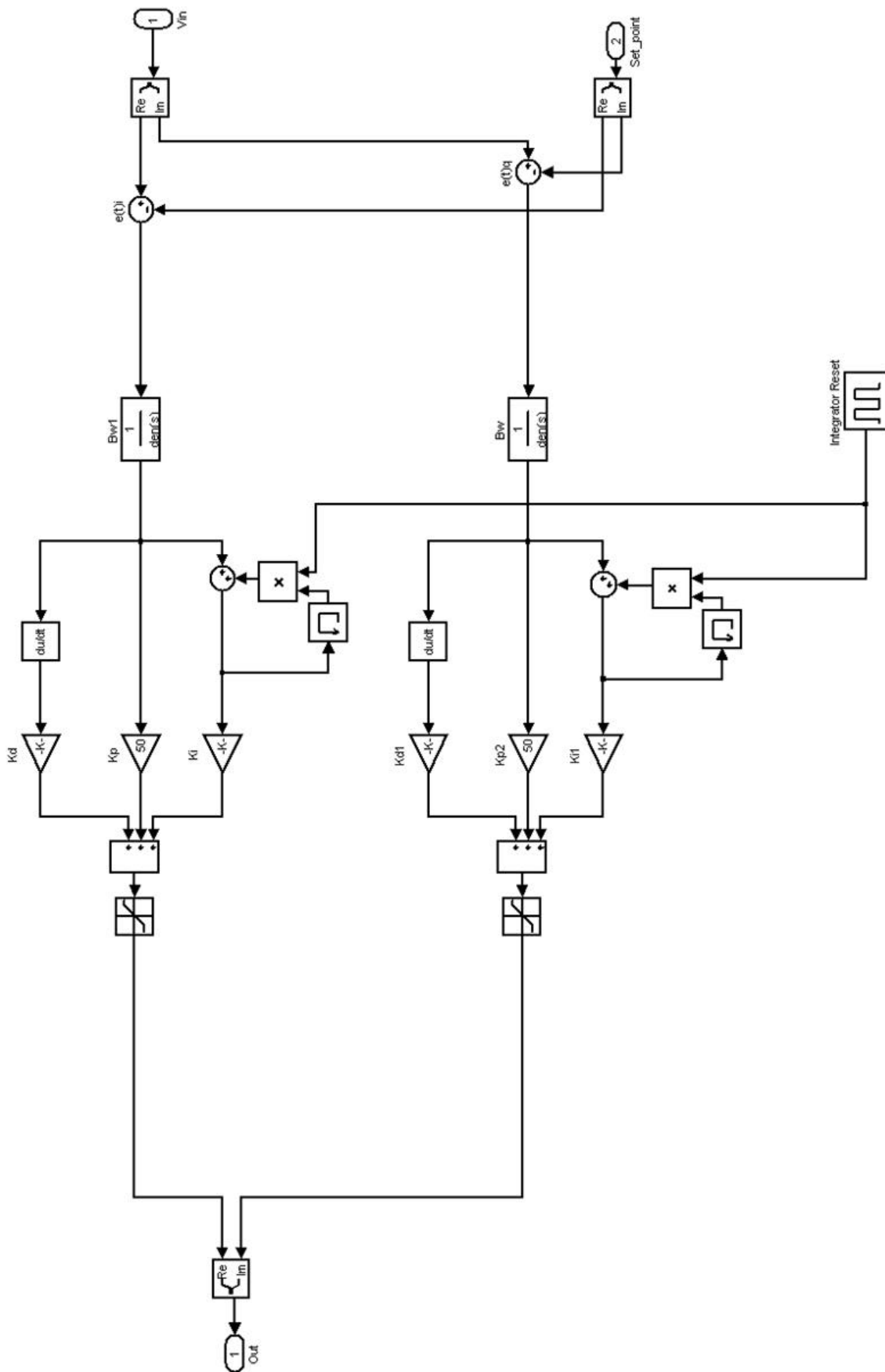


Figure 4.12: PID feedback SIMULINK model



## 4.4 Dual Cavity Model

Figures 4.14 and 4.15 show the layout for the two-cavity case. Both cavities are identically modelled but some of their values can vary slightly to observe the effects of a slight mismatch between the cavities in the actual SPL design. The real innovation in this model is the feed-forward scheme using Kalman filters. The filters find the cavity detuning using a best fit from the cavity voltage and a first order relationship between this voltage and the Lorentz detuning. Figures 4.16 and 4.17 show the Kalman filter model and its operation. It is important to mention that the Lorentz detuning input to the filter model is set to zero as the pickup from the cavity looks that way due to feedback. The feedback loop works on the vector average of the outputs from the individual cavities (figure 4.13).

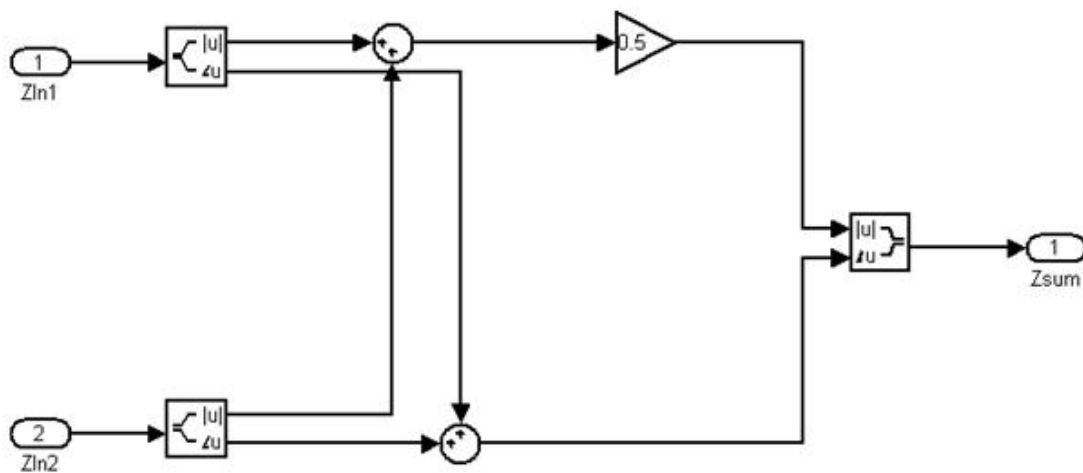


Figure 4.13: Vector average block

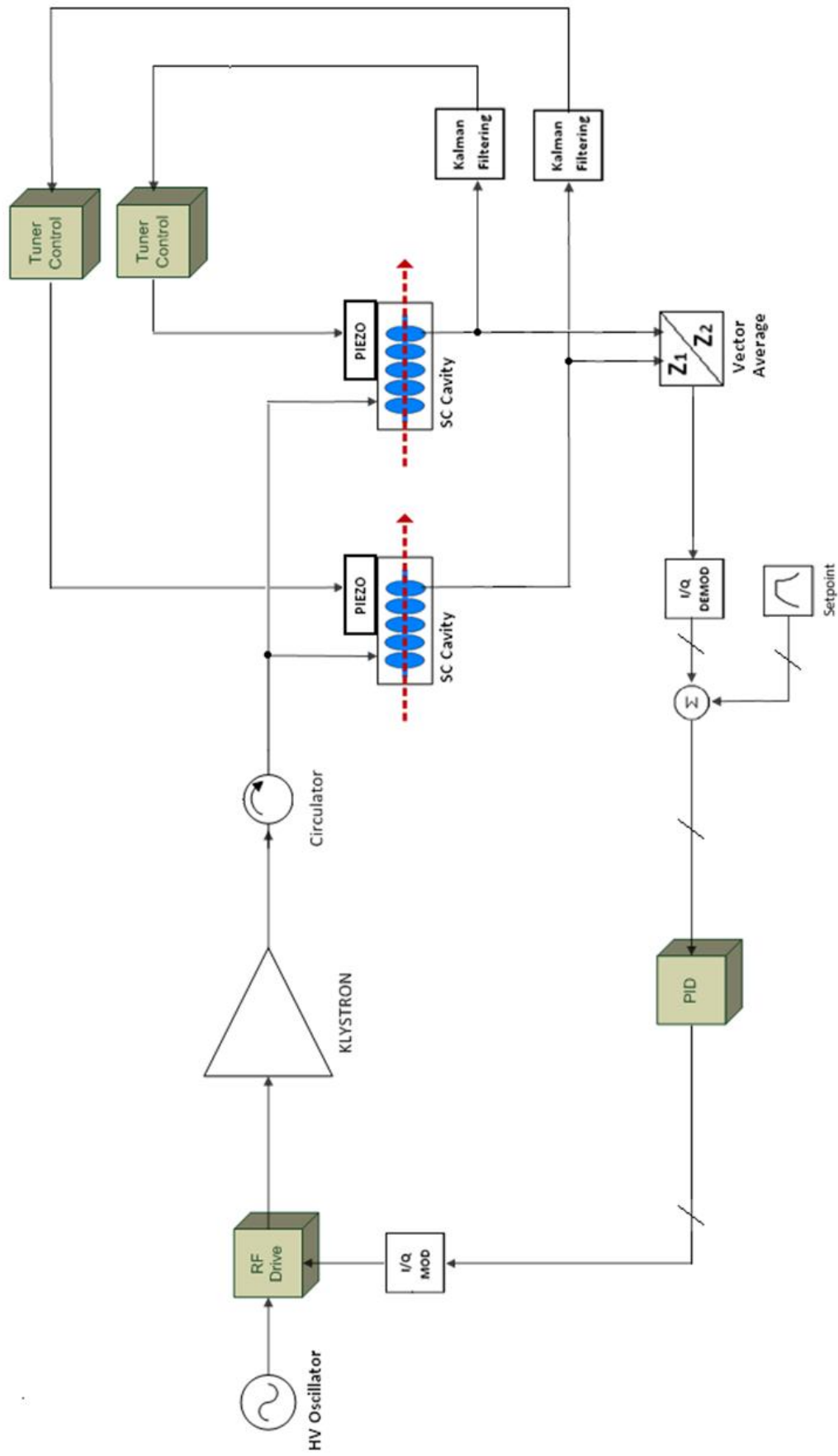


Figure 4.14: PID feedback loop high-level diagram

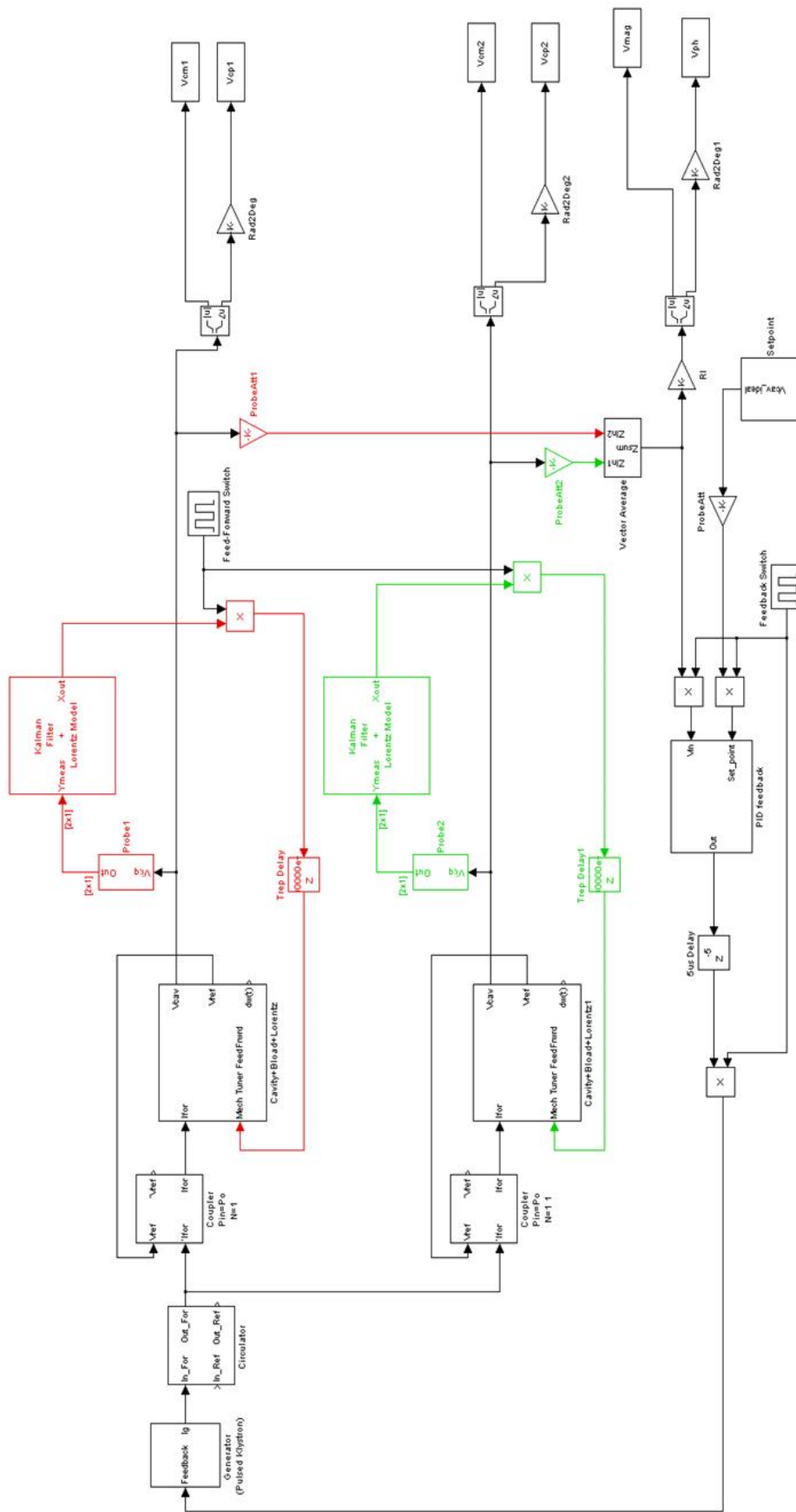


Figure 4.15: PID feedback SIMULINK model

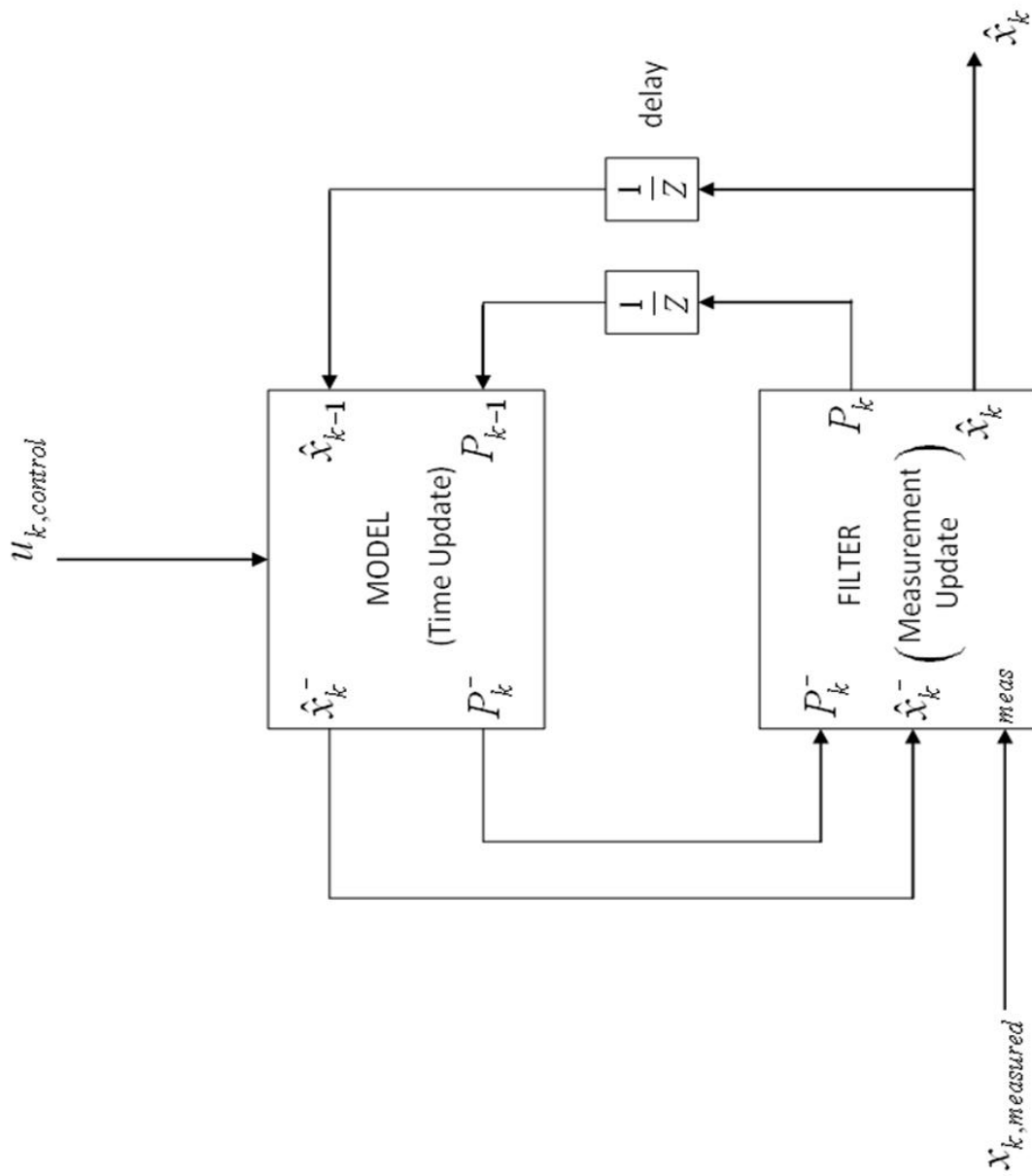


Figure 4.16: Kalman filter high-level diagram

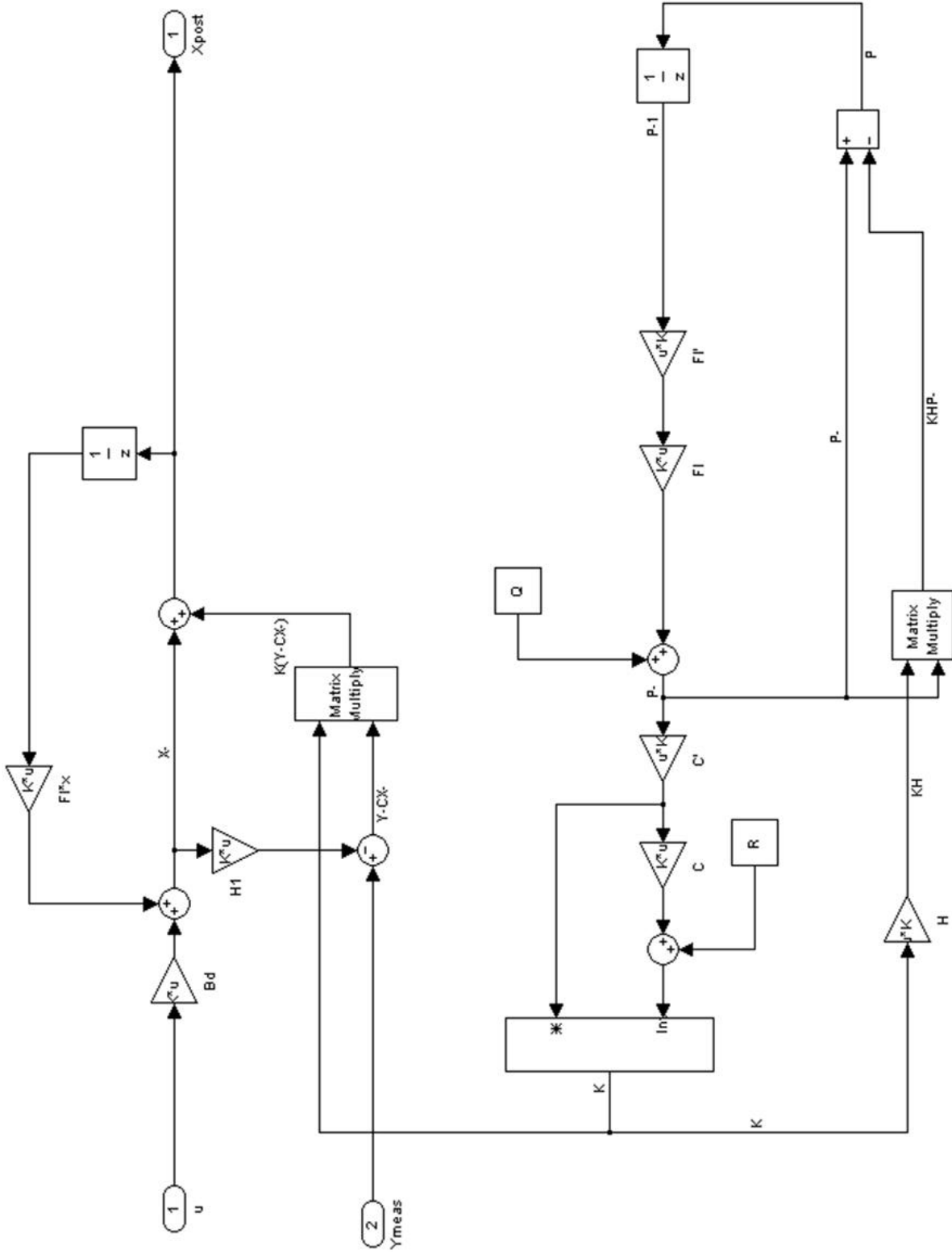


Figure 4.17: Kalman filter SIMULINK model

## 4.5 Graphical User Interface (GUI)

Last but not least, in order to be able to display results quickly and conveniently, add versatility to the model and shield the user from the low-level design of the project, a GUI has been designed, striving to be a user-friendly tool for the interpretation of data derived from the model. The GUI, at its present state, can analyze the behaviour of single, double and quad-cavity operation with control loops in many different scenarios, depending on user inputs and display choices. A .exe file was also created in MATLAB for portability. It is, thus, not necessary to have MATLAB installed in the machine to operate the GUI. The GUI is displayed in figures 4.18, 4.19 and 4.20; following is an explanation of its main features:

- **Start Simulation:** the button group labelled as such allows choosing between single, double and quad-cavity operation in closed-loop and open-loop, as well as possible feed-forward in the multiple cavity case. Simulation begins when the Simulate button is activated.
- **Operating Parameters:** within this box, the user can specify cavity, generator and beam parameters to match their application. The loaded quality factor can be specified as fixed or left blank, in which case the program will calculate the optimum for simulation. The Simulate button in the Start Simulation button group will not be enabled until numerical inputs for these values are added. Inputs that are not critical are set to zero without user input.
- **Progress Bar:** As it is impossible to maintain processing speed and output data from SIMULINK while a simulation is running, the progress bar does not show the time left for the simulation to finish, but notifies the user when it has, and shows the time elapsed during the last simulation.
- **Axis Control:** Both axes in the GUI behave in exactly the same way. There are two for the purpose of visually comparing graphs and result displays. Using the popup menu on the right, the user can choose to display different results for interpretation. These include cavity voltage amplitude and phase, forward and reflected power, power consumed by feedback loop, frequency shift with Lorentz detuning, Kalman filter outputs, and a phasor diagram of the effects of beam loading with synchronous angle  $\phi_s$ . Most graphs can also be zoomed to view critical areas in more detail. In addition, the plot to figure button can be chosen to plot outside the GUI, for saving or manipulating the graphs further.

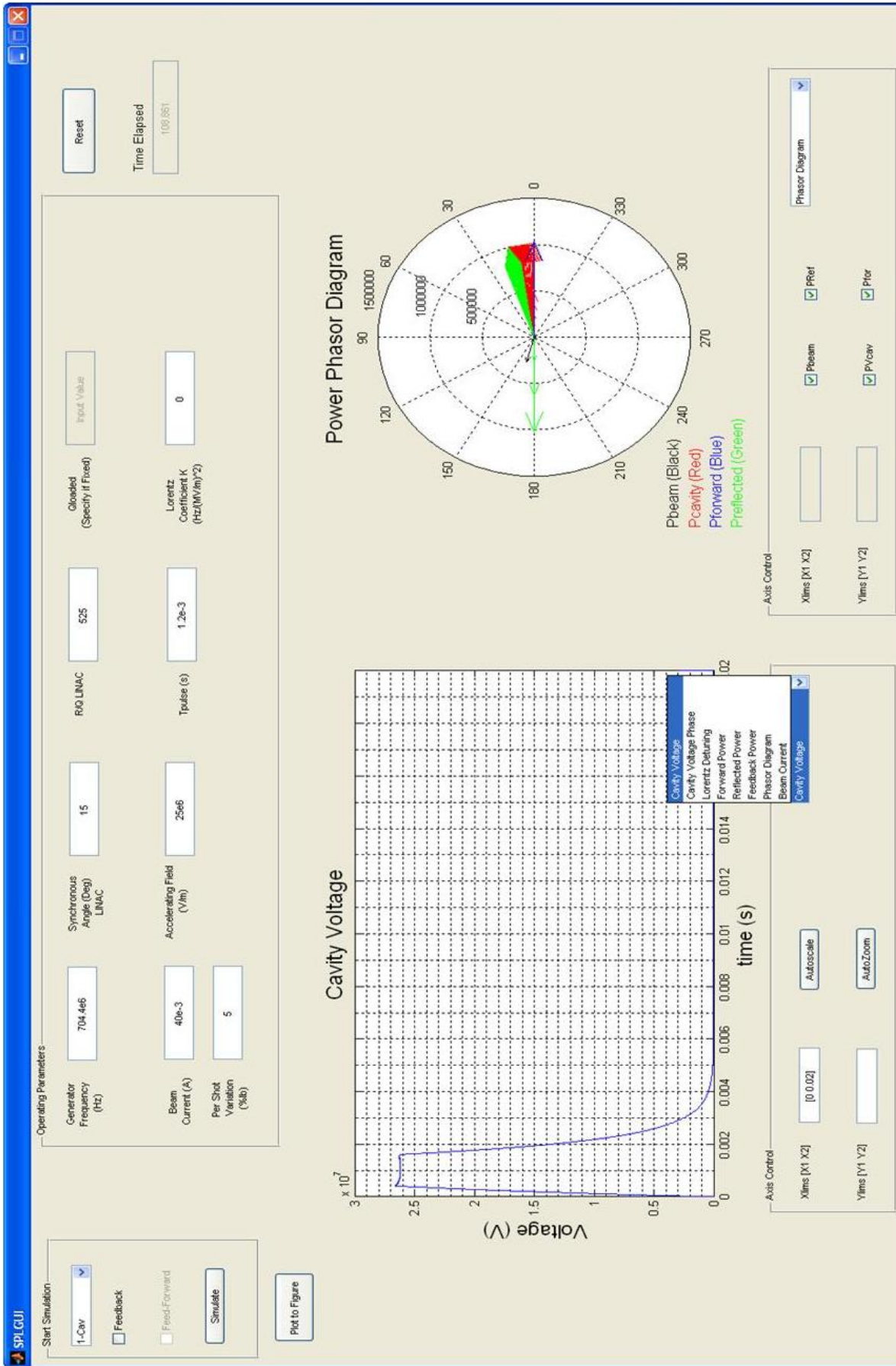


Figure 4.18: Graphical user interface (1-Cavity)

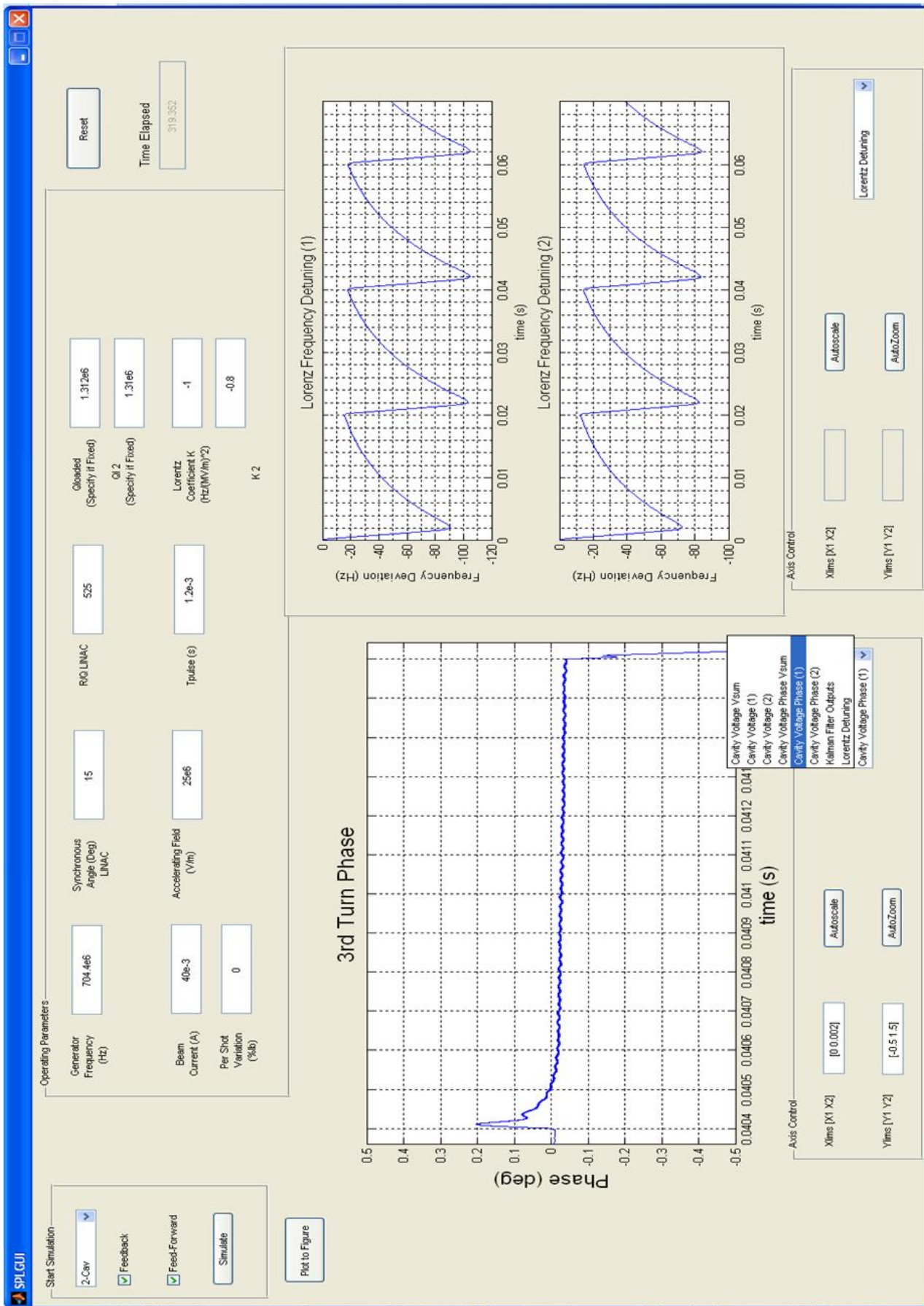


Figure 4.19: Graphical user interface (2-cavities)



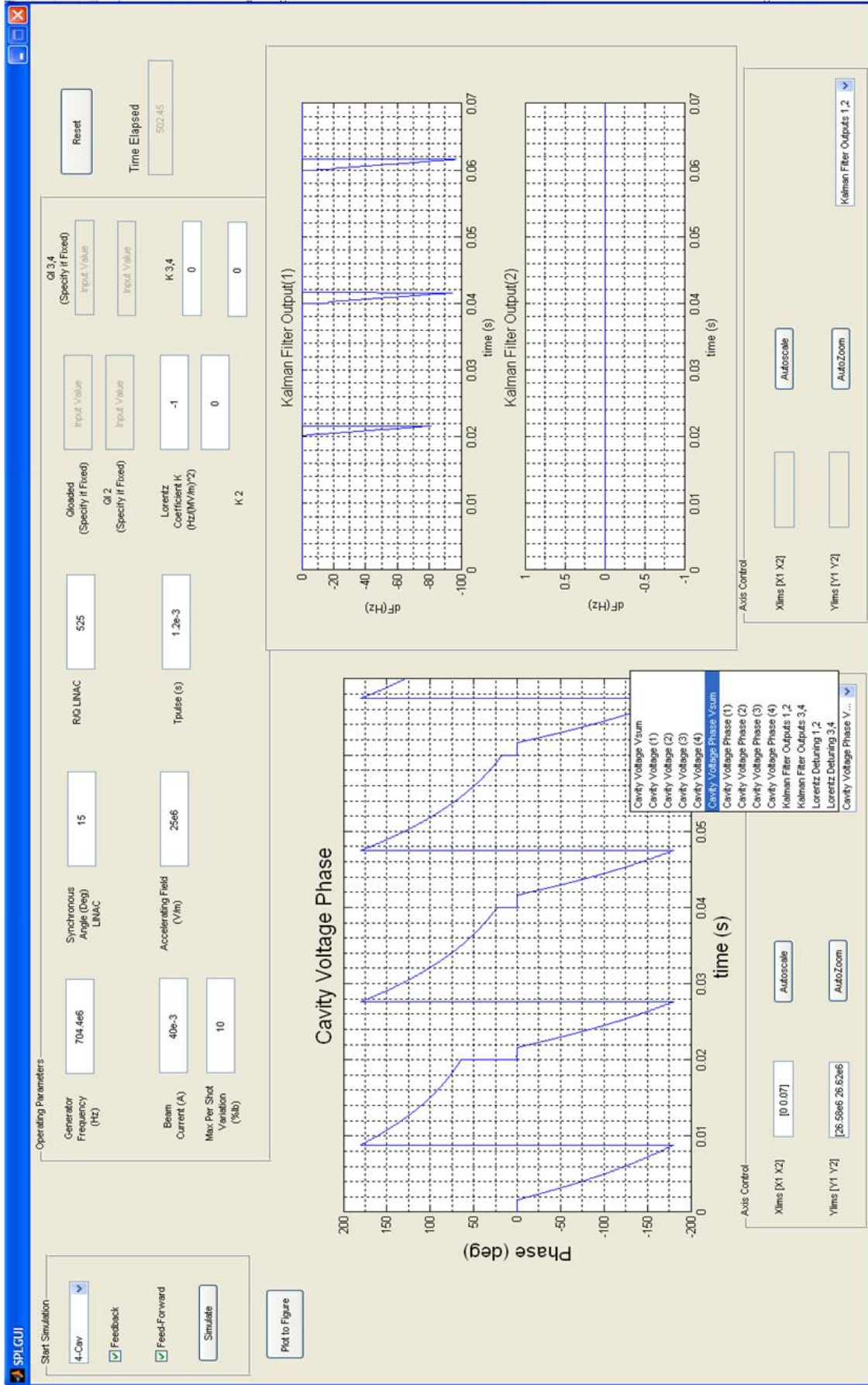


Figure 4.20: Graphical user interface (4-cavities)

# Chapter 5

## Results of Model Analysis

In this section, modelling results are portrayed in a gradual fashion. The single cavity case is observed for the ideal case, in the presence of Lorentz detuning and finally results are shown for the dual-cavity behaviour. Bear in mind that all angles in the phase of the cavity voltage are those of the cavity with respect to the generator.

### 5.1 Single Cavity in the Absence of Lorentz Detuning

#### 5.1.1 Open Loop

We start off with the simplest case, a single cavity with a matched loaded quality factor to beam current. At the time of injection, given by

$$t_{inj} = \ln 2\tau_{fill}$$

the beam arrives with a phase shift given by the synchronous angle  $\theta_s$ . This explains the fact that the power delivered by the generator is not entirely absorbed by the beam and the cavity voltage increases with time. As the cavity is uncompensated, the unsynchronised beam causes the voltage amplitude to rise above the 0.5% tolerance level and detunes the cavity phase with respect to the generator (0 degree) phase towards 15 degrees. This also means that some reflected power is observed during beam loading.

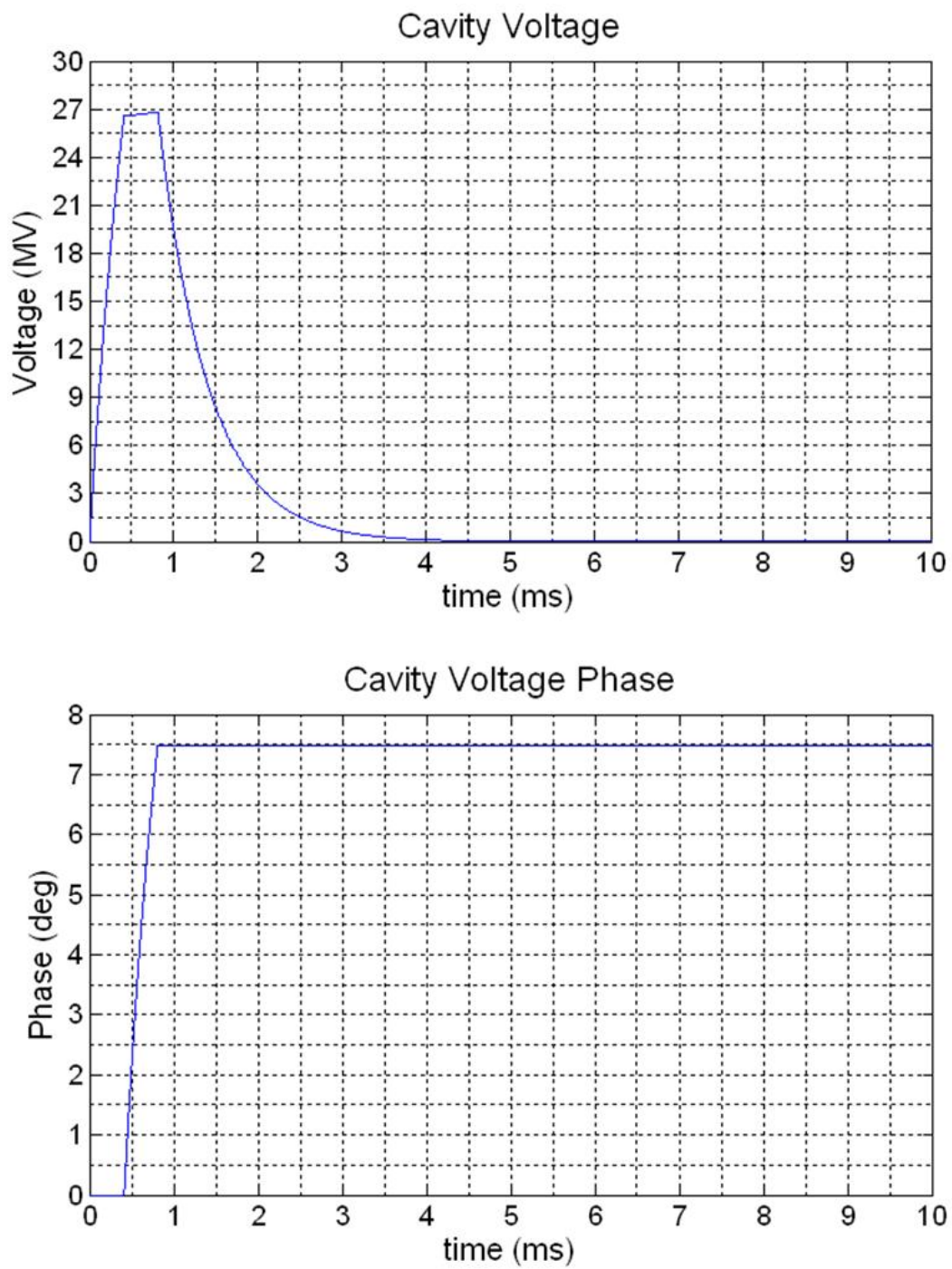


Figure 5.1: Cavity voltage magnitude and phase in the absence of Lorentz detuning (open loop)

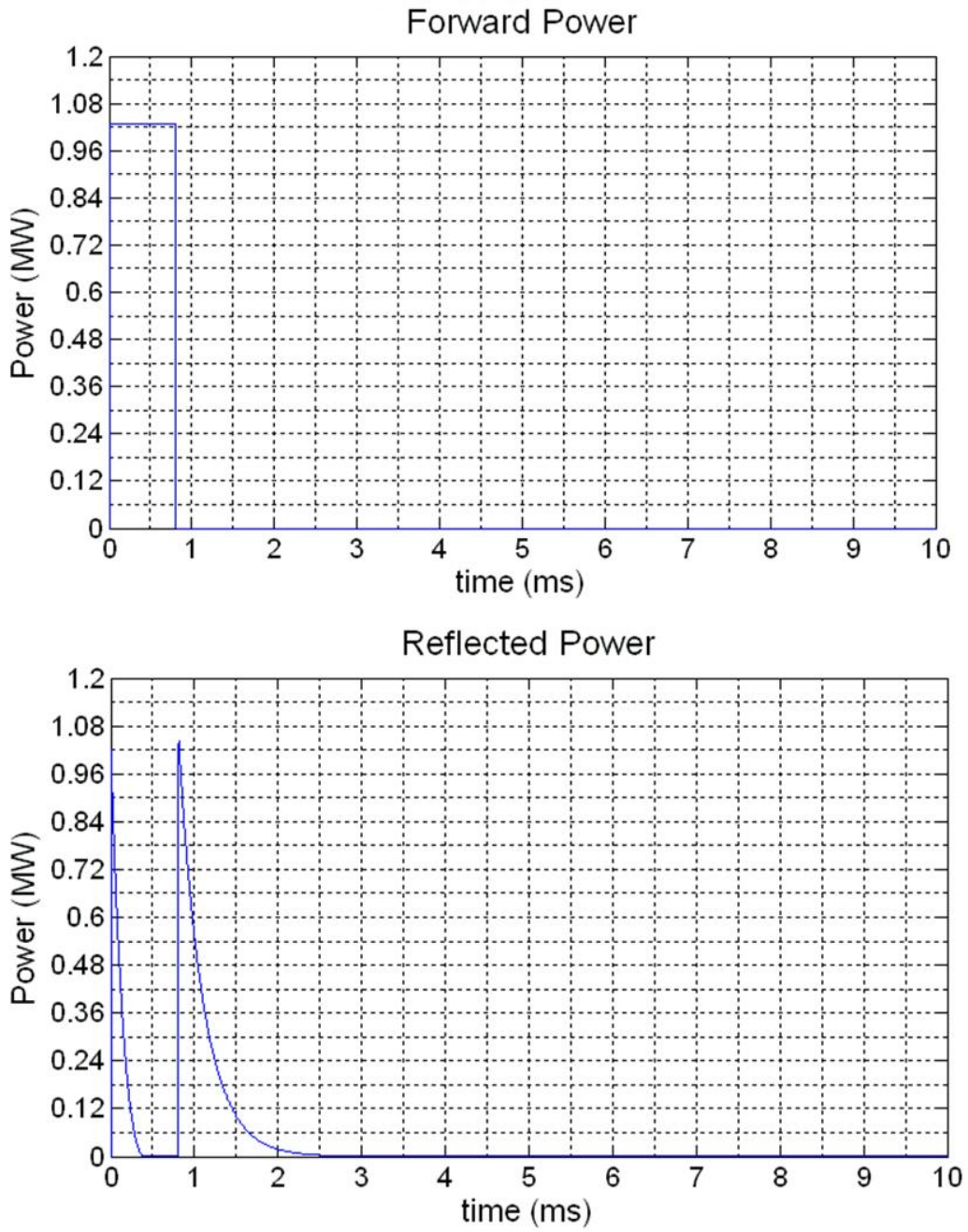


Figure 5.2: Forward and reflected power in the absence of Lorentz detuning (open loop)

## 1st Turn Power Phasor Diagram

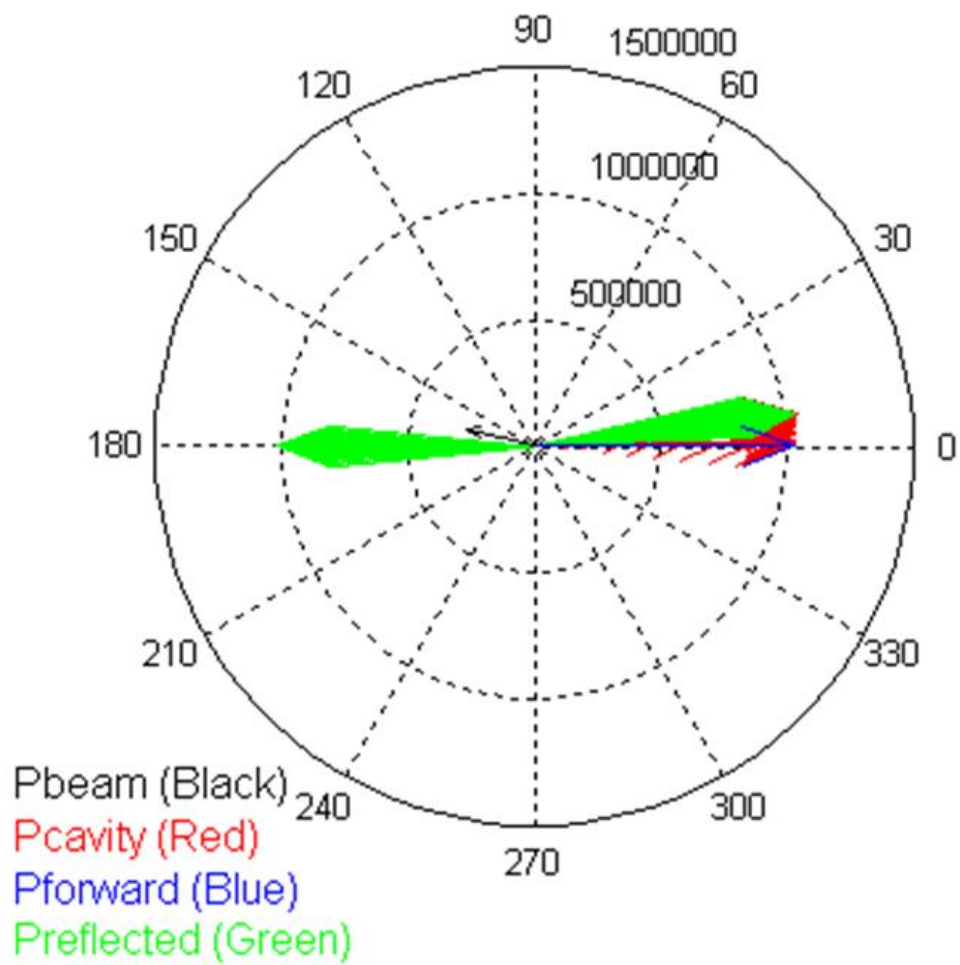


Figure 5.3: Power phasor diagram for open loop system

### 5.1.2 Closed Loop

It is clear from the results in the previous sub-section that feedback is necessary for the correct operation of the system output. The following results were obtained by adding PID feedback with an ideal cavity output as a setpoint. The proportional gain was set by stability considerations, assuming a feedback loop delay of 5 microseconds. The integral and differential gains were set by trial and error. Both the cavity magnitude and phase are now within the design specifications, as shown by figure 5.4. The feedback loop is closed (ON) right after the generator pulse begins, which means it is already ON when the beam arrives. Right after the beam has passed, the feedback loop is turned OFF to save power, leaving the cavity detuned at a constant value depending on the oscillations resulting from the end of beam loading. The forward and reflected powers are as before, with the addition of the feedback compensation. The power consumed by the feedback peaks at around 23 kW at the moment of beam injection.

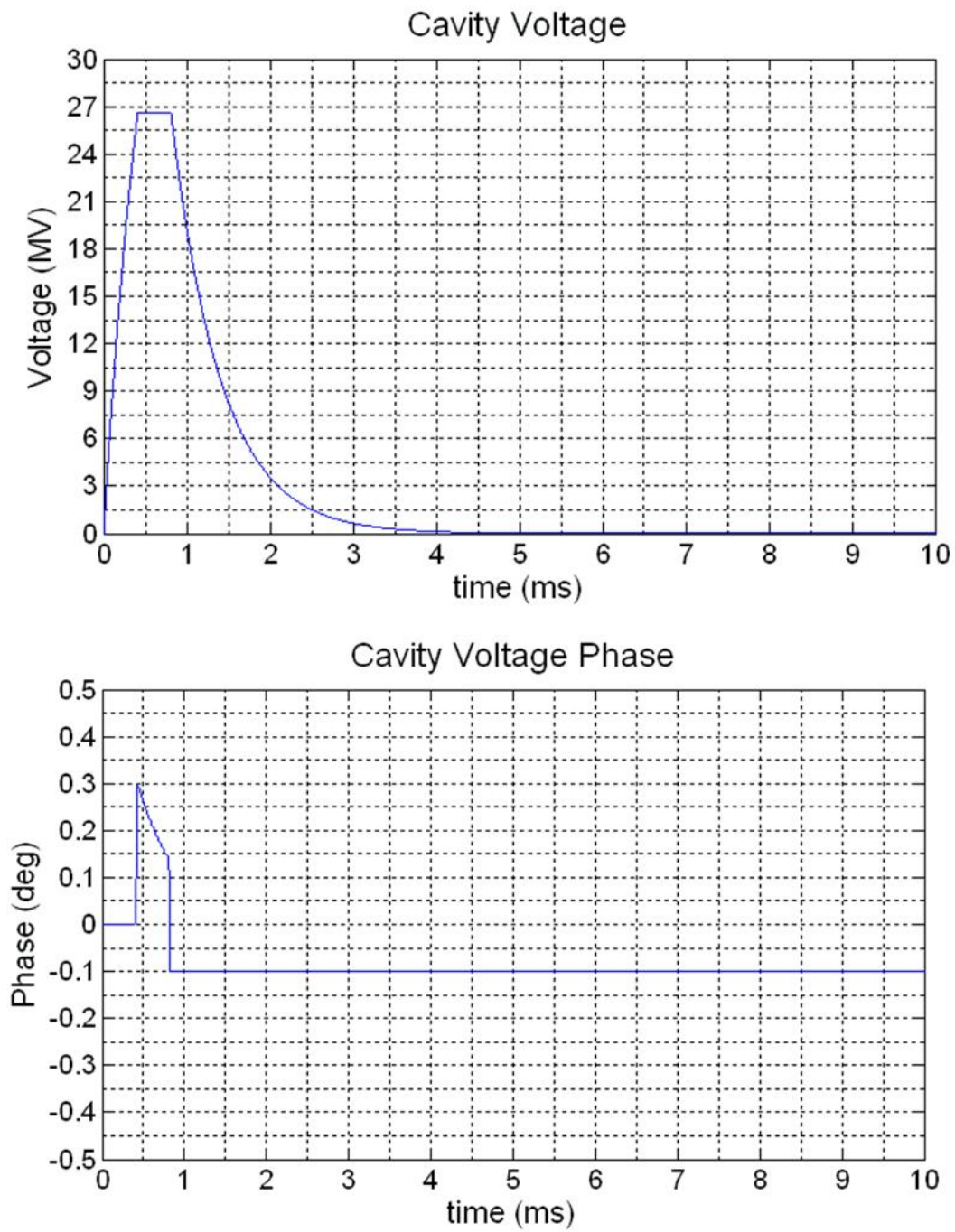


Figure 5.4: Cavity voltage magnitude and phase in the absence of Lorentz detuning (closed loop)

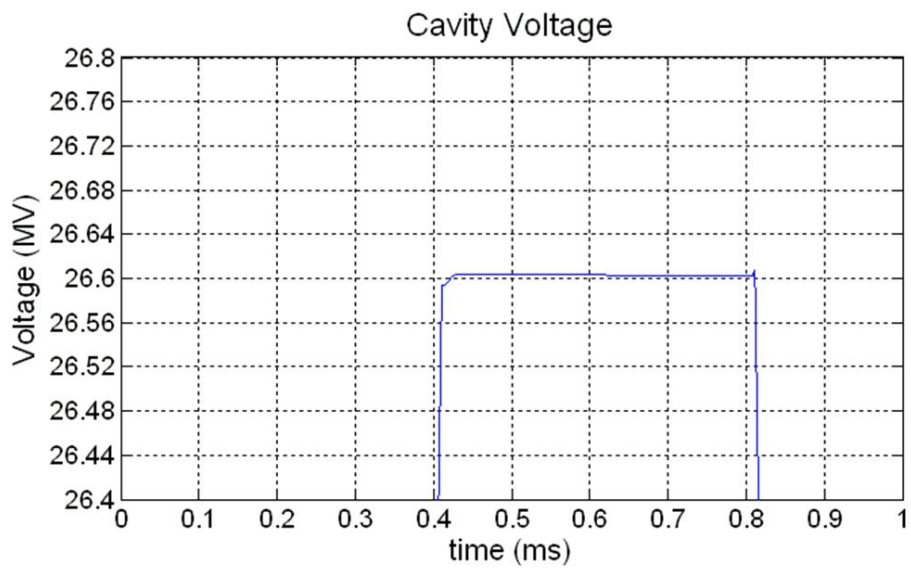


Figure 5.5: Cavity voltage magnitude detail



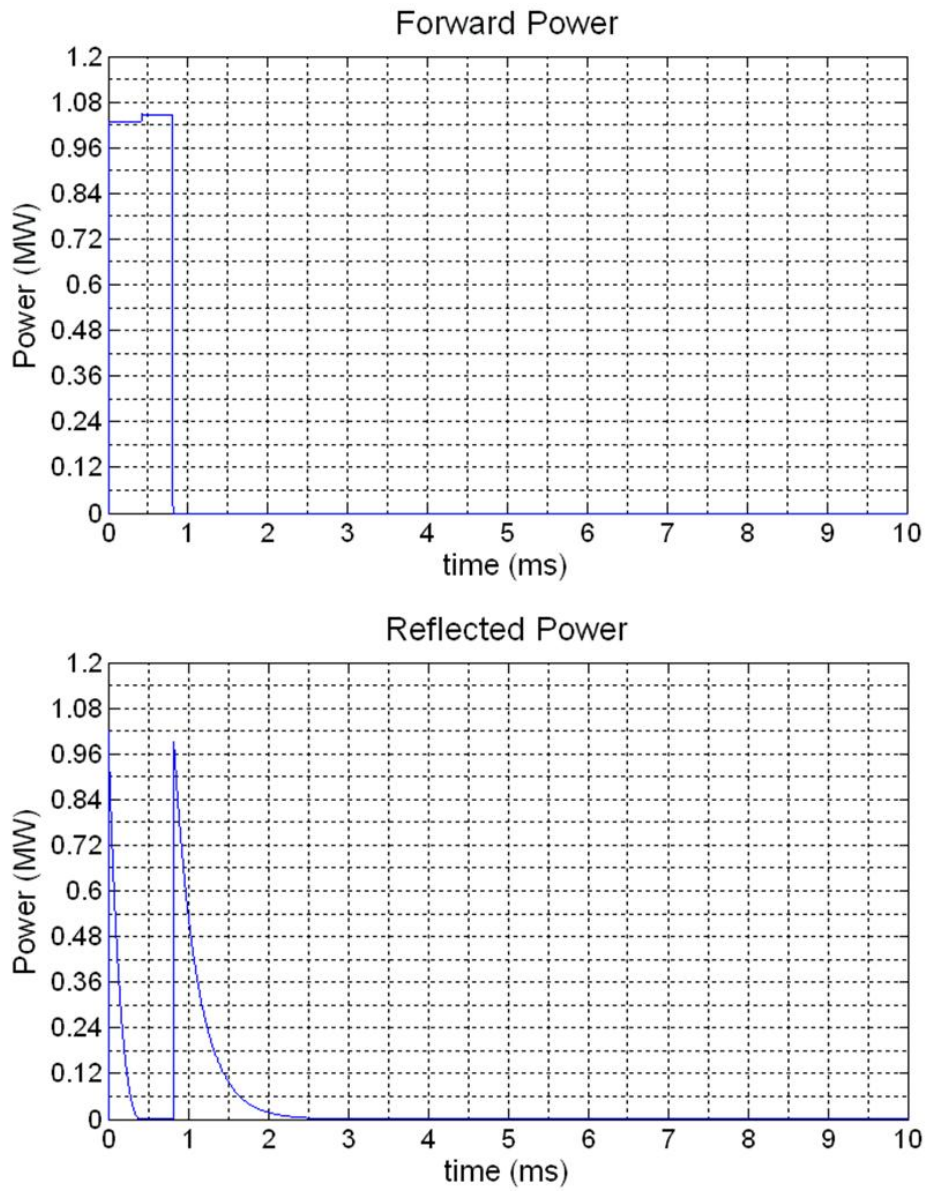


Figure 5.6: Forward and reflected power in closed loop operation

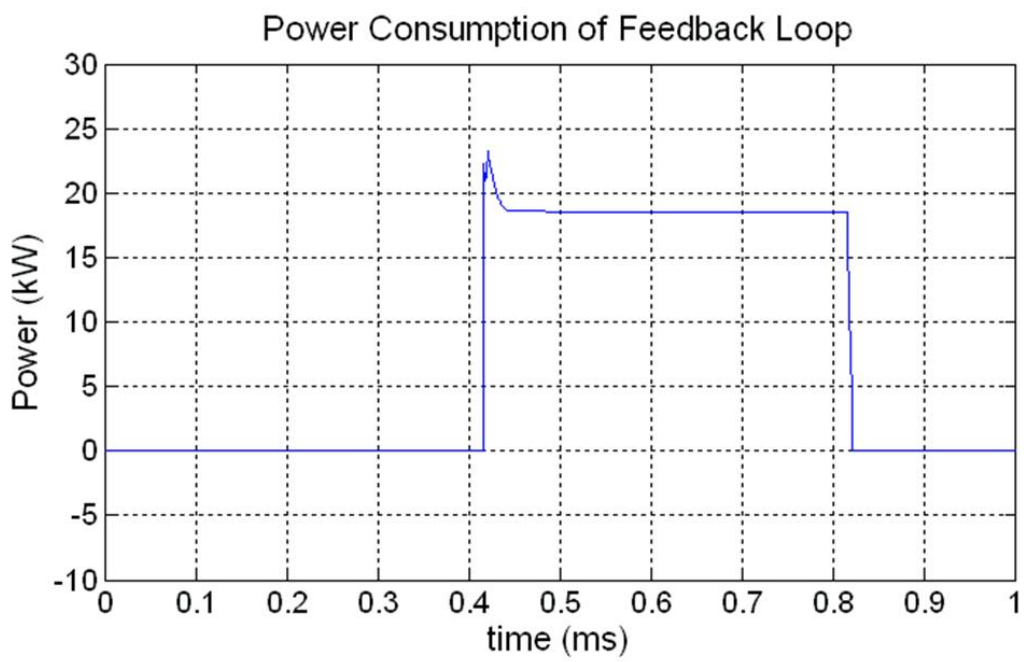


Figure 5.7: Feedback power added

# 1st Turn Power Phasor Diagram

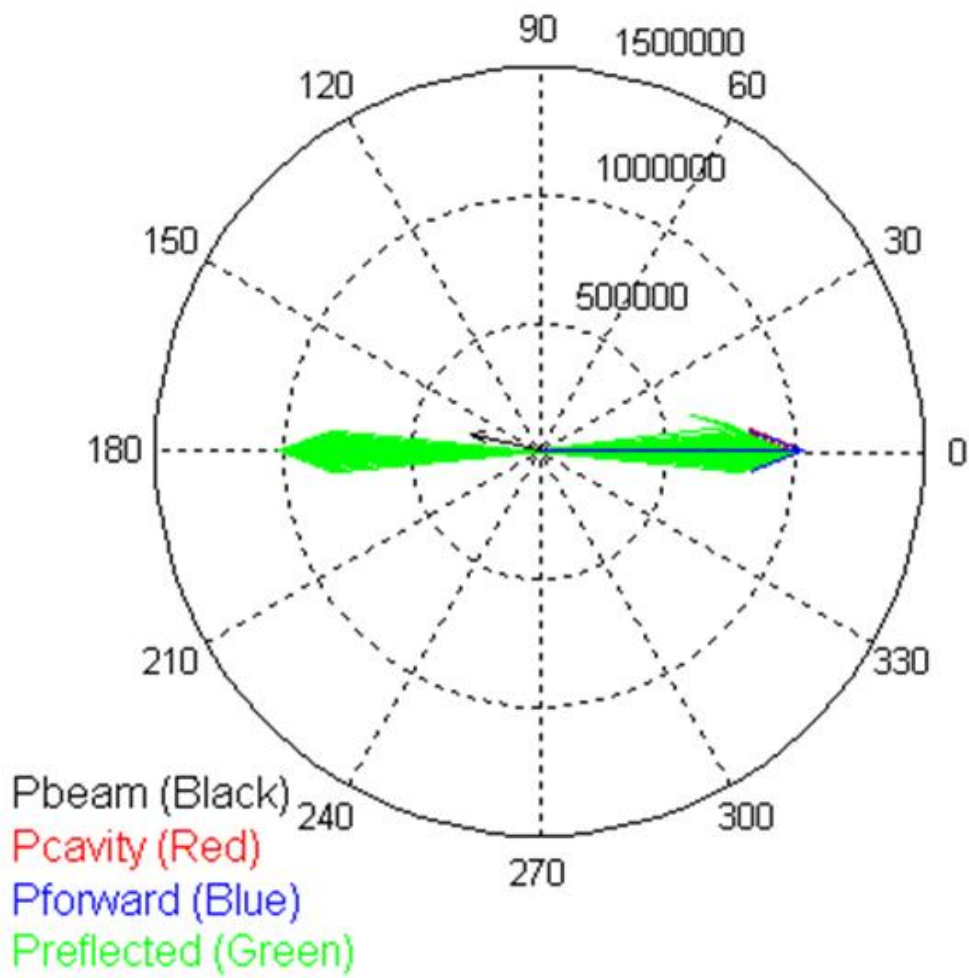


Figure 5.8: Power phasor diagram for closed loop system

## 5.2 Single Cavity with Lorentz Detuning Effects

When a high electric field, and its associated magnetic field, is contained within a resonant cavity, the pressure exerted on the cavity walls due to their magnitudes is known as Lorentz force. Lorentz force can result in the physical deformation of the cavity, which, from the RF point of view, is seen as a damped variation in the resonant frequency of the cavity. This means the cavity is no longer matched to the generator frequency, and this has repercussions on the cavity voltage and power, which means it has effects on the total beam acceleration during beam loading. Taking into consideration the stiffness of the cavity and using experimental results from CEA Saclay, the Lorentz detuning coefficient was set to be of  $-1 \text{ Hz}/(\text{MV}/\text{m})^2$  for the purposes of our model. This results in a time-dependent frequency shift given by a first order differential equation as shown in figure 5.9.

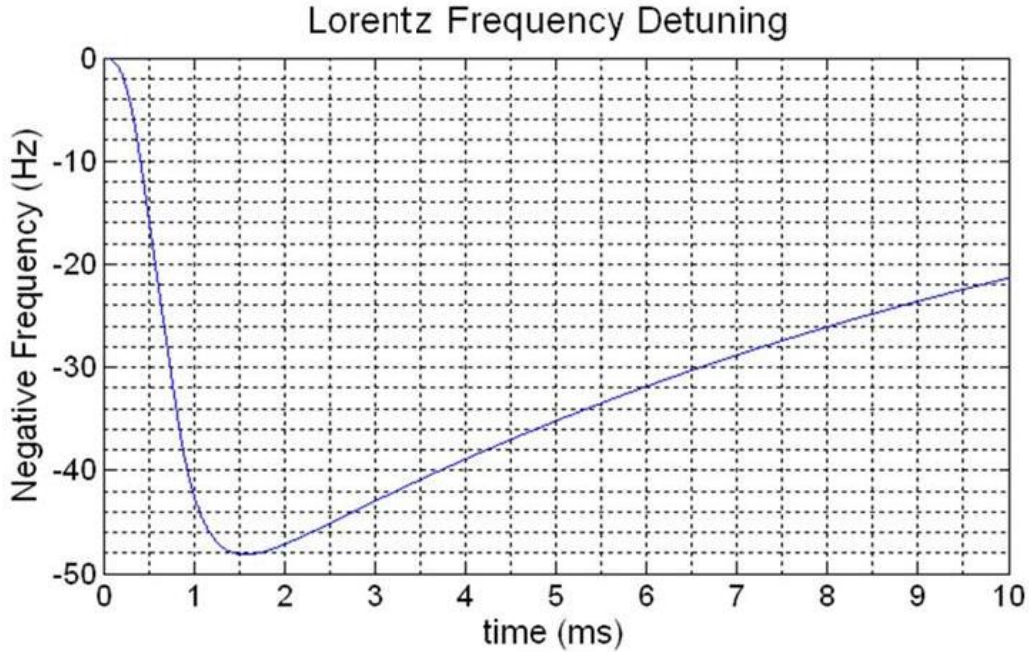


Figure 5.9: Resonant frequency shift due to Lorentz force cavity deformation

$$\frac{d\Delta\omega(t)}{dt} = \frac{1}{\tau} (2\pi K E_{acc}^2 + \Delta\omega_T - \Delta\omega(t)) \quad (5.1)$$

Thus, a frequency shift of  $-1 \text{ Hz}/(\text{MV}/\text{m})^2$  results in about a 50 Hz decrease of the cavity's resonant frequency for the given beam + generator pulse time.

### 5.2.1 Open Loop

The open-loop analysis reveals the effect of Lorentz force detuning on the cavity output, particularly in its output voltage phase. The effect of Lorentz detuning on the cavity voltage magnitude opposes the effect of the beam angle mismatch; now the beam absorbs less power from the generator but due to Lorentz detuning

the generator also delivers less power to the cavity. The Lorentz force (negative coefficient) also opposes the phase shift in the cavity voltage resulting from the beam synchronous angle. After beam loading, however, the cavity is out of tune and the voltage phase will oscillate with a gradient proportional to the detuning. Once again, some reflected power will be observed during beam loading, but it is negligible compared to the filling and dumping of the cavity before and after beam loading.

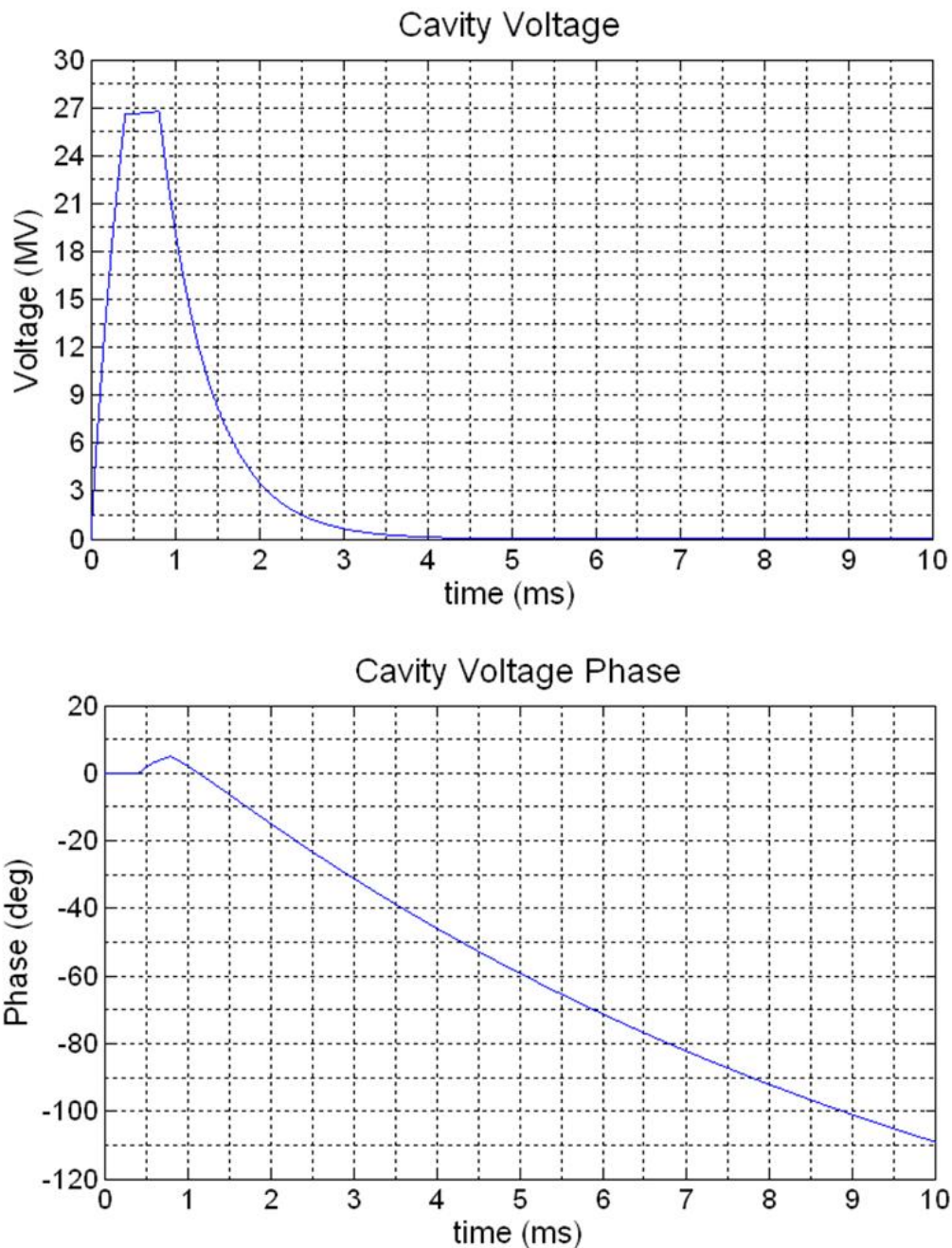


Figure 5.10: Cavity voltage magnitude and phase with Lorentz detuning (Open Loop)

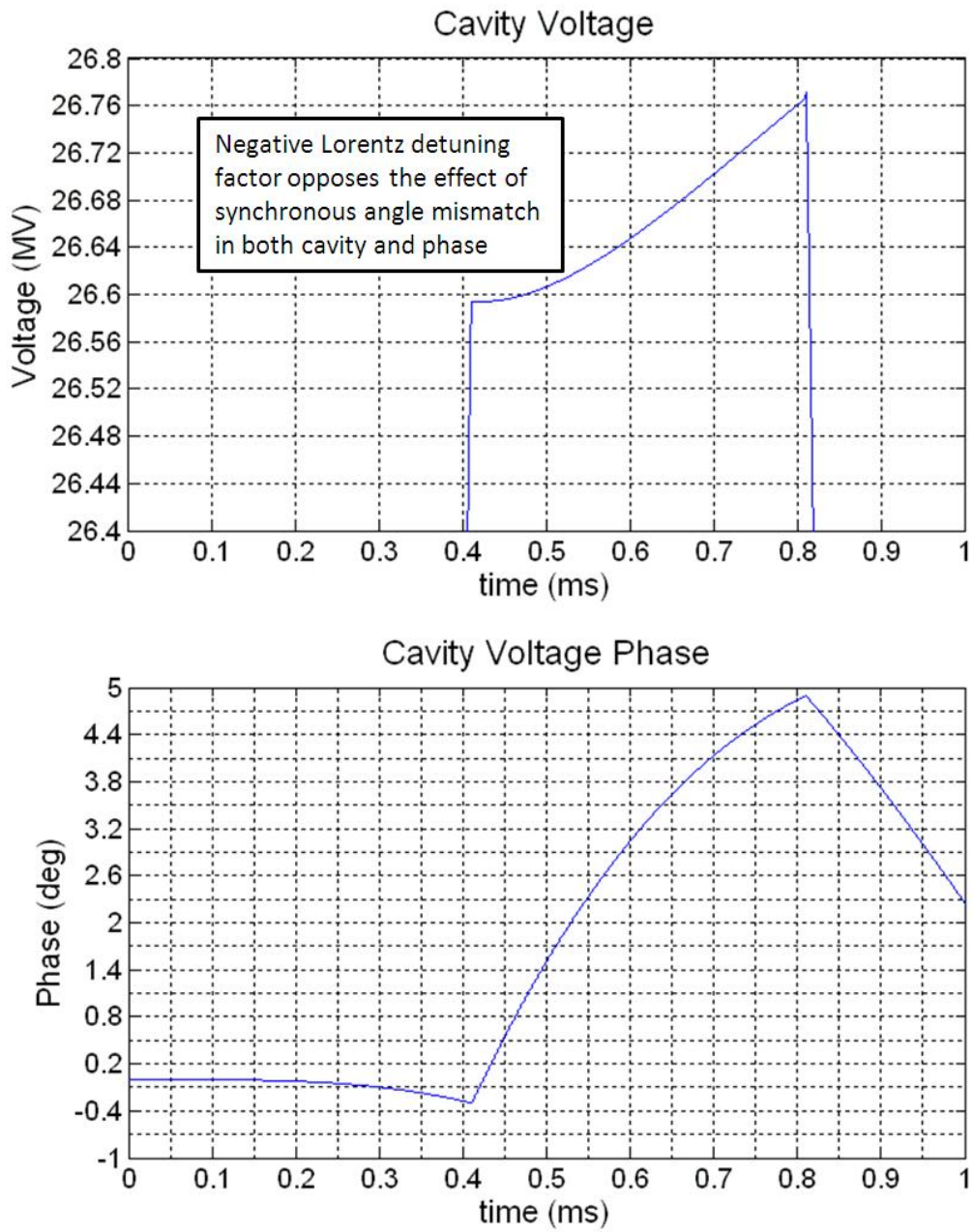


Figure 5.11: Cavity voltage magnitude and phase detail

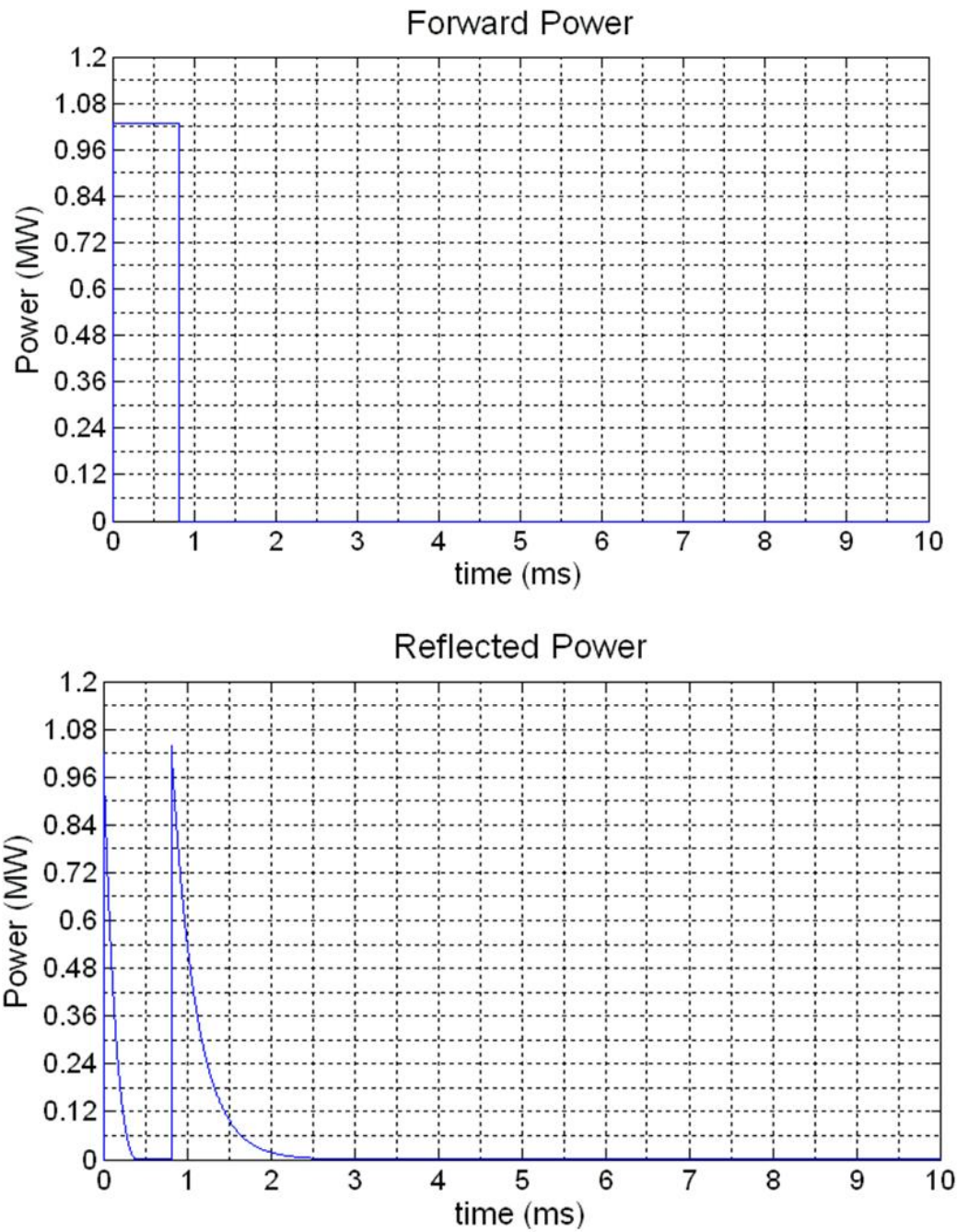


Figure 5.12: Forward and reflected power with Lorentz detuning

## 1st Turn Power Phasor Diagram

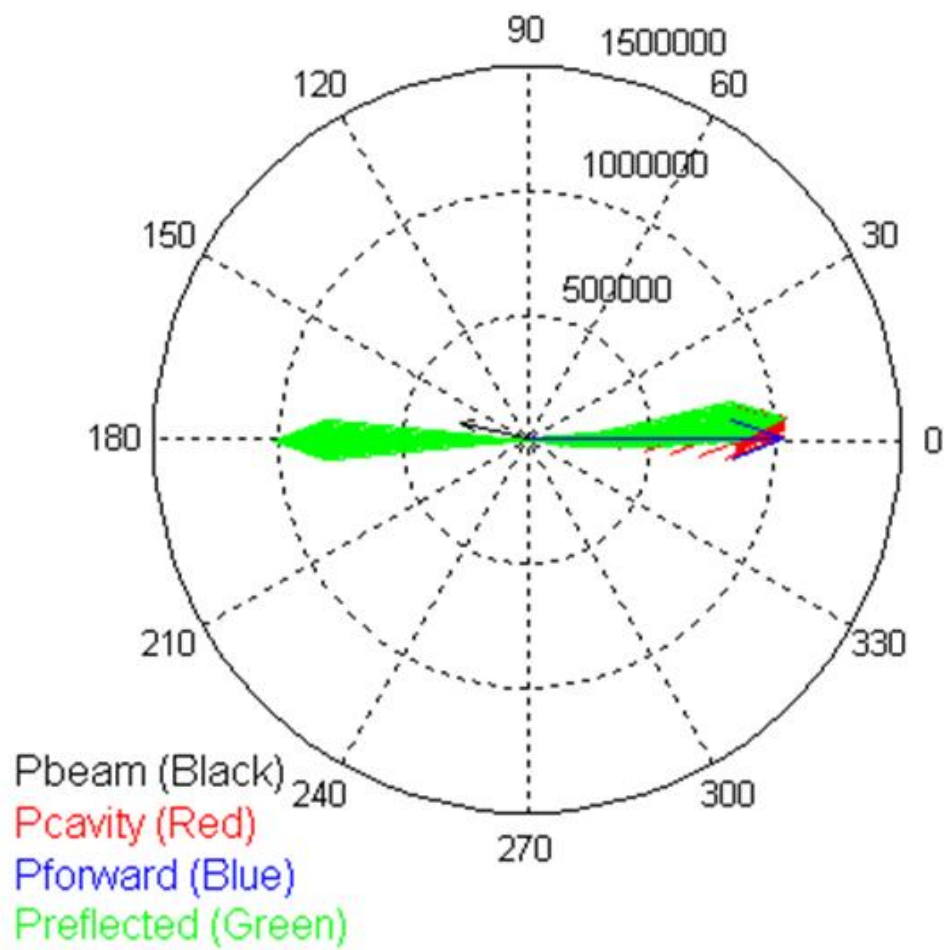


Figure 5.13: Power phasor diagram for open loop system



### 5.2.2 Closed Loop

It is clear that for the correct operation of the system, the feedback needs to compensate for Lorentz detuning and beam angle effects. Now, as mentioned before, the feedback loop is closed (ON) during beam loading, and open (OFF) right after until the next generator pulse. We can now see that both the cavity voltage magnitude and phase are within design parameters, with the added phase shift when the loop is OFF due to the mismatch between generator frequency and cavity resonant frequency. Due to the fact that negative Lorentz detuning opposes the effect of beam angle mismatch in both the cavity voltage amplitude and phase, the feedback power required is actually lower than for the former case (no Lorentz detuning) as the beam pulse progresses. For the case of a beam passing with a 15 degree synchronous angle through a cavity with a Lorentz coefficient of  $-1 \text{ Hz}/(\text{MV}/\text{m})^2$ , driven by a 1.03 MW generator, the maximum feedback power required is of about 23 kW, but it decreases during the beam pulse due to the Lorentz effects.

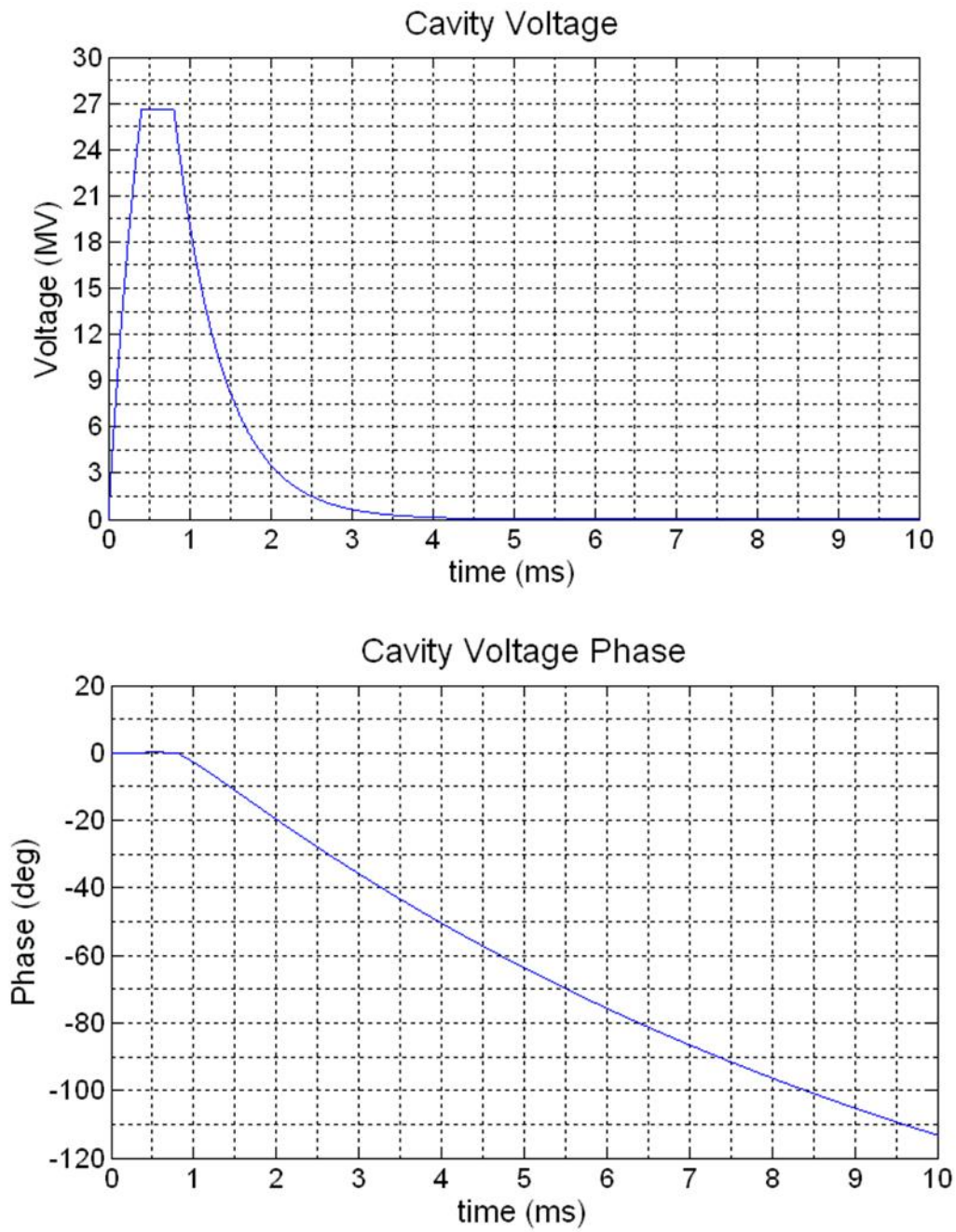


Figure 5.14: Cavity voltage magnitude and phase with Lorentz detuning (Open Loop)

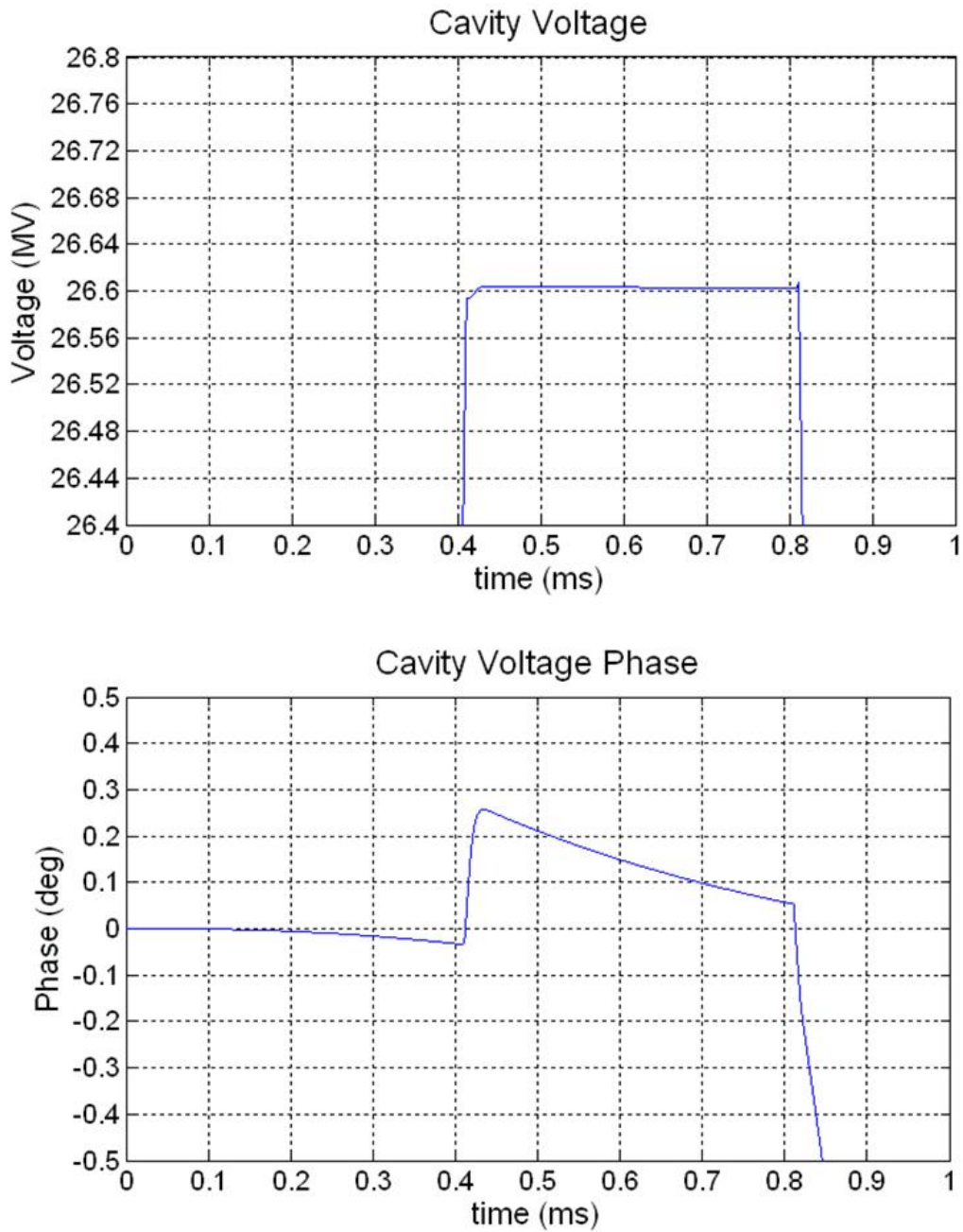


Figure 5.15: Cavity voltage magnitude and phase detail

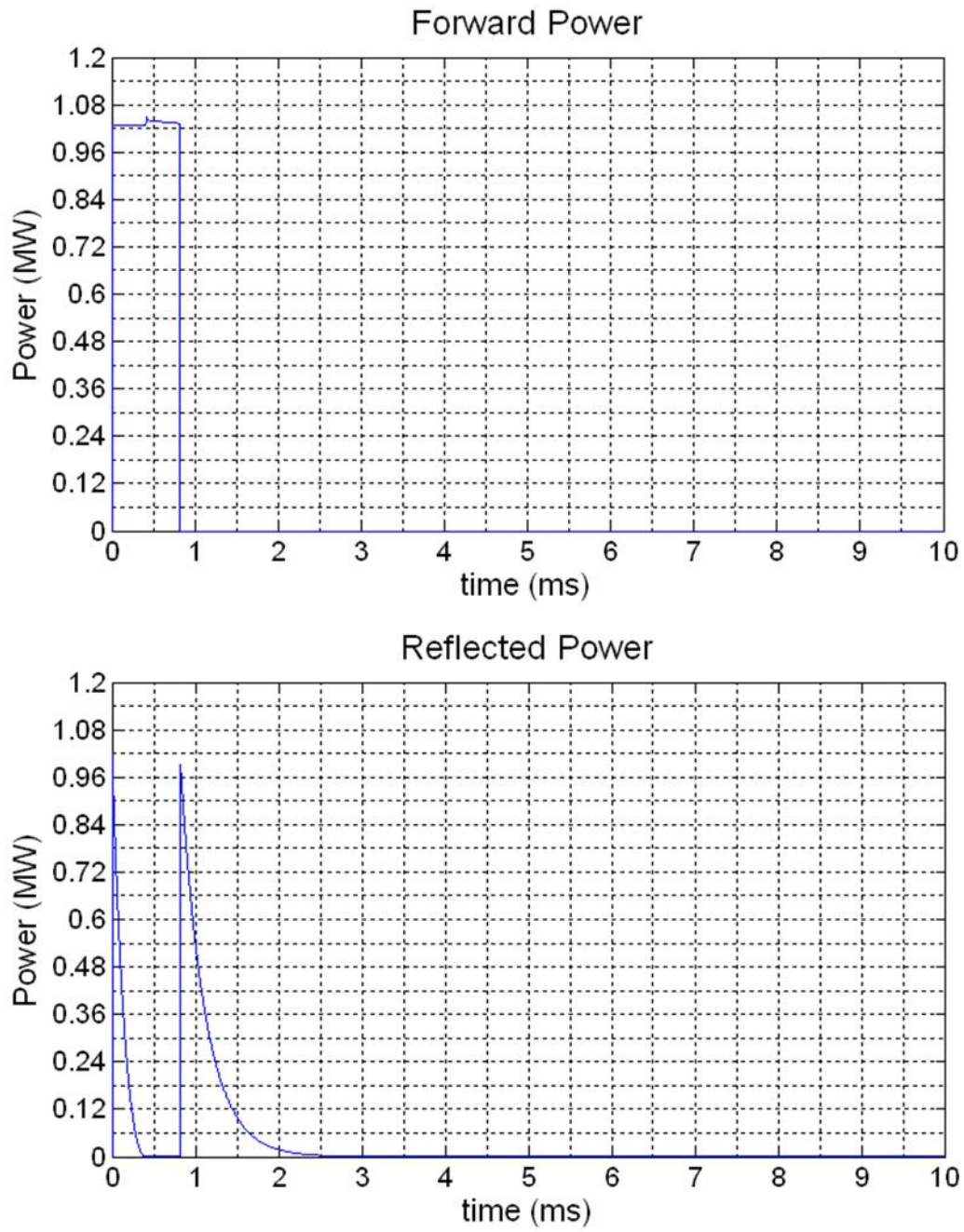


Figure 5.16: Forward and reflected power with Lorentz detuning

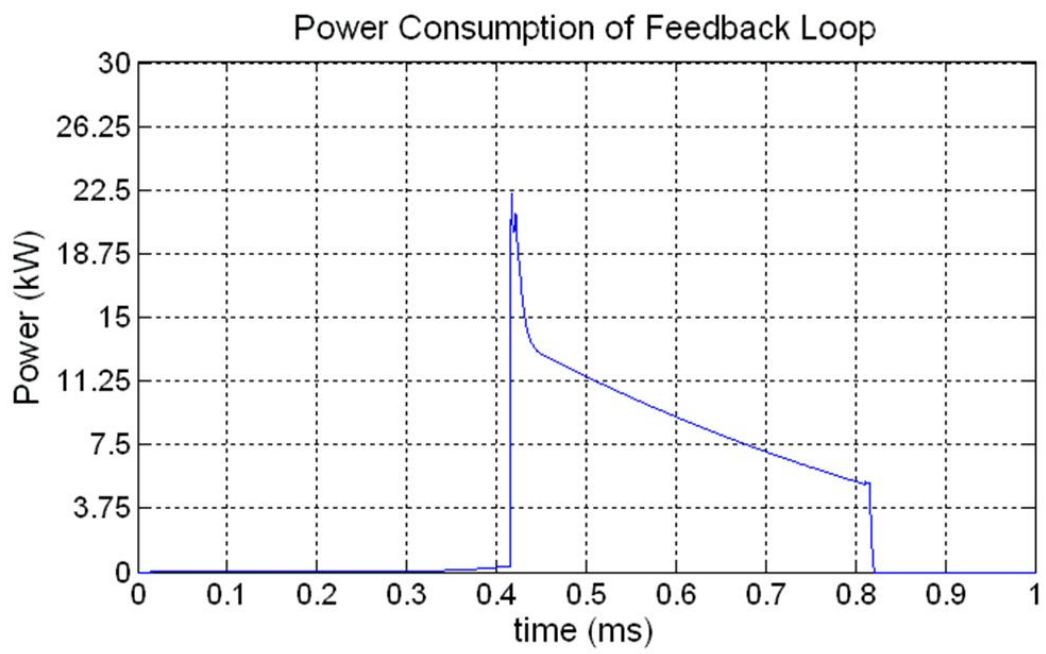


Figure 5.17: Feedback power added

# 1st Turn Power Phasor Diagram

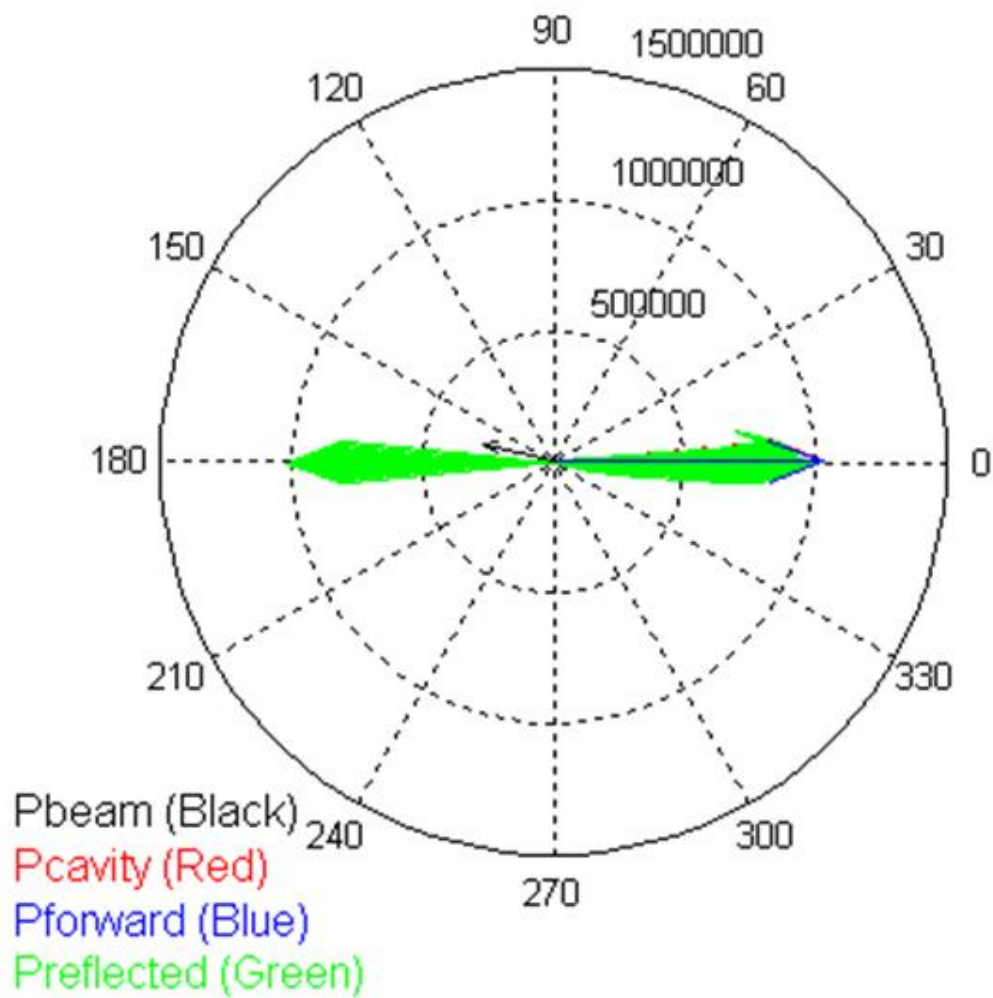


Figure 5.18: Power phasor diagram for open loop system

### 5.2.3 Variation of Source Beam Current: Low and High Power SPL Operation

In both high current and low current operation cases for the SPL specifications, the source repetition rate is of 50 Hz. The hydrogen ion source for the LINAC has a specified beam current that can vary within the beam pulse. This variation has been observed to be up to 5% of the nominal beam current. For the purpose of our simulations, we added this variation to ensure that the control loop was adequate. As shown in the following results, the feedback loop has no trouble compensating for the current variations, provided enough power is available. The feedback power requirements were found to be around 30kW/mA for the matched case, and around 20kW/mA for the mismatched (20mA beam current) case. The 20 mA SPL operation has no significant differences with the 40 mA case with respect to cavity voltage phase and magnitude behaviour. It is interesting, however, to note the effects of the power mismatch prior to beam loading and the effects of the mismatched beam on the feedback loop. This would be the case if a lower current beam is sent to an RF system with a loaded quality factor that is optimised for 40 mA operation. This will give us an idea of the power requirements for mismatched operation.

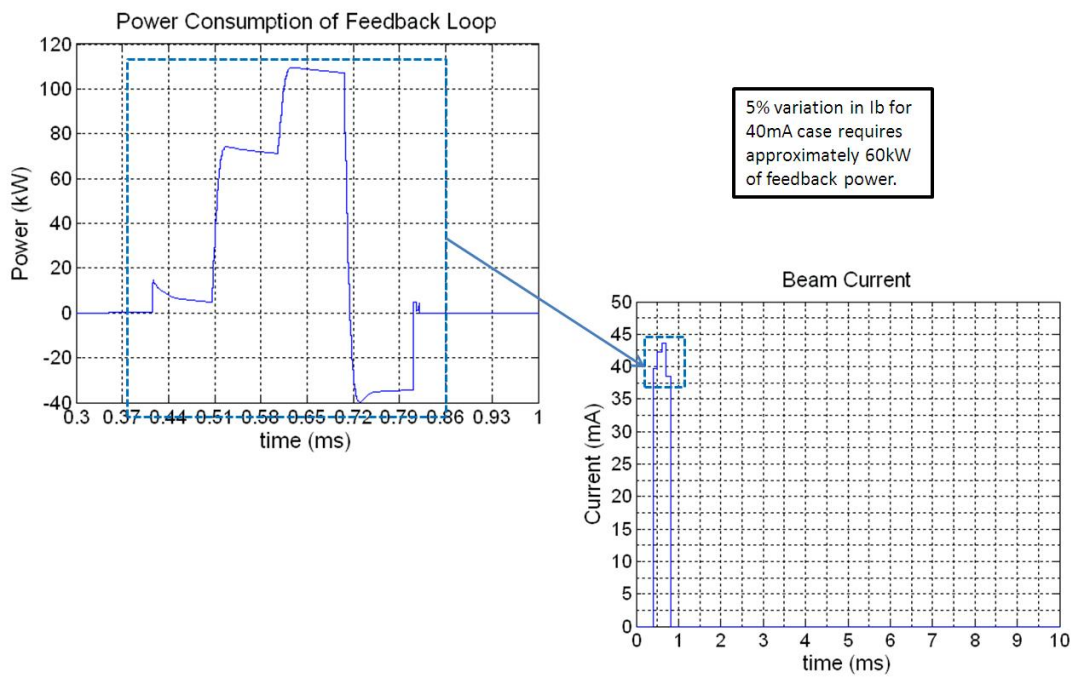
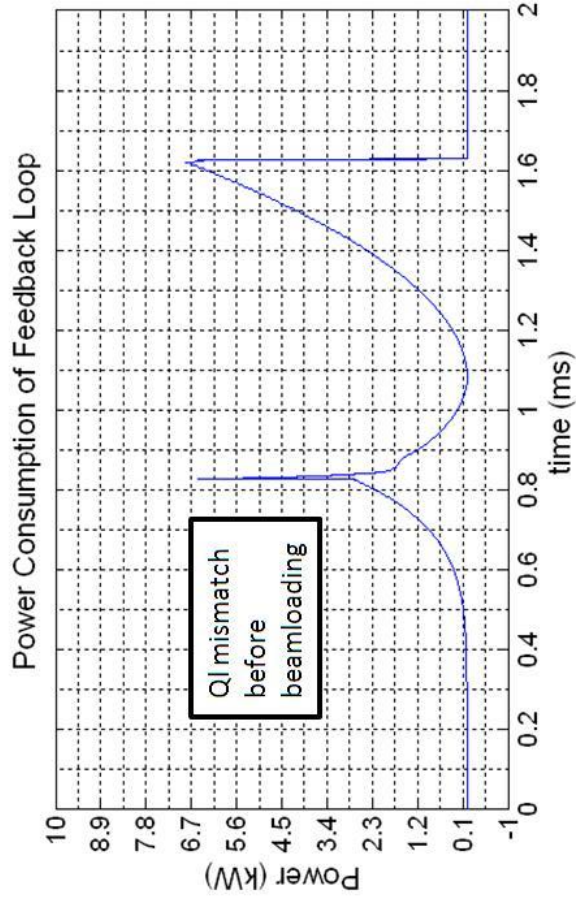
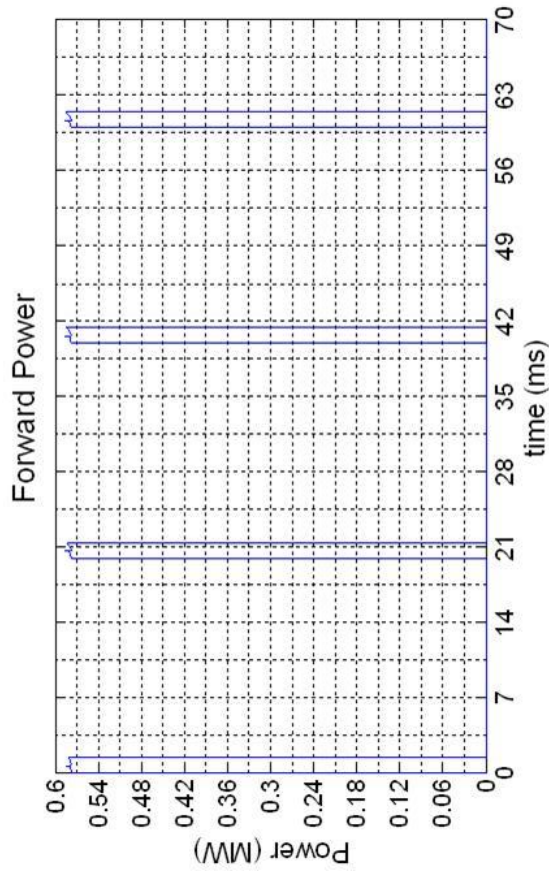


Figure 5.19: Effect of beam current variation on feedback power (matched operation)



$$I_{b,DC} \cong 20 \text{ mA}$$

$$P_b = V_{acc} \times I_{b,DC} \times \cos(\phi_s) \cong 514 \text{ kW}$$

$$Q_{L, \text{fixed}} = R \frac{V_{acc}}{\frac{1}{Q} \times I_{b,40\text{mA}} \times \cos(\phi_s)} \cong 1.3113 \times 10^6$$

$$I_g = \frac{V_{acc}}{R_L} + I_{b,DC} \cos(\phi_s) = 58 \text{ mA}$$

$$\alpha = \frac{I_g}{I_{b,DC} \cos(\phi_s)} = 3$$

$$\tau_{fill} = \frac{2Q_L}{\omega_{RF}} = 0.5926 \text{ ms}$$

$$t_{inj} = \tau_{fill} \ln(\alpha) = 0.6510 \text{ ms}$$

$$P_{fwd} = \frac{1}{4} R_L |I_g|^2 = 578 \text{ kW}$$

$$t_{pulse} = 0.8 \text{ ms}$$

Figure 5.20: Low-power operation of SPL (power considerations)



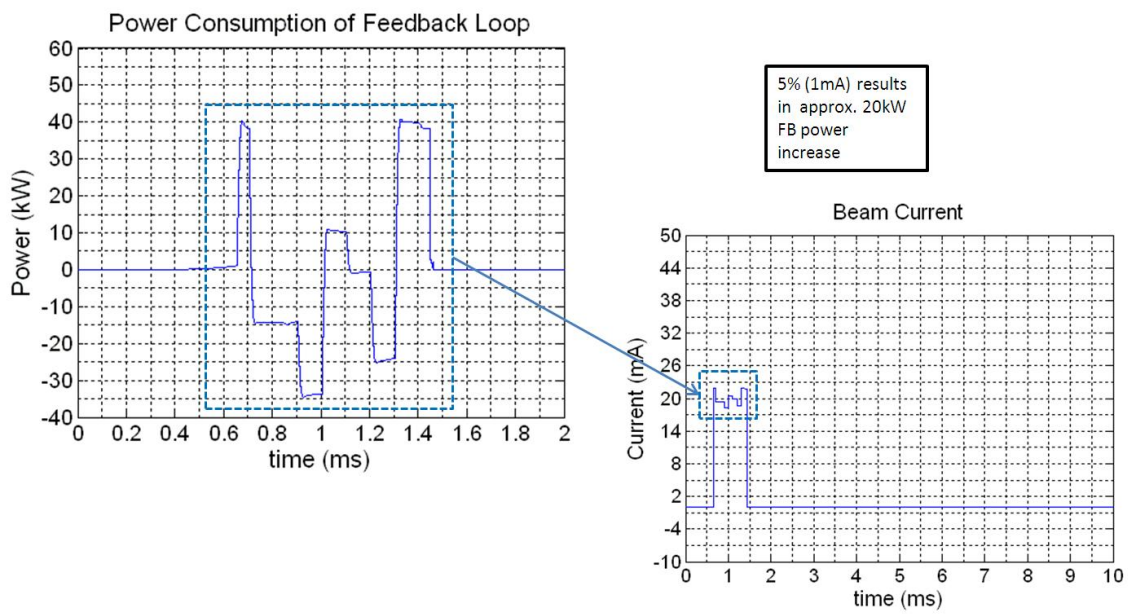


Figure 5.21: Effect of beam current variation on feedback loop power consumption (mismatched operation)

## 5.3 Dual-Cavity Case

### 5.3.1 The Need for Feed-Forward

In context with the superconducting SPL project, there are a few possible schemes to use as a solution for power requirements and design constraints. Until this point, this report has dealt with the case of one 1.6 MW Klystron driving a single cavity to accelerate a 40mA or 20mA beam, the following results deal with a different possible scheme in which a single Klystron will be used to supply two cavities, and the model is capable of dealing with a quad-cavity scheme driven by a single Klystron. As the results for the 4-cavity case do not reveal new information on the operation of the feedback and feed-forward loops, or on power requirements, the results are not displayed in this report. They are observable, however, using the graphical user interface. Figures 5.22, 5.23, and 5.24 below show the cavity voltage of both cavities separately and of their vector sum. The cavities are identical but for their Lorentz detuning coefficient (-1 and -0.5 Hz/(MV/m)<sup>2</sup> respectively). If we are able to control only the vector sum output of two cavities, it is possible, as the figures suggest, to observe a vector sum within specifications resulting from two cavities whose phases are well outside the acceptance range of 0.5 degrees. The cavity voltage magnitude is controlled acceptably for both cavities but, if the individual phase of each cavity is critical, the necessity for the addition of feed-forward becomes quite clear.

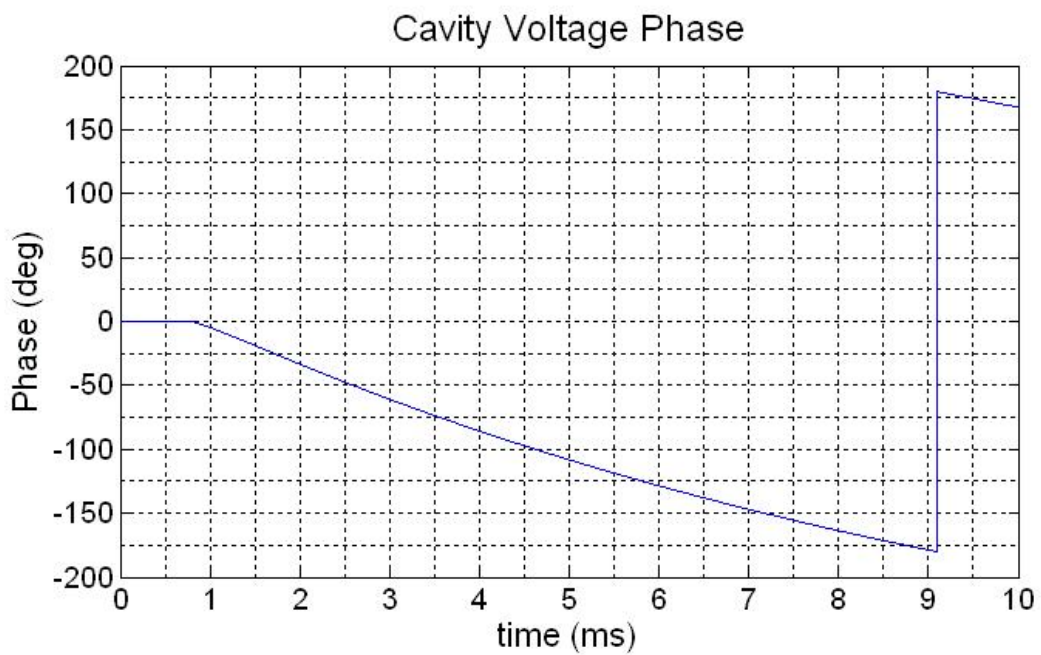
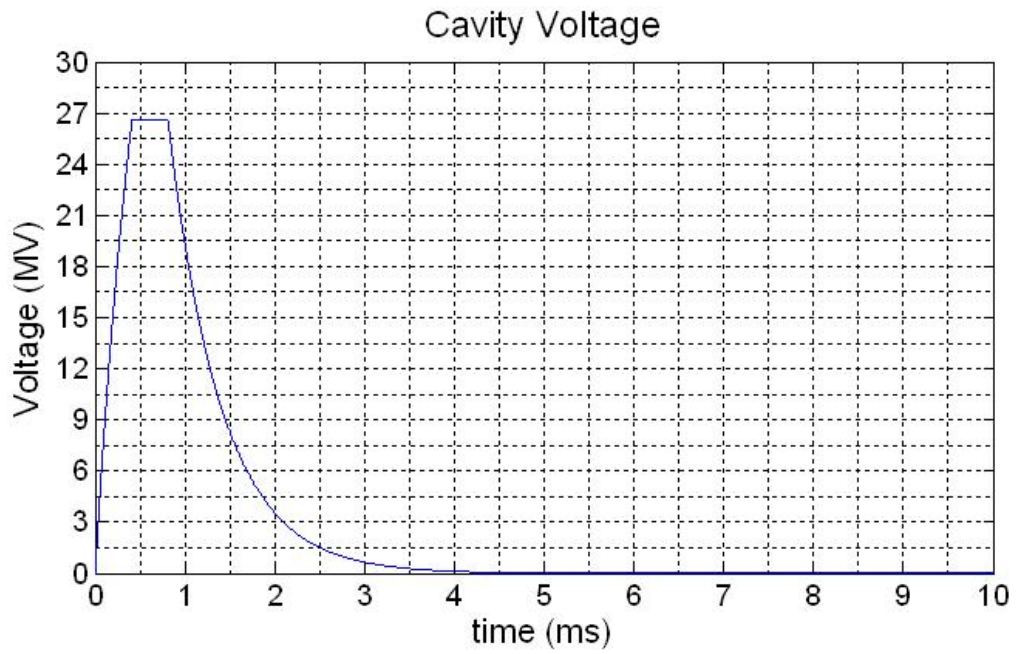


Figure 5.22: Cavity voltage magnitude and phase of vector sum output, feedback loop is ON

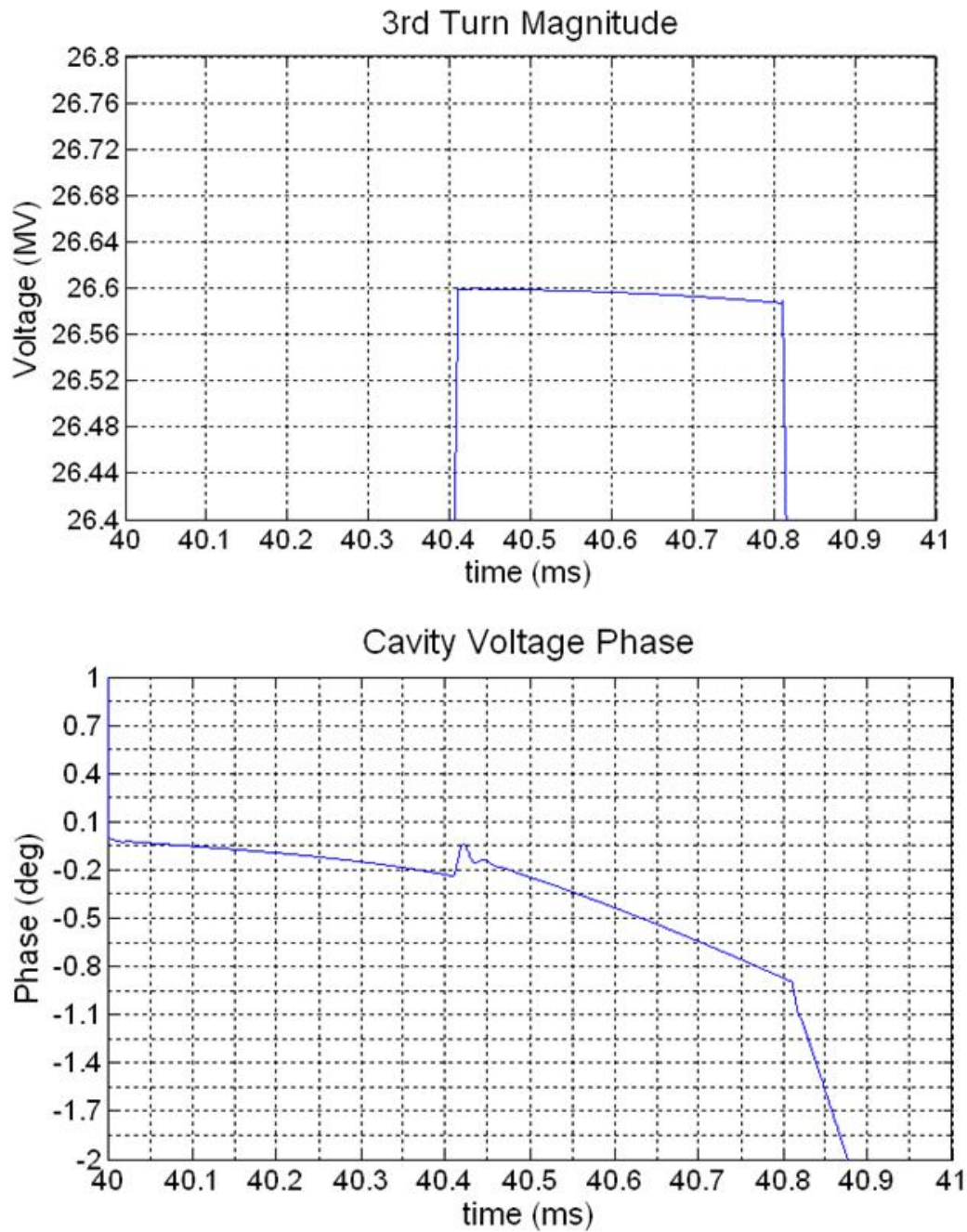


Figure 5.23: Cavity voltage magnitude and phase for cavity 1

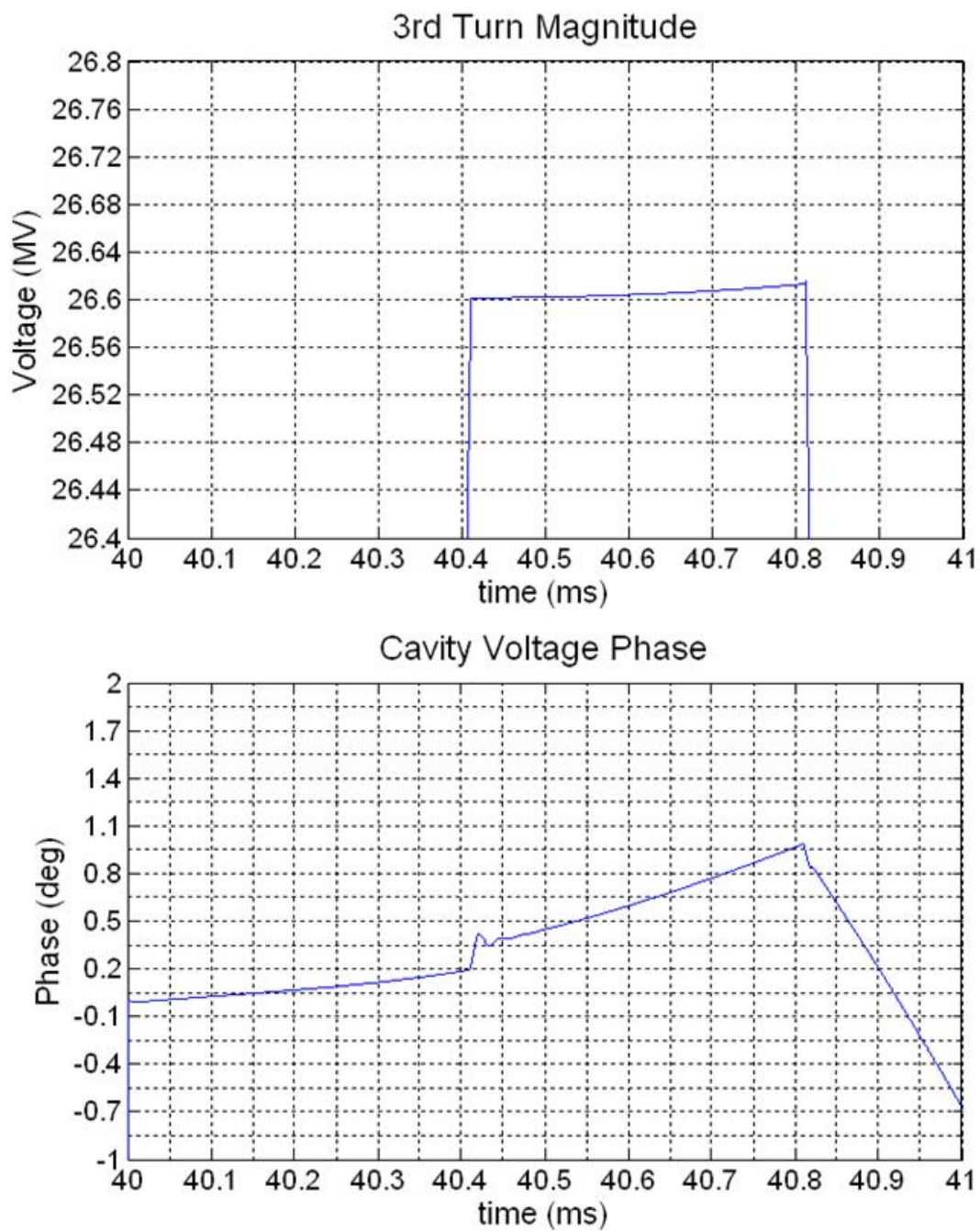


Figure 5.24: Cavity voltage magnitude and phase for cavity 2

### 5.3.2 Dual Cavity with Feed-Forward

The following results show the output of the cavity when using feed-forward. The model uses Kalman filtering to estimate the cavity voltage magnitude from a noisy measurement of the cavity voltage I/Q components. This is then used to estimate the Lorentz force detuning due to that (estimated) voltage and finally the estimated detuning is directly subtracted from the actual detuning within the model in an effort to imitate the effects of a similar waveform produced by the piezoelectric circuitry installed in the real cavities. There are a couple of shortcomings with this model that can be foreseen; first of all, the tuning of the Kalman filter will have to be set in real life as the Kalman filter process model might be too close to the actual model as they are both done in SIMULINK (as opposed to real life and FPGAs), and more importantly there is the need for transfer function characteristics and power consumption of the piezoelectric circuit to really model the actual performance. This can introduce noise of its own and, once again, some tuning might be necessary for practical applications.

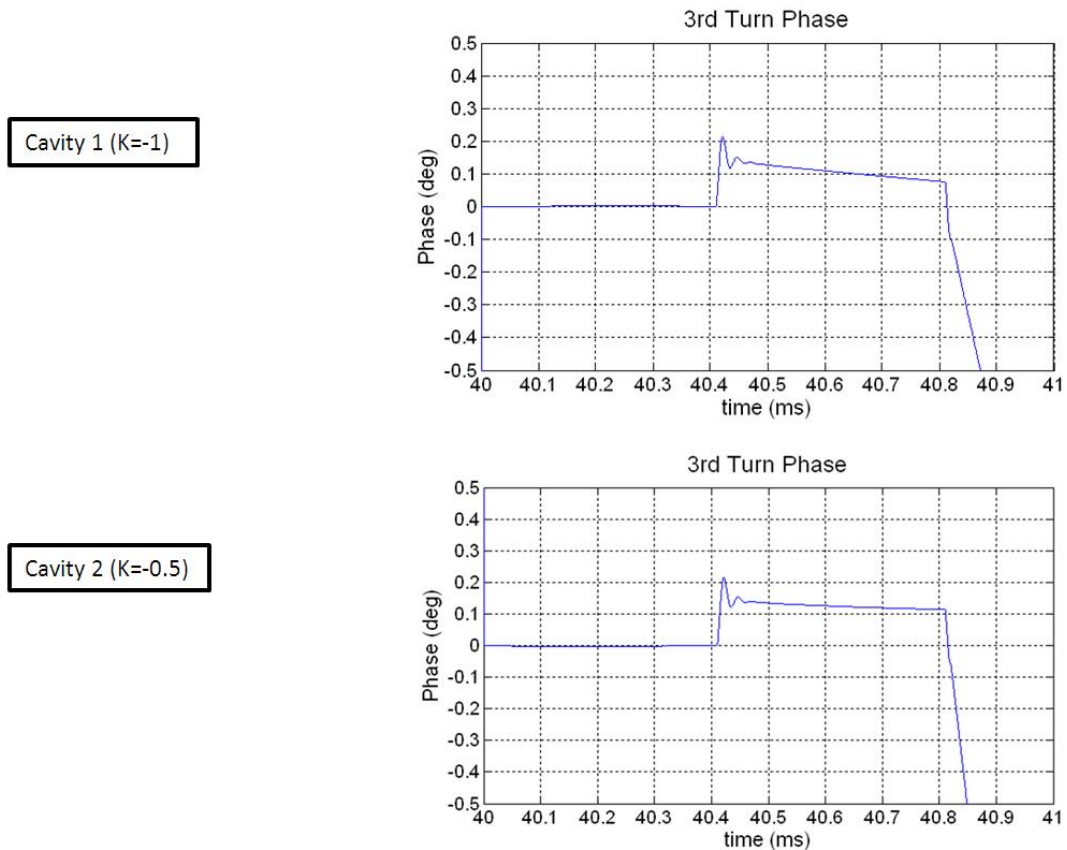


Figure 5.25: Cavity phase for cavities controlled by a single loop, feed-forward correction is applied

### 5.3.3 Loaded Quality Factor Mismatch

As previously mentioned; when feeding multiple cavities using a single Klystron, it is not possible to control each cavity output individually, but rather the vector sum of each voltage. This means that there is nothing we can do with the control loop to compensate for variations within the individual cavities in loaded quality factor. The control loop will optimise the vector sum while the individual cavities might diverge from the specifications of SPL operation. According to modelling results, for the deviation constraints for the cavity voltage magnitude of  $\pm 0.5\%$  of the total ( $26.6 \times 10^6 MV$ ), we find that the limit of  $Q_L$  difference lies around 1.5% difference in value between both cavities, where the optimum value is  $1.3113 \times 10^6$ .

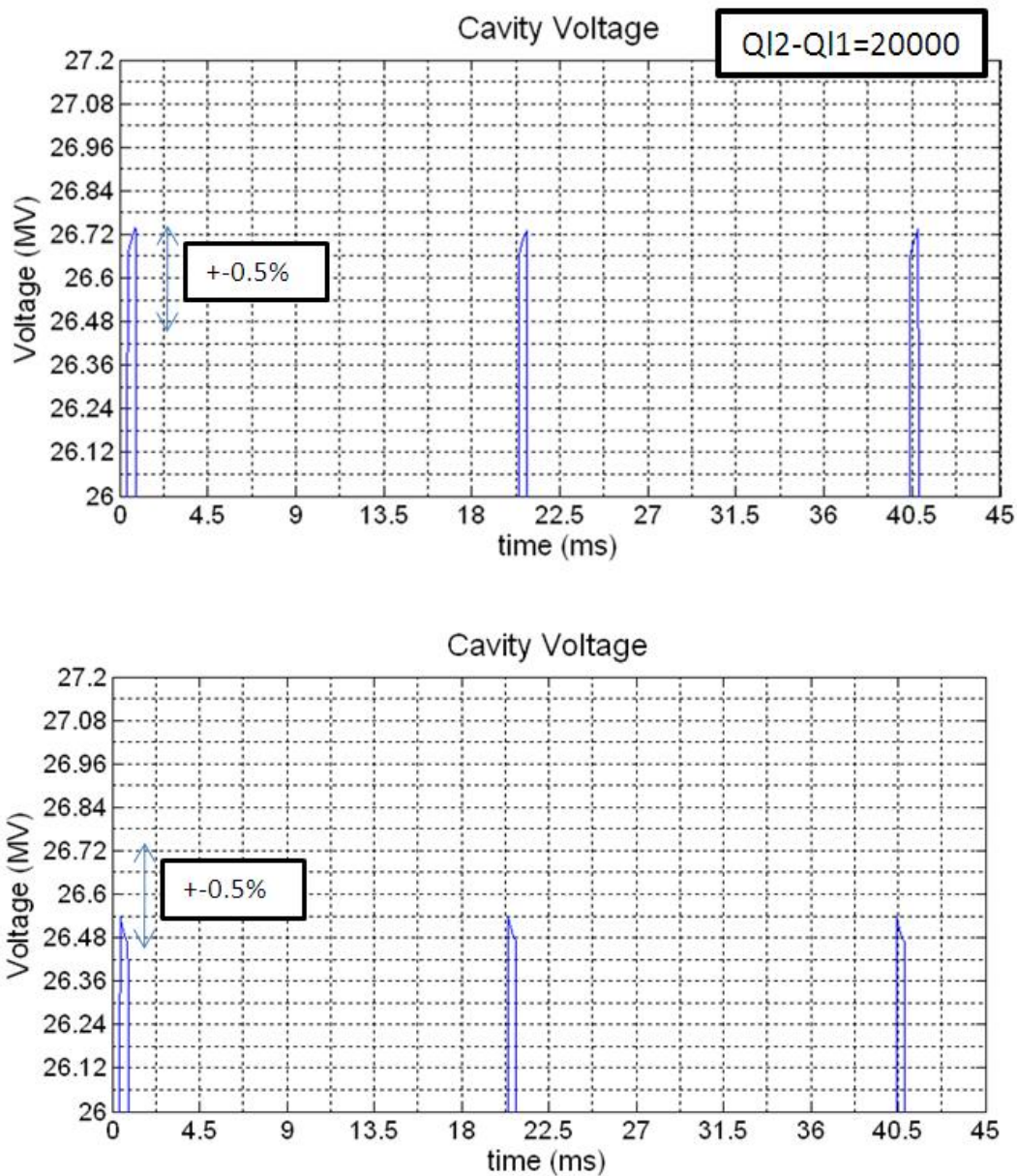


Figure 5.26: Effect of 20k (1.5%) difference between loaded quality factors of resonant cavities

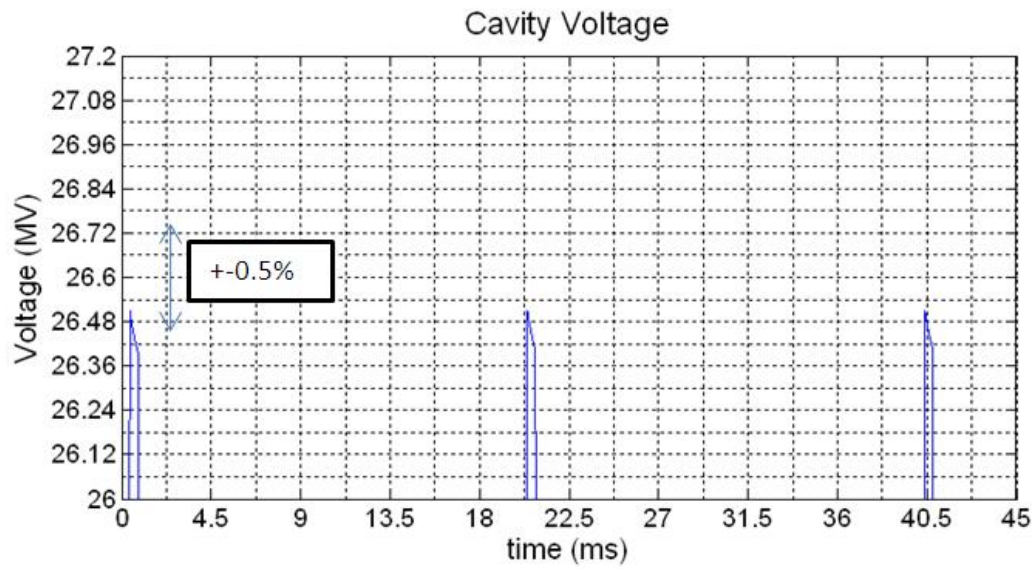
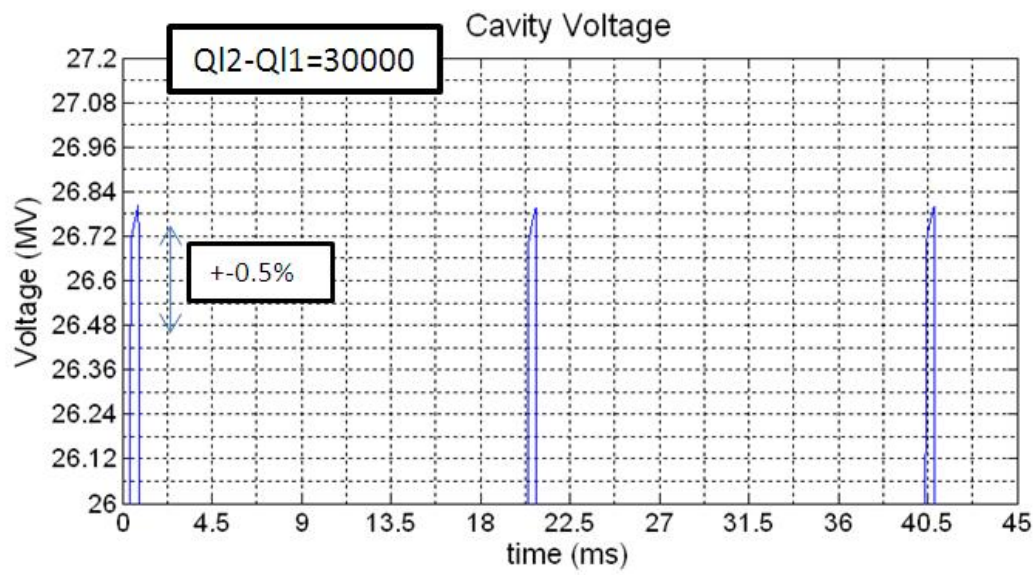


Figure 5.27: Effect of 30k (2.2%) difference between loaded quality factors of resonant cavities



## 5.4 Error Analysis and Stability Considerations

Until this point in the report, we have shown the versatility of the model with regard to the stabilisation of the electric field within superconducting RF resonant cavities with the specifications needed to build the SPL. However, no analysis is full without pointing out some of the limitations of the system. As shown in the last chapter, a  $>1.5\%$  difference in the cavities' quality factor can result in a deviation on cavity voltage magnitude that cannot be resolved using feedback or feed-forward when more than a single cavity is driven by one Klystron. The feedback loop compensates the vector sum of the cavity voltages, keeping it within specifications (0.5% magnitude and  $0.5^\circ$  phase deviations), but that does not mean that each cavity separately is also exhibiting the same behaviour. The cavity voltage magnitudes vary with the difference in the loaded quality factors and their magnitudes and phases vary with the difference in their Lorentz detuning coefficients. To observe the extent of these variations, a simulation sweep was carried out, recording the voltage magnitude difference at the output, as well as the phase difference (voltage of cavity 1 minus voltage of cavity 2). For both the loaded quality factor ( $Q_L$ ) and Lorentz detuning coefficient sweeps (K), it was found that fitting a curve based on the results was more suited than an analytic approach. With this curve, an exhaustive analysis using a model for the whole SPL length can be developed as a parallel project, to observe if the beam cannot ultimately tolerate the single cavity variations even though their overall effect (vector sum) might appear within specifications. The results are as follows:

### Cavity voltage difference between two cavities with different loaded quality factors

$$Q_{L\_optimal} = 1.3113 \times 10^6$$

Measurements of the voltage difference between both cavities were taken with feedback control on their vector sum. As the quality factor of the cavities has no impact on their voltage phases, the analysis is restricted to cavity voltage magnitudes. The sweep was done using values for  $Q_{L1}$  and  $Q_{L2}$  (for cavities 1 and 2 respectively) from  $1e6$  to  $1.5e6$  at  $1e4$  intervals resulting in 51 different values of  $Q_L$  and  $51*51=2601$  different  $Q_{L1}, Q_{L2}$  combinations minus redundant values. Thus, the obtained  $V_{diff} = f(Q_{L1}, Q_{L2})$  curve was fitted using 1326 points. The polynomial equation relating the voltage output difference to the individual loaded quality factors of the cavities was found to be of the form

$$V_{diff}(x, y) = p00 + p10x + p01y + p20x^2 + p11xy + p02y^2 \quad (5.2)$$

where  $x = Q_{L1}$  and  $y = Q_{L2}$ , with coefficients:

$$p00 = 1.725 \times 10^6$$

$$p10 = 34.88$$

$$p01 = -37.66$$

$$\begin{aligned}
p20 &= -8.311 \times 10^{-6} \\
p11 &= 1.527 \times 10^{-7} \\
p02 &= 9.27 \times 10^{-6}
\end{aligned}$$

Figure 5.28 below shows the curve fit. The blue points are given by model experimental results, while the continuous plane is given by the equation above. The individual cavity voltages can be reproduced as  $V_{cav1} = V_{acc} + \frac{V_{diff}}{2}$  and  $V_{cav2} = V_{acc} - \frac{V_{diff}}{2}$ , where the low voltage corresponds to the cavity with lower  $Q_L$ .

### Cavity voltage difference between two cavities with different Lorentz detuning coefficients

$$K_{optimal} = 0 \text{ Hz}/(\text{MV}/\text{m})^2$$

As before, measurements were taken in closed-loop operation with no feed-forward. In this case, however, both the cavity voltage magnitude and phase are affected by varying Lorentz detuning coefficients. Two curves are therefore fitted, with values of  $K$  from  $-1 \text{ Hz}/(\text{MV}/\text{m})^2$  to  $+1 \text{ Hz}/(\text{MV}/\text{m})^2$  using  $0.01 \text{ Hz}/(\text{MV}/\text{m})^2$  intervals (20301 points). Figures 5.29 and 5.30 show the fitted surfaces for magnitude and phase difference respectively. The respective polynomials for the voltage magnitude and phase difference were found to be:

$$V_{diff}(x, y) = p00 + p10x + p01y + p20x^2 + p11xy + p02y^2 \quad (5.3)$$

with coefficients:

$$\begin{aligned}
p00 &= 25.8 \\
p10 &= -2.05 \times 10^{14} \\
p01 &= 2.014 \times 10^{14} \\
p20 &= -3.496 \times 10^{28} \\
p11 &= -1.565 \times 10^{26} \\
p02 &= 3.505 \times 10^{28}
\end{aligned}$$

and:

$$V_{diff}(x, y) = p00 + p10x + p01y \quad (5.4)$$

with coefficients:

$$\begin{aligned}
p00 &= -0.0004408 \\
p10 &= 3.768 \times 10^{12} \\
p01 &= -3.768 \times 10^{12}
\end{aligned}$$

where  $x=K1$  and  $y=K2$ .

Once again, the individual cavity voltage magnitudes can be found using the aforementioned formula centered at  $V_{acc}$ . The phase equation is centered at  $0^\circ$ .

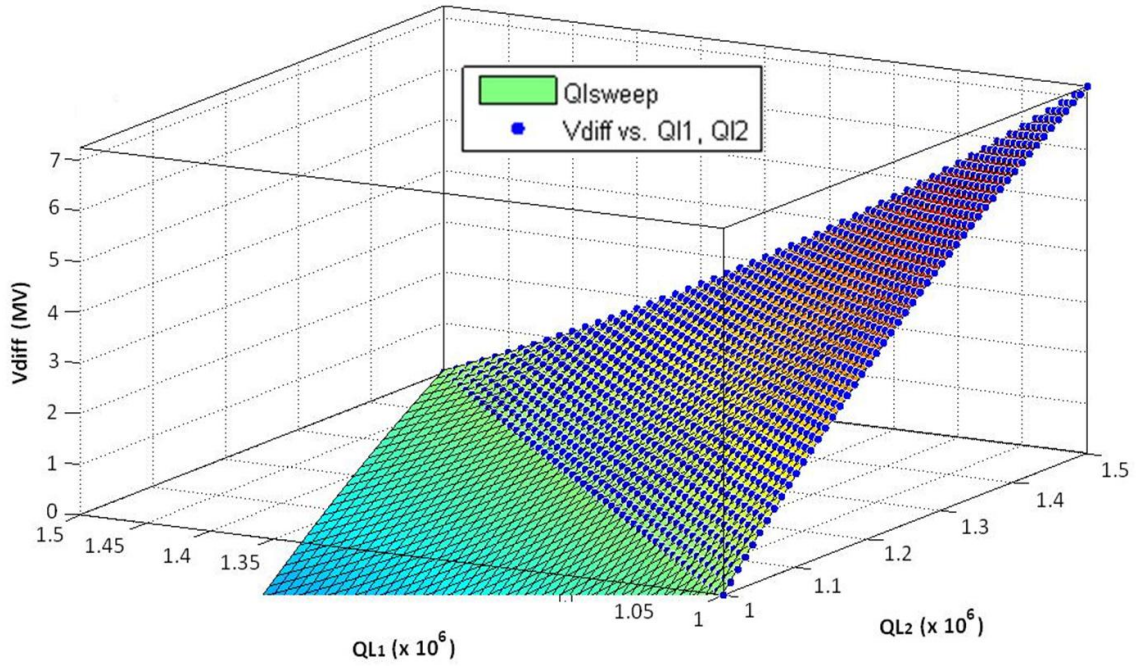


Figure 5.28: Curve fit for cavity voltage difference with varying loaded quality factor

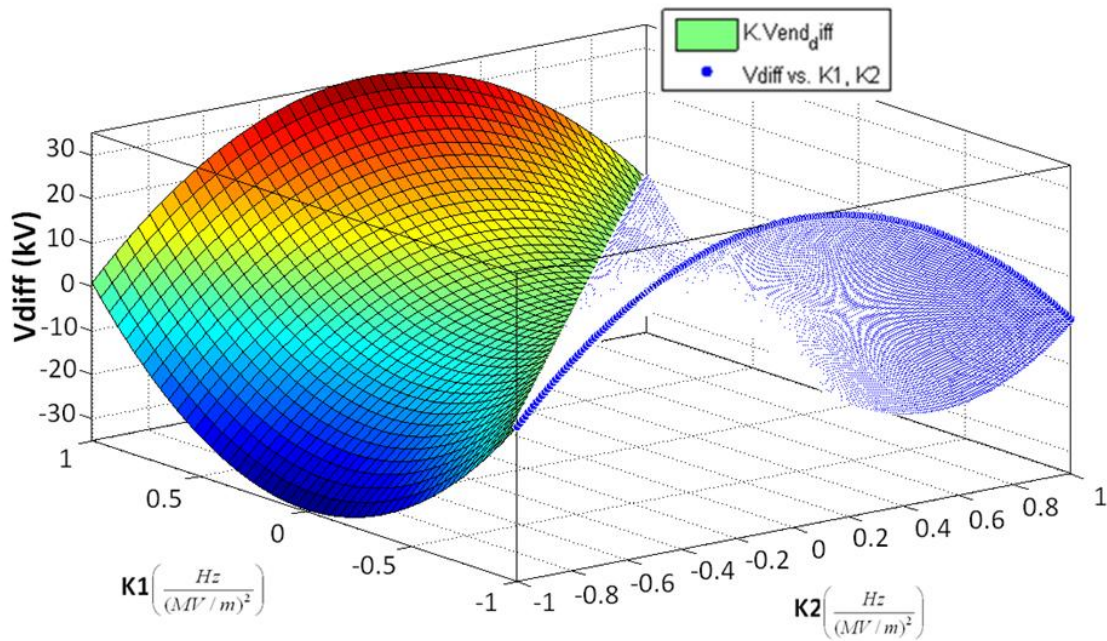


Figure 5.29: Curve fit for cavity voltage magnitude difference with varying Lorentz force detuning

All system configurations described are part of an analysis whose goal is to prove the viability of a superconducting, high-power proton LINAC from the point of view of

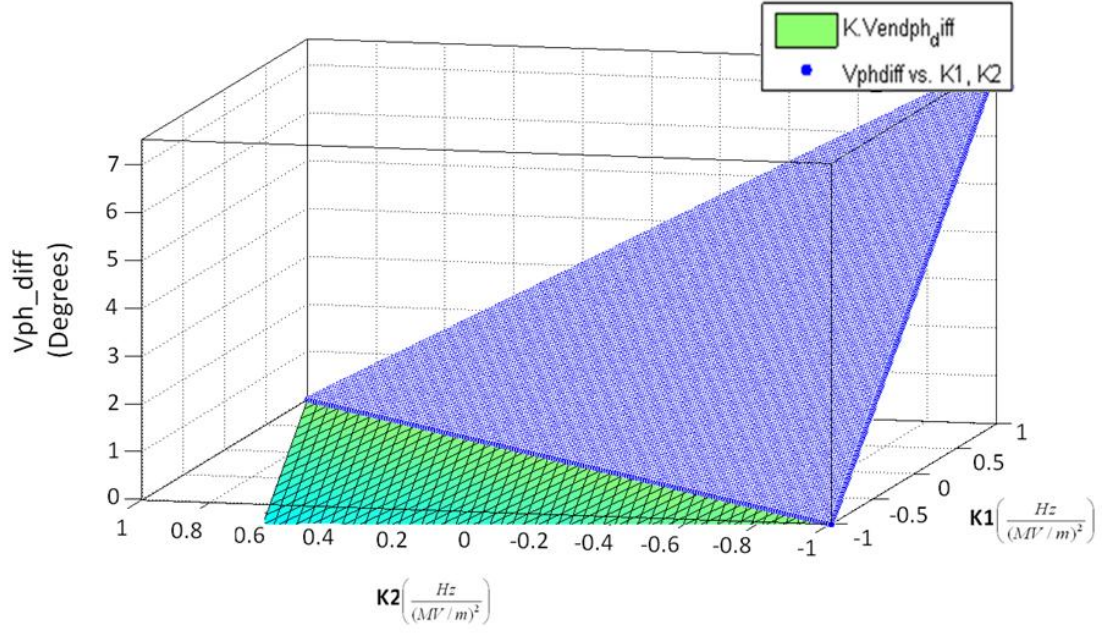


Figure 5.30: Curve fit for cavity voltage phase difference with varying Lorentz force detuning

the RF systems. The SPL is not only a challenge because of the energies and bunch densities involved, but the fact that the underground cavities are driven by pulsed klystrons operating from the surface adds complexity to the situation. The time delay of the feedback loop becomes an issue when the connectors are of considerable length, and the operating frequency of the system is of the order of hundreds of megahertz. In addition to this effect, pulsed generators introduce transients to the system with components in the whole frequency spectrum. A feedback delay of 5  $\mu$ s is included in the model, and stability analysis was carried out using low-pass filters to model the feedback loop and generator frequency responses. Finally, the proportional feedback gain was set to ensure that the system is stable [Gar96] [Hof]. The open-loop transfer function is given by:

$$H_{SPL}(s) = H_{FB}(s)H_{Kly}(s)H_{Cav}(s)H_{Delay}(s)H_{probe}(s) \quad (5.5)$$

where

$$H_{FB}(s) = \frac{G_{FB}}{\frac{s}{2\pi f_{cFB}} + 1} \quad H_{Kly}(s) = \frac{G_{FB}}{\frac{s}{2\pi f_{cKly}} + 1} \quad (5.6)$$

$$H_{probe}(s) = G_{probe} \quad H_{Delay}(s) = e^{-s\tau} \quad (5.7)$$

$$H_{Cav} = \begin{bmatrix} H_s(s) & -H_c(s) \\ H_c(s) & H_s(s) \end{bmatrix} \quad (5.8)$$

The cavity self and cross-coupled transfer functions are given by

$$\begin{aligned}
H_s(s) &= \sigma R \left[ \frac{s + \sigma \left(1 - \frac{\Delta\omega}{\omega_R}\right)}{(s + \sigma)^2 + (\Delta\omega)^2} \right] \\
H_c(s) &= \frac{\sigma^2 R}{\omega_R} \left[ \frac{s + \left(\sigma + \frac{\omega_D \Delta\omega}{\sigma}\right)}{(s + \sigma)^2 + (\Delta\omega)^2} \right]
\end{aligned} \tag{5.9}$$

where

$$\sigma = \frac{\omega_R}{2Q_L}$$

$\omega_R$  is the resonant frequency of the cavity, and  $\Delta\omega = \omega_R - \omega_0$  is the frequency deviation between RF source and resonant frequency of the system. The value was chosen as the maximum value observed in simulations.

We find that the problem of observing the characteristics of the system transfer function is not as straightforward as expected, as the behaviour of the model is the result of a coupled action between in-phase and quadrature signal components. The output of the system can be expressed using the following coupled equations:

$$\begin{aligned}
Y_I(s) &= H_K(s)H_s(s)X_I(s) - H_K(s)H_c(s)X_Q(s) \\
Y_Q(s) &= H_K(s)H_s(s)X_Q(s) + H_K(s)H_c(s)X_I(s)
\end{aligned} \tag{5.10}$$

where

$$H_K(s) = H_{FB}(s)H_{Kly}(s)H_{Delay}(s)H_{probe}(s)$$

I/Q refer to inphase and quadrature components, and s/c refer to the self and cross-coupled components of the cavity transfer function respectively. X and Y are inputs and outputs to the system. If we assume a purely inphase unit step input to the system to begin with, the system equations simplify to yield

$$\begin{aligned}
Y_I(s) &= H_K(s)H_s(s)X_I(s) \\
Y_Q(s) &= H_K(s)H_c(s)X_I(s)
\end{aligned} \tag{5.11}$$

and so we can investigate the stability behaviour of the system by analyzing the transfer function given by

$$H_K(s)(H_s(s) + iH_c(s))$$

in both magnitude and phase.

We want to find  $G_{FB}$  such that the open-loop transfer function is such that the closed-loop system is stable. For a feedback loop with a 100 kHz bandwidth and a 1 MHz bandwidth klystron driving an SPL cavity at its resonant frequency of 704.4 MHz, we find a gain margin of about 43 dB (x150) as shown in figure 5.31.

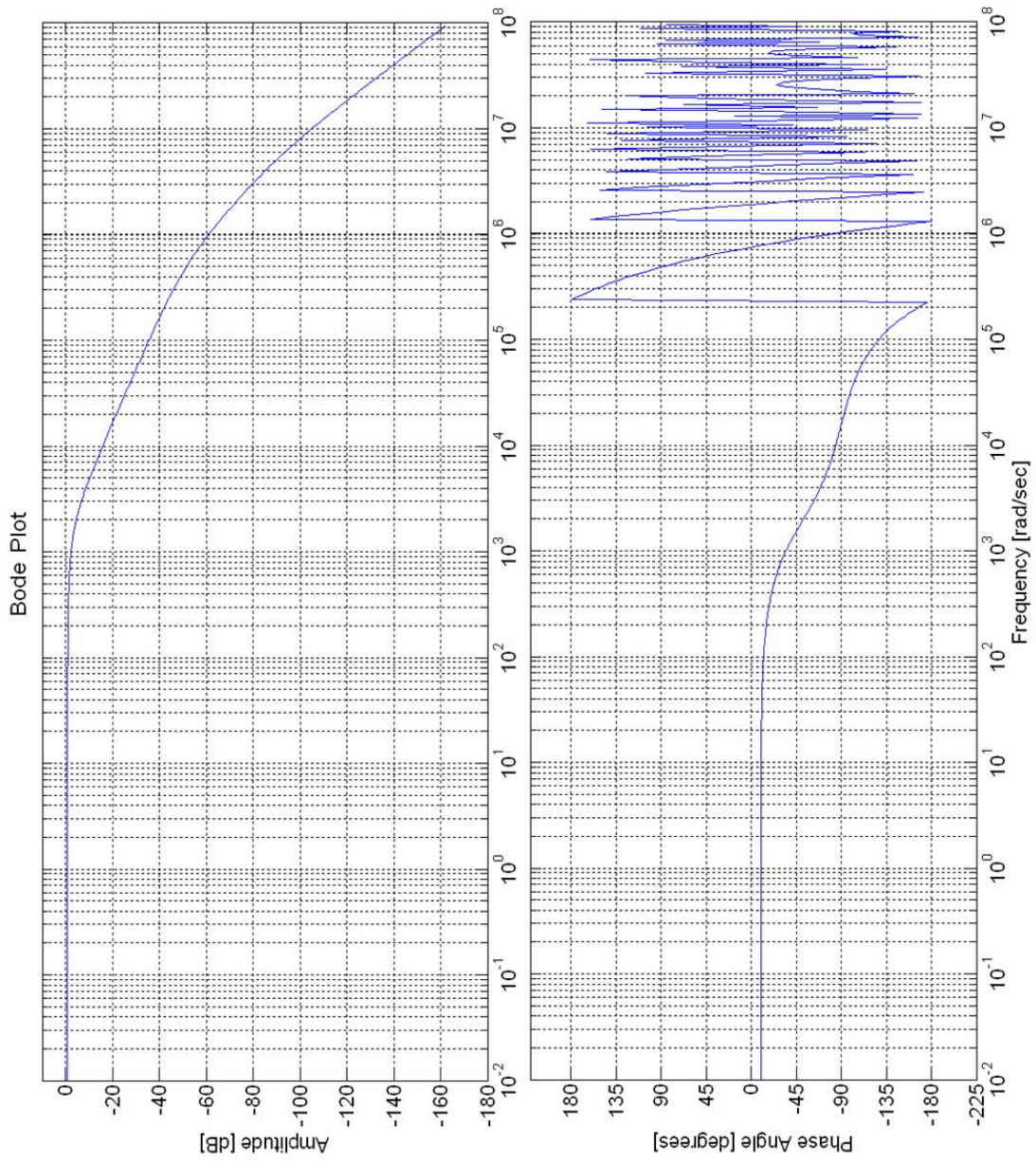


Figure 5.31: Open plot of open-loop system, gain margin of about 43 dBs

# Bibliography

- [AM] K. J. Astrom and R. M. Murray. **Feedback Systems, PID Control**. <http://www.cds.caltech.edu/~murray/amwiki>.
- [Bou86] Daniel Boussard. **Beam Loading**. In *Cern Accelerator School Proceedings*, Oxford, UK, September 1986.
- [G<sup>+</sup>10] Roland Garoby et al. **sLHC-PP 2nd Periodic Report**. Technical report, CERN, Geneva, Switzerland, May 2010.
- [Gar96] Roland Garoby. **Low-Level RF and Feedback**. In *Joint US-CERN-Japan Accelerator School on Frontiers of Accelerator Technology*, Tsukuba, Japan, September 1996.
- [Ger07] Frank Gerigk. **SPL parameter table**. <https://twiki.cern.ch/twiki/bin/view/SPL/SPLparameterList>, 2007.
- [Hof] Wolfgang Hofle. **Cavity-Laplace**. IQ transfer function.
- [Hof07] Markus Hoffman. **Digital Signal Processing Maths**. In *Cern Accelerator School Proceedings*, Sigtuna, Sweden, May-June 2007.
- [Hof09] Wolfgang Hofle. **SPL LLRF Simulations Feasibility and Constraints for Operation with more than one Cavity per Klystron Power Overhead**. In *3rd SPL Collaboration Meeting*, Geneva, Switzerland, November 2009.
- [Hol07] J. Holma. **The Model and Simulations of the LHC 400 MHz Cavity Controller**. Technical report, CERN, Geneva, Switzerland, February 2007.
- [Le 00] J. Le Duff. **High Frequency Non-Ferrite Cavities**. In *Cern Accelerator School Proceedings*, Seeheim, Germany, May 2000.
- [LP07] Michel. Luong and Olivier Piquet. **High Frequency Non-Ferrite Cavities**. In *IP-Eurotrans*, June 2007.
- [May79a] Peter S. Maybeck. *Stochastic Models, Estimation, and Control*, volume Volume 1, chapter Chapter 1. Academic Press, New York, San Francisco, London, 1979.

- [May79b] Peter S. Maybeck. *Stochastic Models, Estimation, and Control*, volume Volume 1, chapter Chapter 3. Academic Press, New York, San Francisco, London, 1979.
- [Ore07] Y. Oren. **Feedforward Control**. [www.bgu.ac.il/chem\\_eng/pages/Courses/oren%20courses/Chapter\\_9.pdf](http://www.bgu.ac.il/chem_eng/pages/Courses/oren%20courses/Chapter_9.pdf), 2007.
- [Sch98] Thomas Schilcher. *Vector Sum Control of Pulsed Accelerating Fields in Lorentz Force Detuned Superconducting Cavities*. PhD thesis, Hamburg University, Hamburg, Germany, April 1998. Dissertation zur Erlangung der Doktorgrades des Fachbereichs Physik der Universitt Hamburg.
- [Tuc04] Joachim Tuckmantel. **Consequences of an RF Power Trip in LHC**. Technical report, CERN, Geneva, Switzerland, January 2004. Appendix.
- [WB06] Greg Welch and Gary Bishop. **An Introduction to The Kalman Filter**. Technical report, University of North Carolina at Chapel Hill, Department of Computer Science, Chapel Hill, NC, USA, July 2006.
- [wik] **PID-Controller**. [http://en.wikipedia.org/wiki/PID\\_controller](http://en.wikipedia.org/wiki/PID_controller).
- [Wil78] Perry B. Wilson. **Transient Beam Loading In Electron - Positron Storage Rings**. 1078. PEP-0276.
- [WKS<sup>+</sup>00] T. Weiland, M. Krasilnikov, R Schuhmann, A. Skarlatos, and M. Wilke. **Review of Theory (I, II, III)**. In *Cern Accelerator School Proceedings*, Seeheim, Germany, May 2000.